University of Alberta

Scaled test estimation of Rolling Resistance

by

Ajoy Anand

A thesis submitted to the Faculty of Graduate Studies and Research

in partial fulfillment of the requirements for the degree of

Master of Science

in

Mining Engineering

Civil and Environmental Engineering

©Ajoy Anand
Spring 2012
Edmonton, Alberta

Dedication

This thesis is dedicated to my parents Amala and Late Ashok K. Haldhar whose

contributions to my life are beyond any words

Abstract

Rolling resistance is a prime factor effecting fuel consumption of an ultra class haul truck. Capital intensive mining industry has always been interested to reduce rolling resistance of haul roads thus reducing operating costs by saving fuel.

In view of the importance of rolling resistance in movement of ultra class haul trucks on haul roads, commonly used materials sand, oil sand, pit run and limestone were tested. Tests were performed with a scaled truck proportionately fifteen times smaller than ultra class haul truck. Oil sand considered as a base material was capped with other materials and tests were repeated. Results obtained from test data was found to be applicable for ultra class haul truck tire and rolling resistance was estimated.

This research will help in selection of materials for haul roads and quantify rolling resistance in mining industry.

Table of Contents

List of Tables

List of Figures and Illustrations

List of Symbols, Abbreviations and Nomenclature

Symbol	Definition
b	Plate width
B	Wheel width
C or C_1 or C_2	Soil constants
C_i	Cone index value
C_{RR}	Coefficient of rolling resistance
D	Diameter
f	Distance between normal reaction and contact point of wheel with ground
F	Resultant force acting on soil tire interface
F_k	Peripheral force (N)
F_r	Resistance force (N)
G	Gradient of cone index
h	Section height
K	Soil deformation constant
K_c,	Modulus of deformation due to cohesive force
K_c' or K_c'	Dimensionless modulus of sinkage
K_f	Modulus of deformation due to friction
l	Length of loading area
M	Moment (N.m)
M	Mobility number
n	Exponent of deformation
P_c	Carcass stiffness
P_g	Ground pressure
P_i	Tire pressure
Q	Vertical load (N)
R	Radius (m)
RR	Rolling Resistance
R_b	Resistance due to horizontal soil displacement
R_c	Resistance due to vertical soil compaction
R_t	Resistance due to flexing of tire
z	Sinkage
δ	Deflection

Chapter One: Introduction

Rolling Resistance (RR) plays an important role in the movement of any vehicle. Movement cannot be defined without RR. This study envelopes RR for composite materials in the mining industry and predicts the RR of heavy haul trucks. Though, a vehicle cannot move without RR, high values of RR create power loss, greater fuel consumption and environmental impact. Efforts have been made to keep RR at a set level. It has been proved that 30 % of total mechanical energy available at tire is wasted to overcome RR (Baglione et. al., 2007). Various efforts have been made to minimize RR and the recent development is hybrid low RR tires.

RR is an opposing force to rolling motion, which prevents vehicle tires from moving. A vehicle moves only when it overcomes RR. Various factors causing RR are deformation of ground, deformation of tires and tire properties (Plackett, 1985). Deforming objects are associated with energy of deformation and energy of recovery. When energy of recovery is less than energy of deformation, a loss of energy occurs which is the main cause of RR. Other factors affecting RR are temperature, vehicle speed, tire inflation pressure and tire construction (Clark et. al., 1979).

A prime concern in the mining industry is to reduce RR to an acceptable level suitable for large heavy equipment where a considerable amount of energy can be saved with appropriate maintenance of roads. Road materials should have lower RR. This research

tested readily available materials sand, pit run and limestone used in the mining industry

as road capping.

Chapter Two: Theory and Interpretation of rolling resistance

The two most important components of vehicle road interactions are RR and peripheral forces. The first evidence of RR was found during the 19th century when Morin (1841) studied the phenomenon of RR against horse drawn wagons. Morin (1841) considered various factors to determine RR of the wagon, which was operated on highways. Rear wheel load, front wheel load and velocity varied to evaluate the effect speed on RR. Morin (1841) also considered the case where rear wheels followed the same path as front wheels (Komandi, 1999).

2.1 Classic theory of rolling resistance

Ground wheel interaction and classic theories of RR are considered a first step in this research. In classical mechanics, and as depicted in Figure 2.1 RR is considered as a result of the movement 'f' of a vertical component of reaction force. Thus, RR is a reaction torque or moment, and not a force (Komandi, 1999).
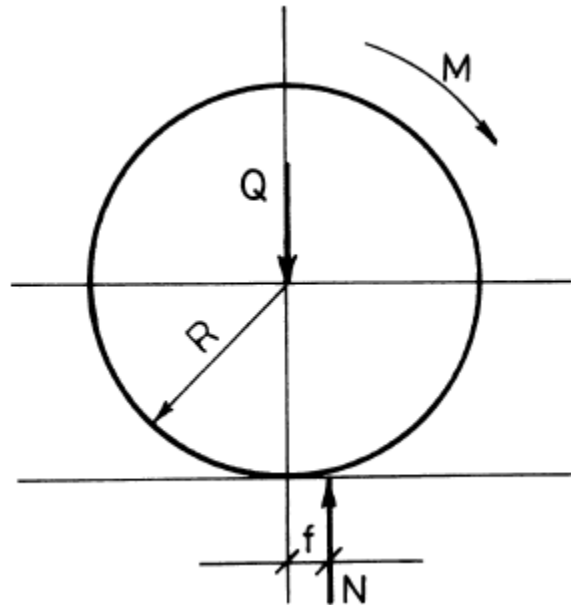
Figure 2.1: Forces and moment on a tire (after Komandi, 1999)

Heyde (1957) analysed the static equilibrium forces acting on a tractor to interpret RR

and develop the mechanics of tractor motion. Heyde's (1957) work can be summarized:

- RR is a moment and calculated from the expression f.Q

- The driving moment overcomes RR and only the balance moment affects the

  wheel-soil interface area

If the driving moment is more than RR moment, then the wheel will spin in its place,

therefore an active force in the direction of travel is required to create rolling motion.

Therefore, rolling is the result of both rotation and forward motion (Komandi, 1999).

$$F = \frac{M - f.Q}{R}$$
2.1

Where, M is the moment and F is the resultant force acting at the soil-tire interface i.e.

the difference of Peripheral force (F_k) and Resistance force (F_r) as shown in figure 2.2

a) a towed wheel b) a driving wheel

a)   b)
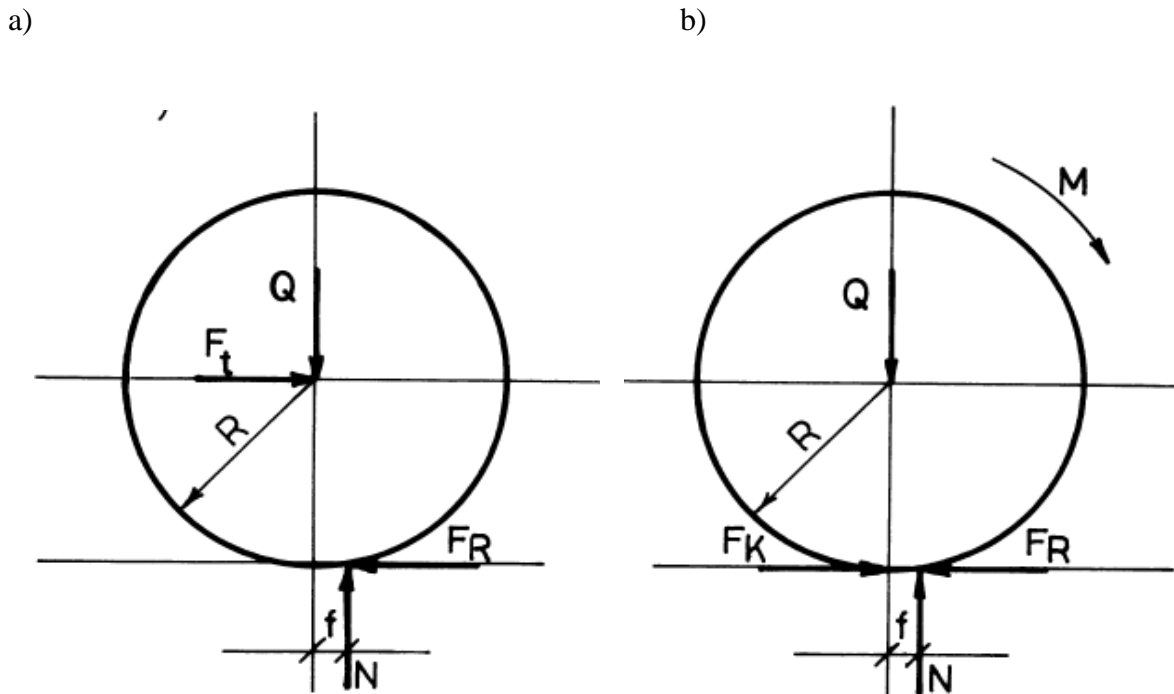
Figure 2.2: Mechanical characteristics of a) Towed wheels and b) Driving wheels

(after Komandi, 1999)

2.2 Similarity between towed and driving wheel under static condition

Under static conditions, the moment required to move a wheel on the ground can be

obtained by taking moments about the center of the towed wheel (figure 2.2 a)

$$f.N = F_r . R \qquad\qquad 2.2$$

which states that both components of normal reaction create an equal amount of moment.

Also, it is clear from figure 2.2 that $N = Q$ and $F_r = F_t$

therefore, $f.Q = F_t . R = M$ \qquad\qquad 2.3

Considering the driving wheel in figure 2.2 b, where conditions are similar to the towed

wheel, the moment equation about the contact point of tire and ground will be

$$M= f.Q \qquad\qquad\qquad\qquad 2.4$$

From equations 2.3 and 2.4, it can be concluded that resistance moment f.Q is equivalent in both cases.

Komandi (1999) concluded the following points:

- Mechanical characteristics of towed and driving wheel under static conditions are similar and analyses can be transferred from one case to the other

- The normal force due to deformation of tire or ground or both have horizontal & vertical components and moments exerted by these about the center of wheel are equal

- RR is a moment. Moments to overcome RR are equivalent for both towed and driving wheels under the same conditions.

This research has been conducted on a test bed where a constant speed motor towed a scale truck. Experiments were performed for different loads and under varying speed conditions. As towed wheel and driving wheel mechanical conditions offers equal RR, this research can likewise be extended to determine RR in the case of a driving wheel.

2.3 A different approach to rolling resistance: Bernstein and Gerstner theory of rolling resistance

In the early 20th century, many researchers investigated about draw bar pull for both on and off road vehicles. Agriculture and military were significant fields where findings were applied. It was imperative to study the soil vehicle interaction to determine the draw bar pull for a particular vehicle. Many attempts have been made to determine the draw bar pull, which is the difference of peripheral force and RR. The attempts subsequently

triggered development of numerous concepts to determine both the peripheral force and RR. Major research organisations and tractor manufacturers developed their own models. WES, NIAE and John Deere are some examples. These models were developed from the respective experience of these entities (Komandi, 1997, 1999).

Bernstein, Gerstner and Bekker offered the most prominent contribution in this stage of research. The majority of contemporary theories have basis on semi empirical methods and are usually devised following numerous estimations and assumptions. (Wills et. al., 1965). A semi empirical approach to predict forces acting on wheel operating in soil was first initiated by Bernstein in 1913. Bernstein and Gerstner (1913) observed that the RR acting on a wheel was due to work done in forming a rut or compression of soil.

Bernstein (1913) intended to determine the pull required to tow a wheel and proposed a theory based on the sinkage characteristics of a rectangular plate placed in soil. Gerstner and Bernstein (1913) applied thorough scientific approach by measuring the soil's resistance to compaction and tried to describe it in mathematical expressions.

Gerstner (1913) suggested that load per unit area of soil surface is

$$P = C_1 z + C_2 z^2 \qquad\qquad\qquad 2.5$$

Where C_1 and C_2 are soil constants and z is sinkage. This equation for load per unit area of soil surface was later modified to $P = C.z$ for simplicity and is hereafter used for calculations.

Considering the static equilibrium of the forces on wheel, Gerstner obtained an expression for the force required to tow a rigid wheel on deformable ground (Komandi, 1999):

$$F_t = 0.54 \left[\frac{Q^4}{(c.B.R^2)} \right]^{1/3} \qquad 2.6$$

Later, Bernstein (1913) found that Gerstner's assumption was not correct and recommended the following experimental expression (Wills et. al., 1965):

$$P = K.z^n \qquad 2.7$$

Where K is soil deformation constant, n is exponent of deformation, which depends on the soil, and the area of the cylinder bottom and z is sinkage. Later Bernstein (1913) found from experimentation on agricultural soil that the value of n is 0.5. Therefore, the expression was further simplified to $P = K.z^{0.5}$ and used for force calculation. Bernstein (1913) stated that RR could be determined by the work required to compress the unit area of soil by z_0. Bernstein's hypothesis proved to be the basis of extensive theories of RR for more than half a century.

Considering static equilibrium and necessary substitution, Bernstein obtained following expression (Komandi, 1999):

$$F_t = 0.57 \left[\frac{Q^{0.5}}{(c.B)^{0.5} .R^{0.75}} \right] \qquad 2.8$$

Bernstein (1913) further stated that soil resistance against vertical compression depends on the area of the cylinder base along with its circumference.

The previous discussion was generalised by theorists and practical experts for both towed and driving wheels. Gerstner and Bernstein defined RR as a force needed to pull a wheel regardless if towed or driven (Komandi, 1999).

According to classical mechanics, RR is a moment which can be calculated by f.Q (Komandi, 1999) while Gerstner and Bernstein (1913) believed that RR is a force needed to pull a wheel in soil.

If deformation of soil and wheel are both considered then a general equation for RR can be written as follows (Plackett, 1985):

$$R = R_c + R_b + R_t \hspace{4cm} 2.9$$

R_c is the resistance due to vertical soil compaction

R_b is the resistance due to horizontal soil displacement

R_t is the resistance due to the flexing of tire

Energy loss in tire can be categorised into three parts: internal, rotational and translational. Internal loss constitutes axle bearing friction, flexure of tire, loss in tread and carcass, etc. Rotational loss is caused by slip and is a part of the tangential force, which is used to support weight of the vehicle. Translational loss is due to the horizontal opposing component of radial force in a wheel following mechanics on deformable terrain (Onafeko, 1969).

2.4 Bekker's theory of rolling resistance

Bekker's theory could be deemed as a significant step forward following the findings of Bernstein. Bekker (1956, 1960, 1965) took into consideration the deformation of tire and ground and subsequently proposed a mathematical expression. Bekker based his analysis on Bernstein hypothesis, $P= K.z^n$. However, he proposed that modulus of soil deformation was composed of two parts, one due to cohesive property of soil other due to friction property of soil (Plackett, 1985). Therefore, Bernstein's equation was modified as follows:

$$P = \left(\frac{K_c}{b} + K_f\right).z^n \qquad\qquad 2.10$$

Where K_c & K_f are modulus of deformation due to cohesive and friction ingredient respectively, and can be obtained by pressure sinkage test in soil. b is the plate width used in experimentation efforts.

Bekker considered the work done in forming a rut and equation 2.10 for pressure distribution beneath a rigid, rectangular and uniformly loaded area. Bekker subsequently proposed the following expression which measured the compaction resistance component of RR R_c (Plackett, 1985)

$$R_{c=} \left(\frac{1}{(n+1).(K_c + b.K_f)^{\frac{1}{n}}}\right).\left(\frac{Q}{l}\right)^{\frac{n+1}{n}} \qquad\qquad 2.11$$

Where l is length of loading area

Later, Bekker considered the curvature of wheel and proposed an expression for compaction resistance and sinkage equation. Bekker also predicted the motion resistance

due to flexing of tire. Bekker considered ground pressure as a combination of tire pressure P_i and carcass stiffness P_c. Therefore, the load carried by flat portion of tire (P_g) can be written as:

$$P_g = P_i + P_c \qquad\qquad 2.12$$

Further, equation 2.11 was modified by incorporating 2.12

$$R_c = \frac{(b.(P_i+P_c))^{\frac{n+1}{n}}}{(K_c+b.K_f)^{\frac{1}{n}}\ (n+1)} \qquad\qquad 2.13$$

Bekker estimated resistance due to horizontal soil displacement R_b and found that it was difficult to express mathematically, largely due to the inability to distinguish between bulldozing and compaction. It was found that bulldozing resistance increased rapidly with an accompanying rising wheel width (Plackett, 1985).

The RR component caused by tire R_t was examined by both Bekker and Semonin (1975). Equations based upon determining the amount of energy used in deflecting the tire was used to compute R_t. Though the model was rather crude in its form, it was accepted due to practicality.

2.5 Development after Bekker

Bekker's theory proved to be milestone in the field of RR and later contributions by various researchers amended the basic theory for application across industry.

Reece (1965-66) investigated the validity of pressure sinkage equation 2.10 and found it unsatisfactory and observed that Bernstein's equation correct in its form. Reece (1965-66) used classical soil mechanics to examine soil failure beneath a strip footing with respect to pressure sinkage relationship and proposed a modified equation considering dimensionless moduli of sinkage $K_c^{'}$ and $K_f^{'}$

$$P = c\, K_c' \left(\frac{z}{b}\right)^n + b\, K_f' \left(\frac{z}{b}\right)^n \qquad\qquad 2.14$$

The Reece relationship was in agreement with Terzaghi's (1944) and Meyerhof's (1951) relationship of strip footing and had a sound theoretical basis. Wills (1976) conducted subsequent and extensive experimental tasks which confirmed the values of the Reece equation.

Onafeko and Reece (1966) investigated the radial and tangential soil stresses and deformations beneath rigid wheels and found that radial stresses beneath a rigid wheel could not be linked to the pressure beneath a strip footing. The actual stress distribution has a peak forward of bottom dead centre which moves further forward with increasing slip or skid which increased RR.

Later Gee-Clough (1976) pointed out that Bekker's equation does not take into account the effect of wheel slip of RR and developed a modified resistance equation inclusive of lift force.

2.6 Various conceptions about rolling resistance

It is clear from the discussion hitherto that RR is a moment according to classical theory, while Bernstein defined it as 'force required to move wheel on deformable terrain.' Bekker considered deformation of both tires and ground and stated that RR is due to soil failure and deformation of tire.

It is observed that definitions of RR have been varied according to interests and fields and thus results likewise have a degree of variation. Some examples include: an automobile engineer concerned with deformable tires on rigid surface; a railway engineer interested in rigid wheel on rigid surface; an agricultural engineer interested in rigid wheel and deformable ground and the two in unison.

This study boasts a broad application in mining and falls in the case of deformable ground and wheel. There is a fair degree of complexity in the latter case due to soil wheel interaction. Researchers have long been interested in discovering the gross force demanded to move a wheel on terrain. Such a pursuit required them to realize RR, as a draw bar pull is the difference of gross force demanded and RR (Komandi, 1999).

2.7 Mobility number approach to rolling resistance

The majority of theories concerned with RR are based on pressure sinkage methods or classical mechanics. However, Firetag (1965) proposed a dimensionless number called the mobility number to predict RR of a tire. Equations later developed included noticing both the coefficient of RR and the mobility number. Firetag (1965) used cone index value

(C) and gradient of cone index (G) to characterise the soil and parameters of load (W),

width (b), diameter (d), section height (h) and deflection (δ) to characterise the wheel.

The mobility numbers proposed by Firetag (1965) are as follows:

Clay mobility number = $(C_i \frac{bd}{W}) (\frac{\delta}{h})^{1/2}$ 2.15

Sand mobility number = $G (bd)^{3/2} (\frac{\delta}{h})$ 2.16

Further modification to the clay mobility number was done by Turnage (1972) which was

used by Dywer et. al. (1975) and later by Gee Clough (1979) to propose following

relation between clay mobility number (M) and coefficient of RR, C_{RR}.

$$C_{RR} = \frac{0.287}{M} + 0.049$$ 2.17

Equation 2.17 was found from experiments with 1.45 m to 1.75 m tires diameter. It was

observed that mobility numbers cannot be extrapolated with confidence.

2.8 Factors effecting rolling resistance

It can be summarised from the discussion hitherto that the following factors affect RR of

a tire movement on deformable ground:

1. Soil type and its failure under the load, soil strength

2. Tire flexing, tire type, inflation pressure and temperature

3. Condition of haul road

4. Wheel loading

5. Internal friction

6. Speed

Additionally, RR is expressed as a percentage weight of vehicle and can be added to grade resistance to obtain gross resistance. This determination can be utilized while working with a particular manufacturer's rimpull -speed- gradeability (Plackett, 1985).

Pope (1969) suggested that RR decreases with increasing speed; the two elements are thus inversely related. Two wheels of 10 inches in diameter, one with solid plate and other with cut away with rim were tested by Pope (1971) to support the effect of speed on RR. Experimental results were found in agreement with the fact the RR decreases with increasing speed.

Knoroz (1968) found that vehicle fuel consumption is related to RR and each vehicle has an operating range where the effect of RR on fuel consumption is maximized. This effect is dependent upon the relationship between tire RR in the overall resistance to motion balance, along with the degree of engine loading and vehicle speed. Tire treads and carcass constitutes major hysteresis loss in a tire causing RR. A reduction of 1 mm to 2 mm of tread thickness reduces RR coefficient by 3 to 4%. Also, every percentage point reduction in RR reduces fuel consumption by 0.25% to 0.35 %.

Chapter Three: Tire flexure test setup

As the research is focused to predict the behavior of an ultra class tire from a scaled tire,

it is important to determine the properties of scaled tire which can be compared with ultra

class tire. In order to determine the properties of scaled tire, a series of tests were

conducted. Various loads were applied on the tire hydraulically. Deformation and foot

print area were measured in each case. Experiments were repeated by adjusting the

inflation pressure in the tire.

The apparatus used for tire flexure are listed below and labeled accordingly in figure 3.1.

1. Frame attached to the table featuring a slot

2. Wooden plank, vertically mobile and fitted to the frame slot

3. Tire holder attached to the wooden plank

4. Cylinder with piston arrangement

5. Piston applying pressure on the tire holder

6. Hydraulic pump to apply load or pressure

7. Pressure regulator

8. 10" diameter tire

9. Hose

3.1 Test procedure

In order to determine the deformation and foot print area of scaled tire a tire flexure test

was conducted as shown in Figure 3.1. A U shaped steel frame (1) was attached to table

and slots were cut both sides of it. A wooden plank (2) was made to fit frame slots such

that it can move up and down in the slot with minimum resistance. Wooden plank was

kept wider in the middle of frame and frame slots provided as a guide for movement. An

inverted U shaped steel tire holder (3) was attached to wooden plank (2) and a through

hole was made in the wooden plank centrally. Piston (5) from the top will pass through

wooden plank hole and would sit on steel tire holder (3). Bottom end of tire holder

contains two holes at the same level through which a small axle holding tire passes.
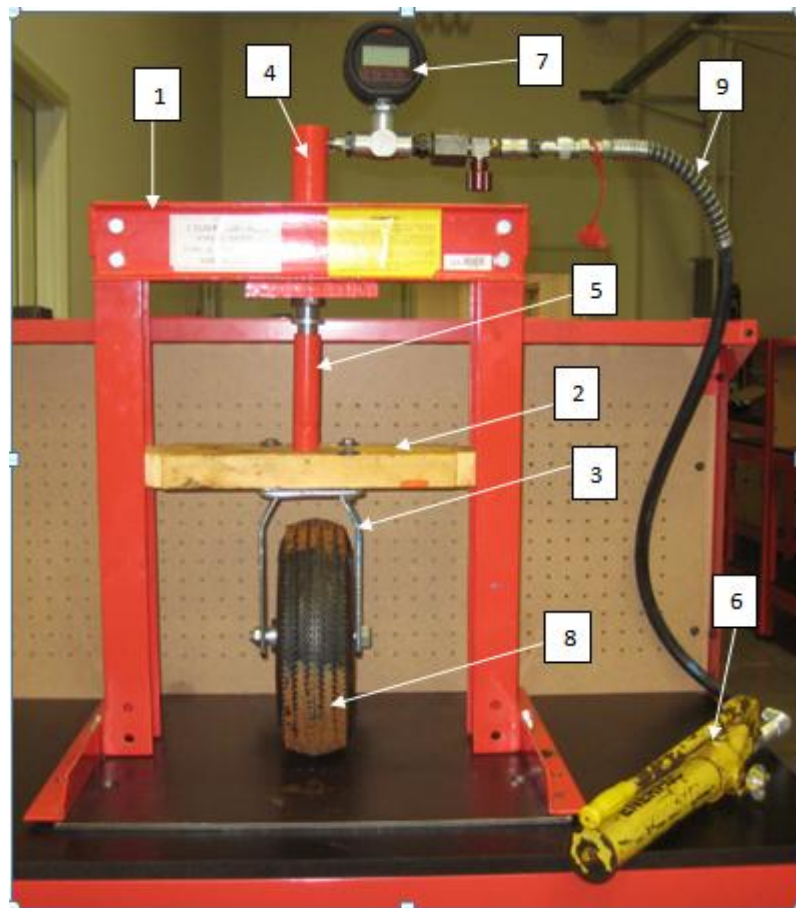
Figure 3.1 Tire flexure test setup
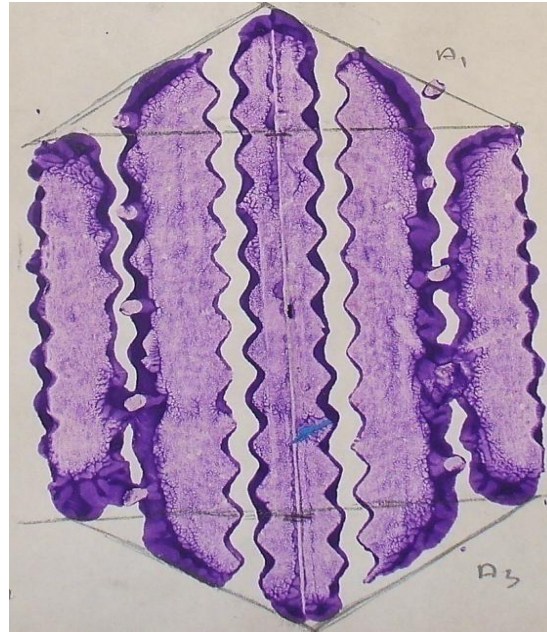
Figure 3.2 Foot print area at 6 psi tire pressure and … psi load

Cylinder (4) and piston (5) arrangement had been fixed on the top of the frame. A

hydraulic pump (6) is connected to cylinder through hose (9). A relief valve pressure

regulator (7) set at 300 psi was fit between pump and cylinder. System was made leak-

proof to avoid inadvertent pressure drop.

Oil was pumped by a manually operated hydraulic pump (6) into the cylinder (4) which

pushed piston (5) out. As piston (5) is sitting on the tire holder (3), it presses the tire

against the ground. The part of tire, which sits on ground, was painted by color and a

white sheet was placed underneath tire. A sample of foot print area obtained after

application of a load on the tire is shown in Figure 3.2.

A mark is placed on the center of the tire. Initial height of tire was measured from

previously stated mark to the ground when piston applied 25 psi pressure to hold the tire

straight. Initial pressure was kept constant afterwards in each case at 25 psi. This was also done to nullify any error in pressure indicator reading.

Further pressure was applied deforming the tire as shown in Figure 3.1 and final height of tire was measured from aforesaid mark to the ground in each case. Difference of initial height and final height was the deformation of tire at that particular pressure. An electronic vernier caliper was used to measure heights to minimize the error. Tire inflation pressure was kept constant for each experiment phase, while the load pressure was varied from 25 psi to 250 psi. Deformation at each pressure load was recorded. Experiments were repeated by changing tire inflation pressure from 2 psi to 10 psi for an interval of 2 psi i.e. 2, 4, 6, 8, 10 Psi.

3.2 Interpretation of tire flexure test data

As tire deformations were obtained at various loads, behavior of the tire under load can be examined. Sample data obtained at 6 psi tire inflation pressure is shown in table 3.1. Similar data at 2 psi, 4 psi, 8 psi and 10 psi were obtained.

Load (N)	Deformation (mm)	% Strain	Foot print area (m^2)	Pressure stiffness (N/m^3)
67.51	4.54	1.70	0.00281	5.3×10^6
104.37	7.21	2.70	0.00429	3.4×10^6
146.51	9.96	3.53	0.00474	3.1×10^6
210.66	12.33	4.62	0.00540	3.2×10^6
251.36	15.62	5.86	0.00682	2.3×10^6
289.90	18.06	6.77	0.00699	2.2×10^6
371.06	23.36	8.76	0.00820	1.9×10^6

Table 3.1 Load flexure test data at 6 psi

A graph measuring respective load and deformation in Figure 3.3 portrays a straight line or constant trend for all inflation pressures the tire is tested for. A horizontal line parallel to the X axis drawn on Figure 3.3 represents deformation at the same load with varying inflation pressure of the tire. Moving on this horizontal line from left to right, it was observed that tire deformed less at a higher inflation pressure with constant load. Therefore, it may be concluded that stiffness of the tire increased following an increasing of inflation pressure. Also, it can be observed that the slope of straight line is increasing with increasing tire inflation pressure, which proves that tire stiffness increased with increasing inflation pressure. A graph between stiffness and tire internal pressure in Figure 3.4 exhibits the linear relation between the two.

Similarly, a graph between foot print area and loads were plotted as seen in Figure 3.5. A horizontal line on this graph exhibits the variation of foot print area with tire inflation pressure at a constant load.

Moving from left to right on the horizontal line one notices that foot print area is less at a higher relative inflation pressure. A vertical line on the same graph reveals that obtaining the same foot print area requires higher load at higher inflation pressure.
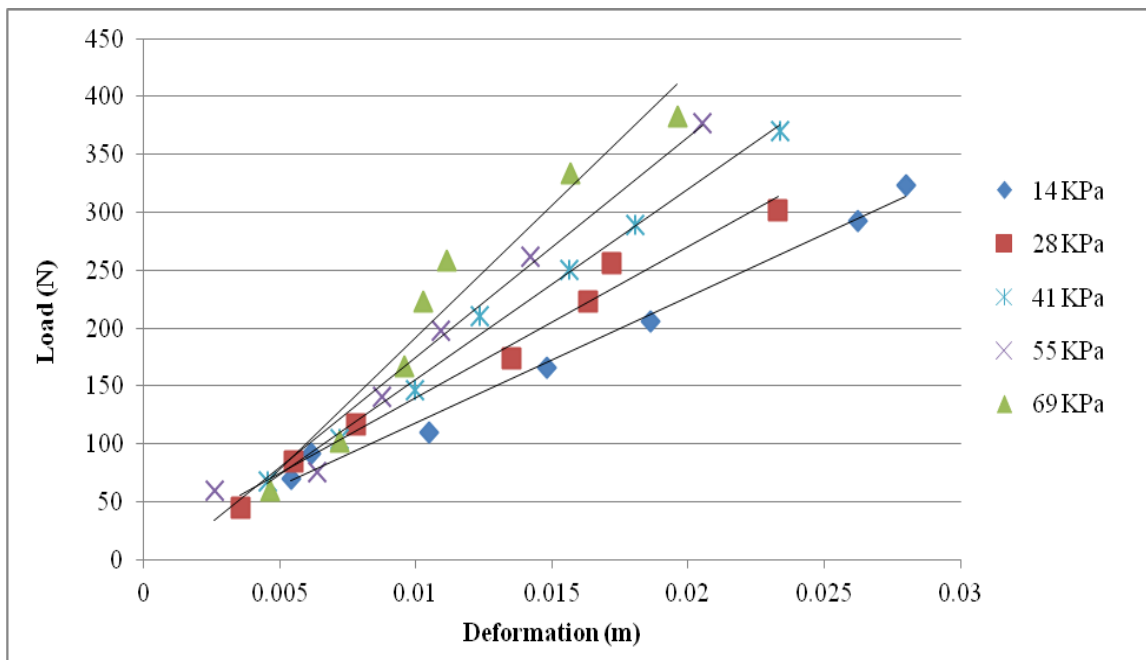
Figure 3.3 Load vs. deformation graph at different internal pressures
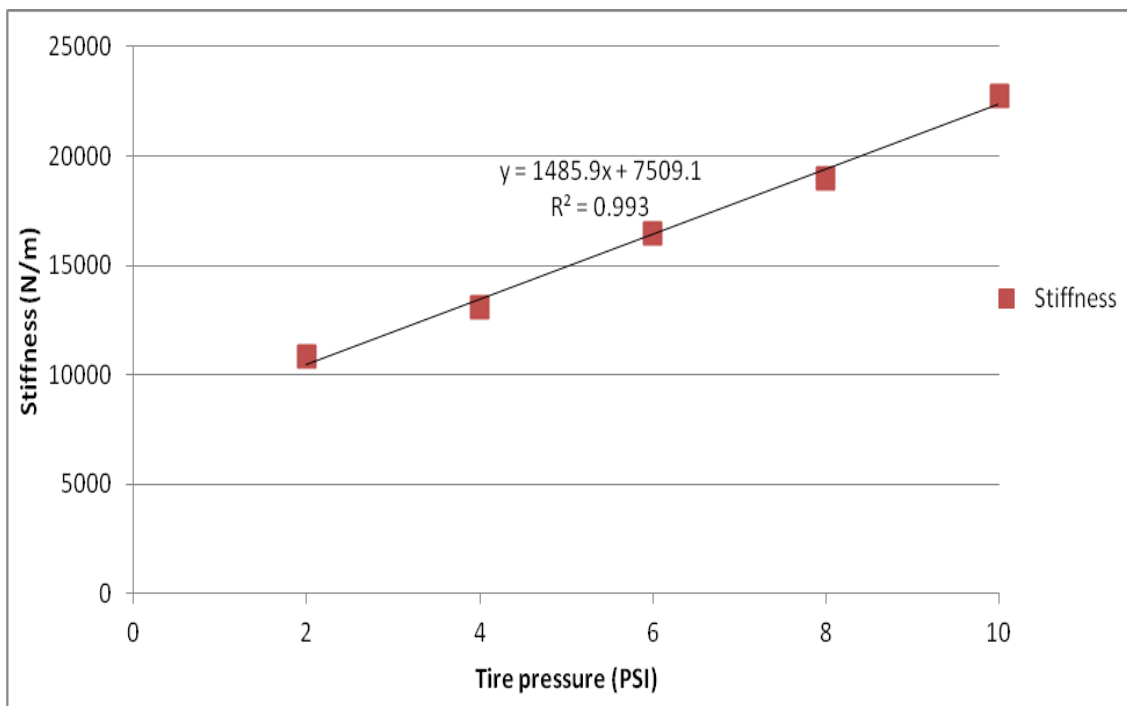
Figure 3.4 Stiffness vs. tire internal pressure
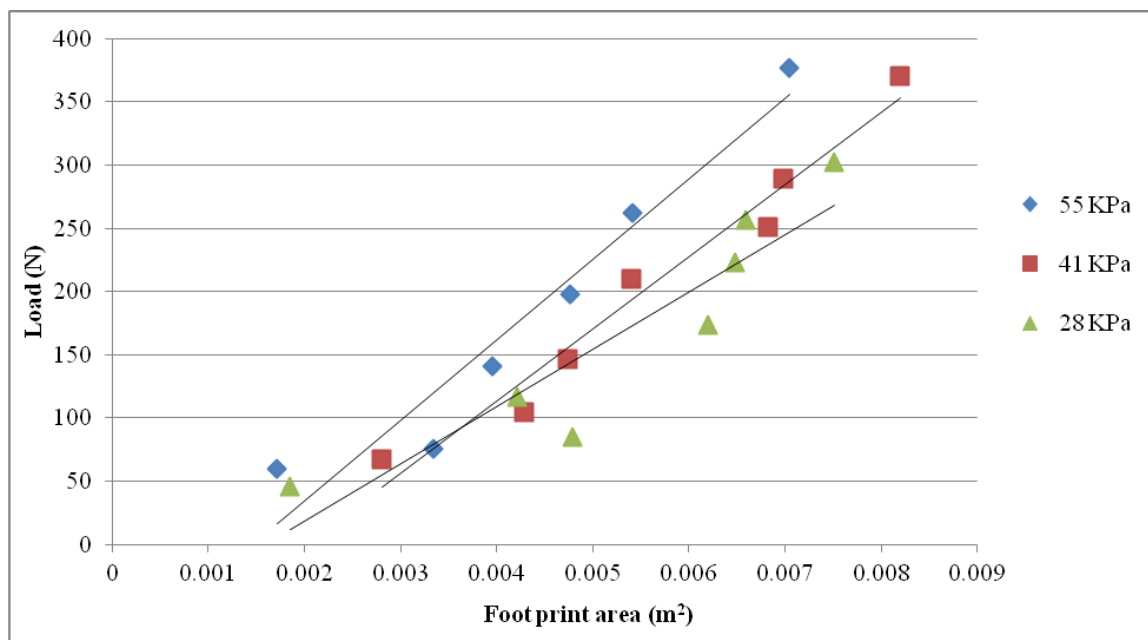
Figure 3.5 Load vs. foot print area at different tire internal pressures

The previous discussion of foot print area, loads and deformation in tire suggests that behavior of the tire can be decided in line with these factors. A parameter comprising these factors can be defined as pressure stiffness in the following form:

Pressure stiffness =   Load

--- 3.1

(Deformation x foot print area of a tire)

Pressure stiffness comprises load, foot print area and deformation of tire, the tires having same pressure stiffness will be equivalent and a scaling factor can thus be calculated in projecting data results from an equivalent tire.

Chapter Four: Concept of scaling and application

The scale model introduces the idea of a miniature version of a larger, original physical system. It simplified and made experiments possible that seemed originally unfeasible. For example the testing of a suspension bridge may be too large for direct experimentation, a spacecraft also may be quite inaccessible but a scale model of these can be created economically and realistically. In order to determine unknown variables, the similar but smaller collection of environment and conditions can be more accessible to researchers. An important factor for reproduction of a particular physical system as a scale model lays in fact that phenomenon might not have a theoretical solution or may ultimately prove to be far more complex than previously thought. Therefore in a relatively more complex experimentation environment certain empirical formulae will dictate the structure of that phase of the research (Schuring, 1977).

A similar situation occurred in this research which demanded an ultra class haul truck for lab experimentation. Commonly used ultra class trucks are CAT 789, CAT 793 and CAT 797 with a hauling capacity of 150, 250 and 400 tonnes and a total weight of 300, 500 and 700 tonnes respectively. Tire sizes used on these trucks are 55/80 R63 or 59/80 R63 having outer diameters of 3.84 m & 4.04 m and rim diameters of 1.60 m respectively. However handling of a mammoth size truck in lab is absolutely impractical. Therefore scaled models of the ultra class trucks were designed and fabricated for the experimentation. Also, deformation of ultra class truck tires was needed to make an

estimation of stiffness and energy lost due to RR. It was not possible to test 55 /80 R63 or

59/80 R63 under the present lab capacity.

Therefore, an equivalent truck having 15 times smaller dimensions was designed and

fabricated for experimentation. Also, selected tire size was 15 times smaller than 151"

tire used in ultra class haul truck. 6 tires of 10" diameter were used in aforesaid truck

with 4 tires in back and 2 tires in front having the same arrangement as ultra class haul

truck. Load distribution on front to back tires was 33% and 67% respectively, which is

equivalent to that of actual ultra class haul trucks. Also, same degrees of scaling were

used for all dimensions. For example, distance between front axle to rear axle and

distance between rear tires has been scaled down 15 times and dimensions of a smaller

truck were found.

It is imperative that the scaled model truck should yield same or equivalent results as

ultra class haul trucks. As discussed in the previous chapter, it was found that tires having

the same pressure stiffness are considered equivalent to each other and a scaling factor

will be calculated to project data from smaller tire data to that of an ultra class truck tire.

It was found in a field study on ultra class trucks weighting 635,000 kg (1.4 million lbs)

and supported on six 55/80R63 tires at 87 psi created a deformation of 0.27 m (10.62

inches) in each tire while load distribution was maintained at 67 % on back tires and 33%

on front tires. Foot print area at this deformation was 1.3 m^2 (2015 in^2). As 55/80R63 tire

has a diameter of 3.84 m, 0.27 m deformation corresponds to 7 % (0.27/3.84) strain in

tires. Pressure stiffness of ultra class truck tire was calculated by equation 3.1 as defined

in section 3.2:

Pressure stiffness =   Load

                                  (Deformation x foot print area of a tire)

$$= \frac{(1.4*1000000) /6 \text{ lbs}}{(10.62 \text{ inches} * 2015 \text{ inch}^2)} = 10.89 \text{ lb/inch}^3 = 3x10^6 \text{ N/m}^3$$

Therefore, 10.89 lb per cubic inch ($3x10^6$ N / m^3) pressure stiffness will make scaled tires

equivalent to ultra class truck tires.

A series of tests were performed and discussed in Chapter 3 in order to determine a viable

combination of load, tire pressure and foot print area. Figure 3.3 shows deformation of

truck tire with varying loads at different internal tire pressure while Figure 3.4 presents

load vs. foot print area.

Pressure stiffness at 4 psi, 6 psi and 8 psi was calculated and properly examined to

determine a viable combination suited for the scaled model truck. The necessary pressure

stiffness of 10.89 lb/inch^3 was found best suited to 6 psi pressure at 35 lbs load.

Deformation of tire was 0.37" (0.0095 m) at this load. Tire inflation pressure higher than

6 psi resulted in the same pressure stiffness at lower loads which would result in

relatively rough travel for the scaled truck, thus the most desirable data points could not

be obtained for subsequent analysis. An internal pressure less than 6 psi required a higher

load which was beyond the capacity of scaled truck. Therefore, 6 psi tire internal pressure

and 35 lbs load were found to be the best suited combination for further experimentation. This combination is highlighted in table 3.1.

A plot between load and percentage strain is shown in Figure 4.1. The selected combination of 6 psi internal pressure and 35 lbs load correspond to 3.5% strain which is shown by the arrow in Figure 4.1. It is evident that load vs. deformation, foot print area and % strain are linear therefore a scaling factor of 2 (7 / 3.5) should be used in a reference equation in order to predict pull forces for scaled trucks such that each tire had 7 % strain while travelling on test bed.
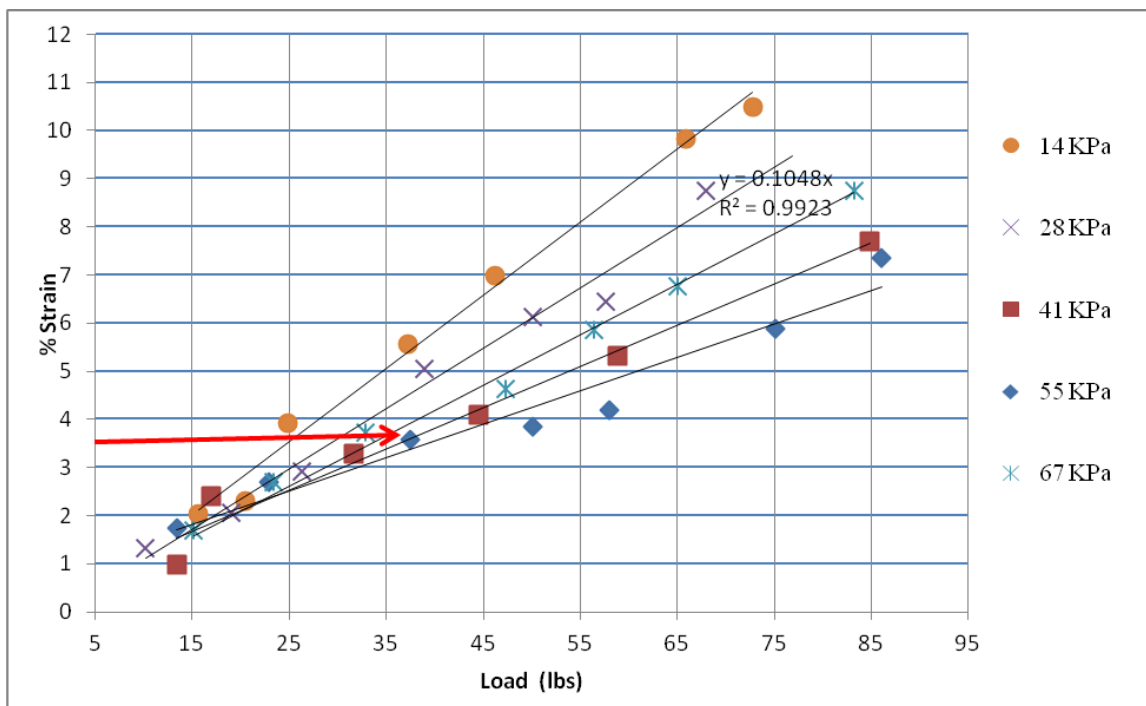
Figure 4.1 Load vs. strain at different tire internal pressures

Chapter Five: Setup design and test procedure for load resistance test

As discussed in Chapter 4, a scaled truck was built with dimensions proportionate to an ultra class haul truck. This truck was designed to run on a test bed filled with different materials in the same manner as ultra class truck runs on a haul road. As the truck is scaled, there is a need to design a haul road suitable for the smaller modeled truck. Also, all components used in research need to be scaled or designed according to scaled truck such that it represents the same situation as ultra class truck running on haul road. Then, an equivalent scale factor will be calculated to project these results on ultra class trucks.

Test Bed – A steel test bed acts as a haul road for the scaled truck. Test bed was 80" long, 32" wide and 5" deep and can be filled with different test materials. Length of the test bed is selected such that all six tires can have two complete rotations. Additionally the test bed included a perfectly plane adjustable ramp (1) with pre set grades of 0, 2.8, 5.1, 7.7, 10.3 and 12.8% inclines (9) as shown in Figure 5.5.

It is known that the depth of influence in operational loading is 2.5 times that of tire width as shown in Figure 5.1. Therefore, arrangements were made so that test bed depth is more than 2.5 times tire width to avoid any interference of bottom surface of test bed. Also, sufficient distance was maintained between truck tires and the sidewall of the said test bed in an effort to eliminate inadvertent interference stemming from sidewalls.

The variable grade test bed discussed above was filled with different materials including sand, oil sand, pit run and lime stone. The scaled truck was to run on these materials in order to determine the behavior of individual materials towards RR. Experiments were repeated with composite materials, which will be discussed in a later section. Properties of materials used in experiments are described below:
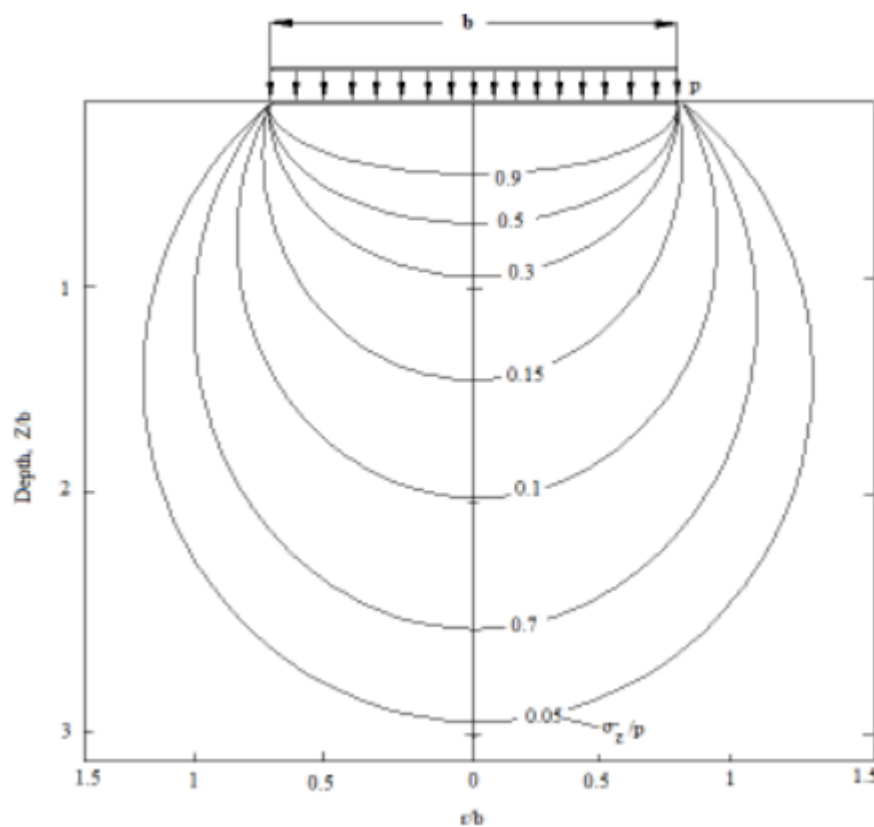
Figure 5.1: Contours of constant vertical stress beneath a uniform loaded circular area (Perloff, 1975)

Oil Sand: Oil sand used in experiments had 11.7% bitumen content, 13.4% fines (including the clay fraction) and 6.8% water. Traces of quartz and other heavy minerals

were evident in oil sand samples. The quartz fraction is described as sub-angular in shape. Grain size of bitumen flushed and dried sand is outlined in Figure 5.2.

Sand: Grain size details of sand used in experiments were not available, however it appeared somewhat finer and less sub-angular in size and shape compared to oil sand screened. Additionally, the sand was deemed reasonable enough to consider their sieve analysis similar and parallel to that of oil sand but slightly to the right, as shown in Figure 5.2.
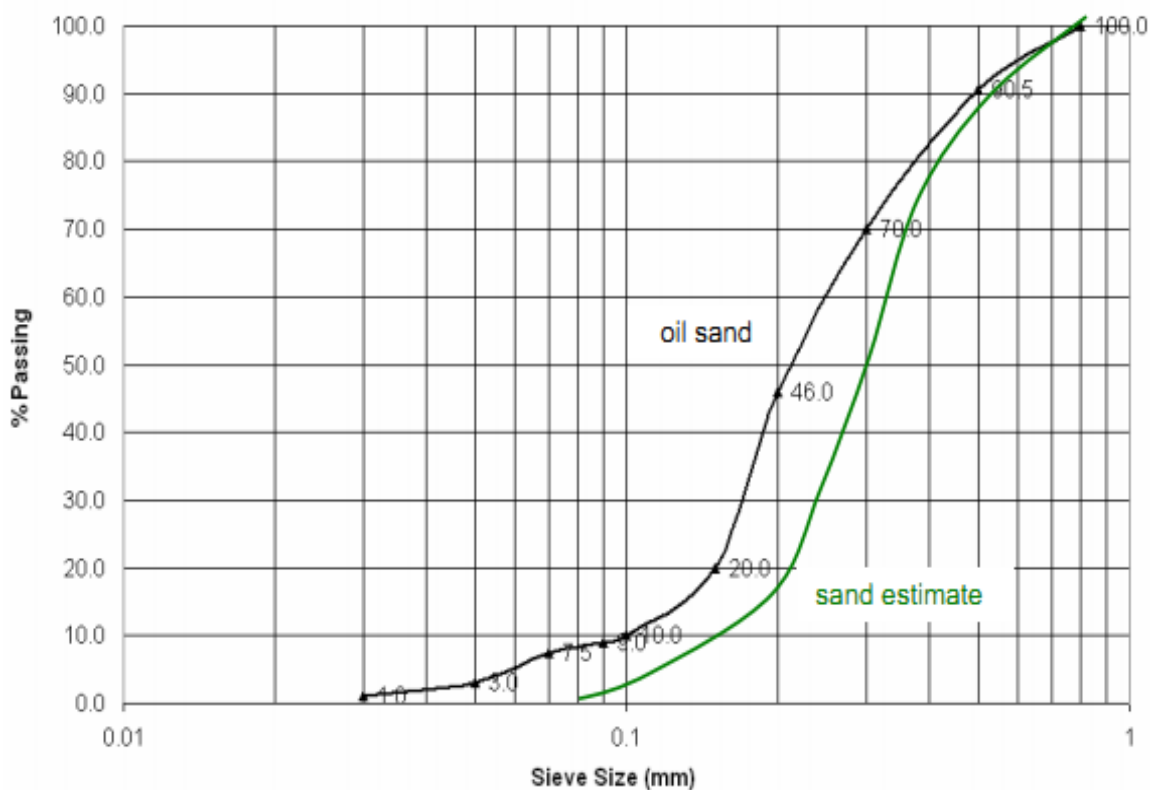
Figure 5.2: 11.7 % bitumen content (flushed) oil sand – dry particulate sample sieve analysis

Limestone: It appears that limestone samples obtained from Birch Mountain had finer grade distribution due to fragmentation in drying process than the material in field conditions or that used in present experimentation. Grain size obtained from sieve analysis is shown in Figure 5.3.

Pit run: It was observed that initial pit run sample had the largest particle size at 200 mm which is $1/7^{th}$ footprint width of an ultra class truck tire. As the experiments were performed with the scaled truck, material needs to be sieved such that maximum particle size in sample should not exceed $1/7^{th}$ (25 mm) of scaled tire footprint width. Therefore, pit run was sieved to 1 inch passing prior to sieve analysis. Grain size obtained from sieve analysis of pit run is shown in Figure 5.4.
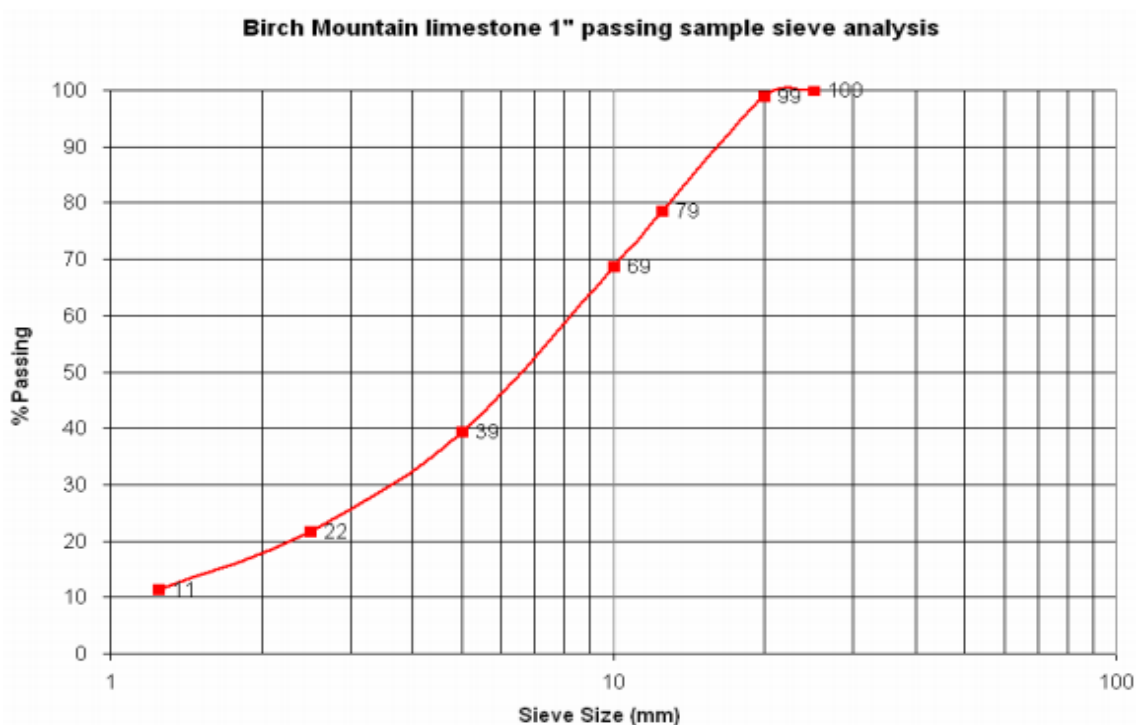
Figure 5.3: Limestone 1" passing sample sieve analysis
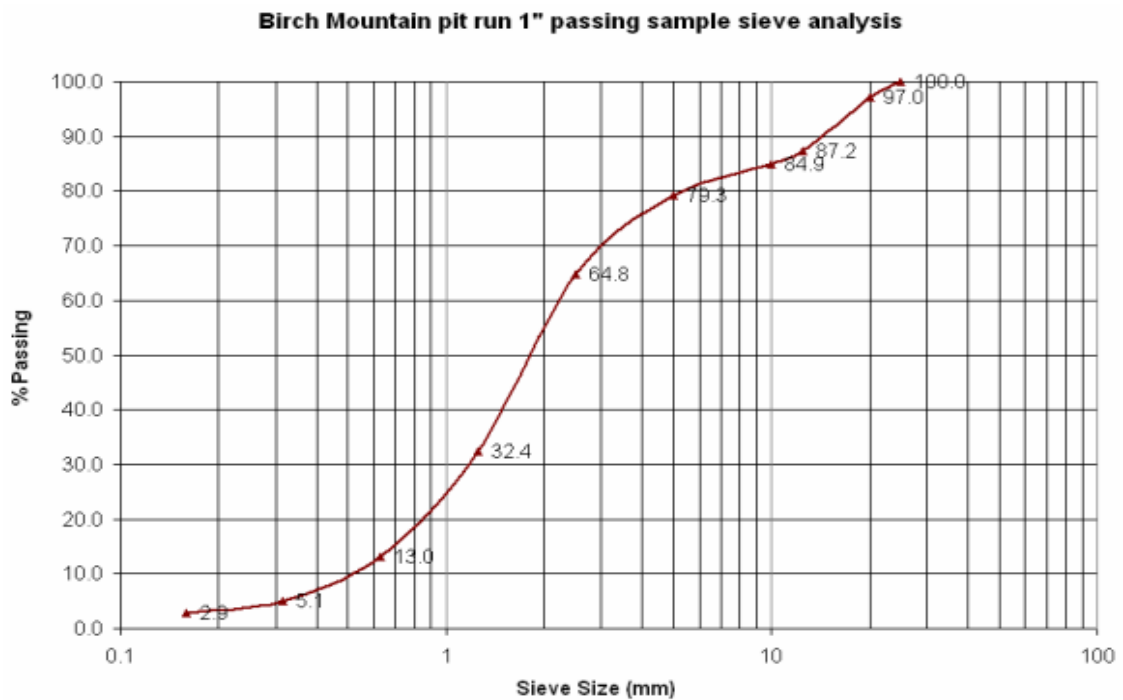
Figure 5.4: Pit run 1" passing sample sieve analysis

All apparatus used in experiments are listed below (Figure 5.5)

1. Test bed or adjustable ramp

2. Scaled truck

3. Load block of 50 lbs and 10 lbs

4. Plate to secure loads

5. Constant speed motor (find out spec)

6. Load cell

7. Wire – load cell to data acquisition system

8. Materials – Sand, Oil Sand, Pit run and Limestone

9. Arrangement to change ramp angle
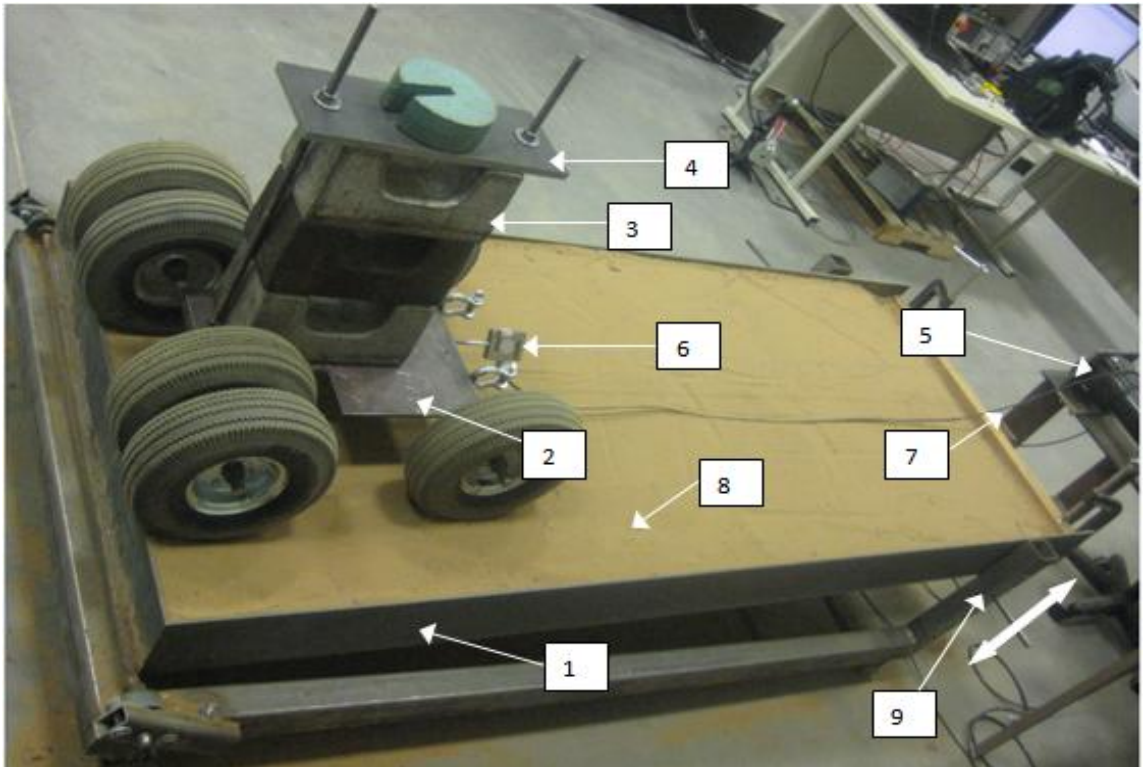
Figure 5.5: Load resistance test set up

5.1 Test on empty bed

Once tire pressure and load on the scaled truck was decided, a number of 50 lb weights

were put on truck such that rear axle had 67% while front axle had 33% of total load. A

complete set up is shown in Figure 5.5. Loaded truck was placed at rear end of empty test

bed which was set at 0 degrees initially. Truck was connected to a constant speed motor

via load cell (6), which gave data input to EDAQ data acquisition system. As soon as

motor was put in 'ON' position, rope (not visible on diagram) experienced a tension and

started pulling the truck across the test bed. Tension in the rope was recorded through the

load cell by a data acquisition system in a connected computer.

Initially the test bed was set at 0 degrees and the test was performed with 160 lbs load at different motor speeds of 60 %, 70%, 80%, 90% and 100%. Three runs were completed at each speed to yield error free data. Then, test bed was varied to 2.85, 5.1, 7.1, 10 and 12.8% gradient and varying speed at each grade with 160 lbs load collected data.

Finally equivalent procedures were repeated for 210 lbs and 260 lbs load. Thus, three variables – load, gradient and speed were considered to establish base line equation. It is clear from this revelation that experiments were performed at three different loads, five different speeds and five different gradients and each test was repeated for three cycles. Therefore, a total of (3x5x6x3) of 270 tests were performed.

Though tire pressure and load was decided to be 6 psi and 210 lbs, initial experiments were performed at different loads of 160 lbs, 210 lbs and 260 lbs to obtain clear understating of reference equation. Later experiments were consistently performed at 210 lbs and 6 psi tire pressure.

5.2 Experiments on sand, oil sand, pit run and limestone

As the research was focused to know the RR of individual material, a number of materials were tested in the test bed. Initially, test bed was set at 0 degrees and filled with sand. Motor speed was kept constant at 60% of maximum speed throughout the experimentation processes. Efforts were made to ensure the sand surface was completely level and lacking any premature compaction. The truck loaded with 210 lbs was run on the sand surface and the pull force recorded. Rut formation was clearly visible on the

sand surface. Seven to ten runs were completed on sand surface and it was made sure that subsequent run followed the same path as pervious run. Initial pull force was seen higher as material was moved by tire to form ruts. Subsequent runs yielded lower forces as truck was running on path made in pervious run and less energy was wasted to move the materials out of the way. These experiments were repeated for 70%, 80%, 90% and 100% of maximum motor speed and pull force was recorded accordingly.

Once the testing on sand was completed, other materials oil sand, pit run and limestone were tested in equivalently by replacing sand in test bed by oil sand, pit run and limestone respectively. Hence, test data for sand, oil sand, pit run and limestone were obtained at different motor speed of 60%, 70%, 80%, 90% and 100%.

5.3 Test on composite material

Further, testing was conducted with composite materials. Composite material consisted 2/3 of oil sand as a base and 1/3 topping of every other materials sand, pit run and limestone in test bed. Experiments were performed equivalently as in the sand test discussed above with the exception of composite materials instead of sand. Composite materials tested are listed below:

    a. Oil sand capped with sand

    b. Oil sand capped with pit run

    c. Oil sand capped with limestone

Hence, data for different composite materials were obtained at different speeds and 0 degree gradient with truck load at 210 lbs. Seven to ten runs were taken at each speed. The above discussion can be grouped into three categories: test performed on empty bed; individual materials; and composite materials. Tests on latter two groups were performed at 0 degree gradient and 210 lbs truck load with varying speed of 60 to 100% with an increment of 10%. By adjusting the gradient, speed and load, tests on the empty bed were subsequently carried out. Tire pressure was kept constant at 6 psi in all tests conducted.

Only sand was tested on all gradients among materials under consideration. Total resistance obtained at each gradient was found to be equal to the sum of grade resistance and RR. Therefore, it can be concluded that RR is a material property and it is same at any gradient. Thus, every other material needs not to be tested at all gradients.

Possible errors while performing experiments may be due to slip in pull rope. Graphical representation of results showed some abrupt high forces and drop off due to this. Surface undulation of material can be neglected as materials were smoothened before experiments. Although, it was tried to make sure that scaled truck follows the same path in subsequent runs, a slight deviation was evident due to difficulty in defining previous path accurately.

Chapter Six: Test Results and Analysis

6.1 Establishing base line equation on a rigid surface

As discussed in Chapter 5, tests were performed with empty bed at variable gradients, speeds and loads. A total of 275 tests were conducted and each yielded similar graphs shown in Figure 6.1 through Figure 6.7. Each test generated more than 450 data points as evident in figures, therefore an enormous range of data were obtained in order to establish a reference equation.

Although graphs for each of 275 tests were drawn for analysis, only seven graphs for rigid surface are presented in Figure 6.1 through Figure 6.7, for convenience. These figures present pull force vs. time plot on empty bed at different gradients and 60% motor speed with 210 lbs truck load. Load cell frequency was set at 10 data points / sec therefore the number of data points can be estimated by 10 multiple of time period shown on X-axis. Pull force values were seen changing rapidly with change of gradient and load. Changing speed had a relatively less significant effect on pull force. Therefore a collection of graphs (Figures 6.1 - 6.7) portraying various gradients was selected for evidence in this section.

Nomenclature on the graph signifies Material, Gradient, % of maximum motor speed and Load i.e. Sand_2.8%_70%_210 graph heading represents the test on sand at 2.8% gradient, 70% of motor speed and 210 lbs load. Maximum speed of motor was considered 100 %. This same nomenclature will be followed for the duration of the

section. Pull force obtained for a rigid surface at 0% gradient, 60% of motor speed at 210

lbs truck load is shown in Figures 6.1 through 6.7:
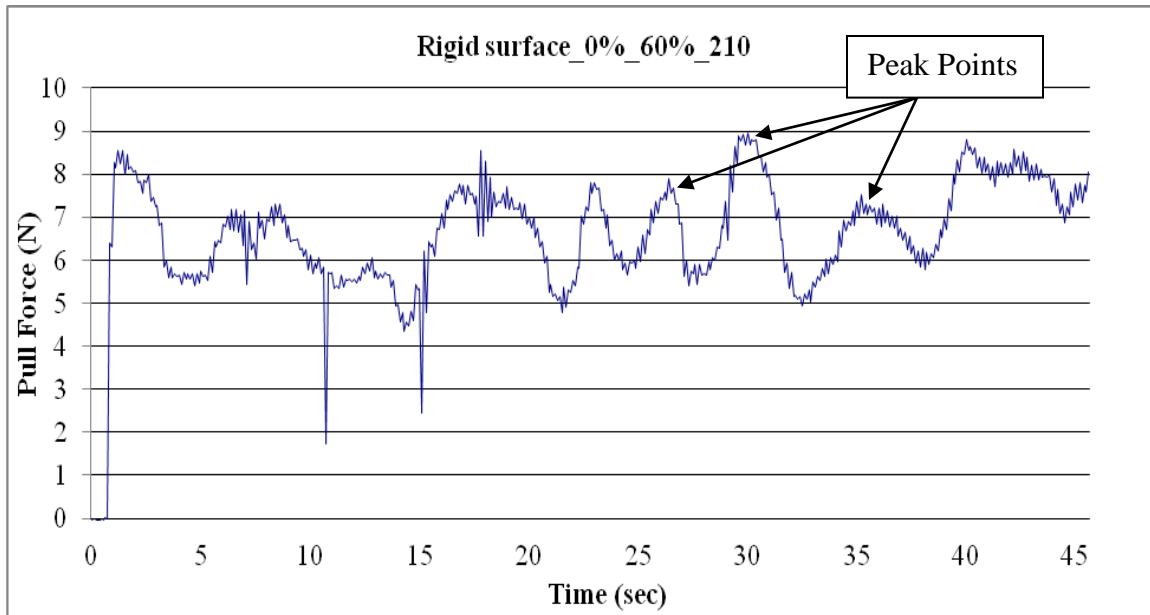
Figure 6.1: Pull force vs. time at 0 % gradient, 60 % speed and 210 lbs load

As three tests were performed under these conditions, graphical representation of all three

combined are shown below (Figure 6.2):
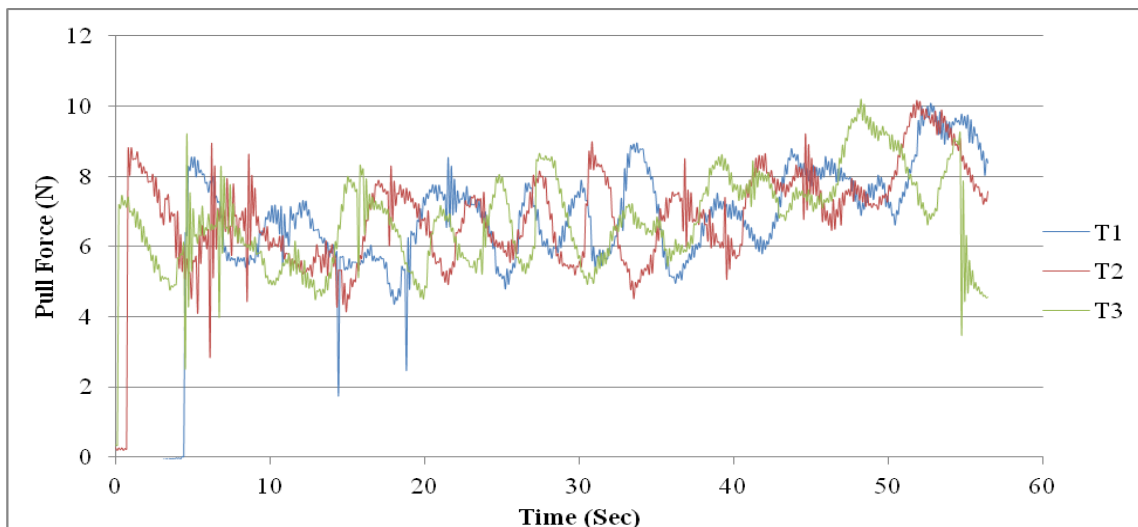
Figure 6.2: Pull force vs. time on a rigid surface at 0% gradient, 60 % speed and 210

lbs load, 3 test runs T1, T2 and T3
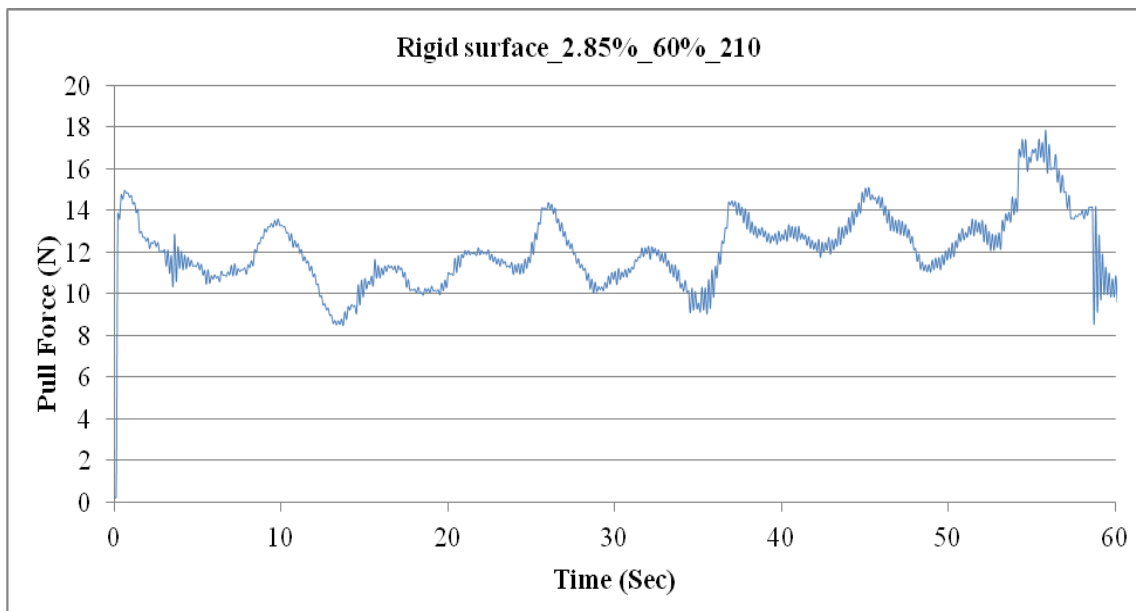
Figure 6.3: Pull forces vs. time graph on a rigid surface at 2.85% gradient, 60% speed with 210 lbs truck load
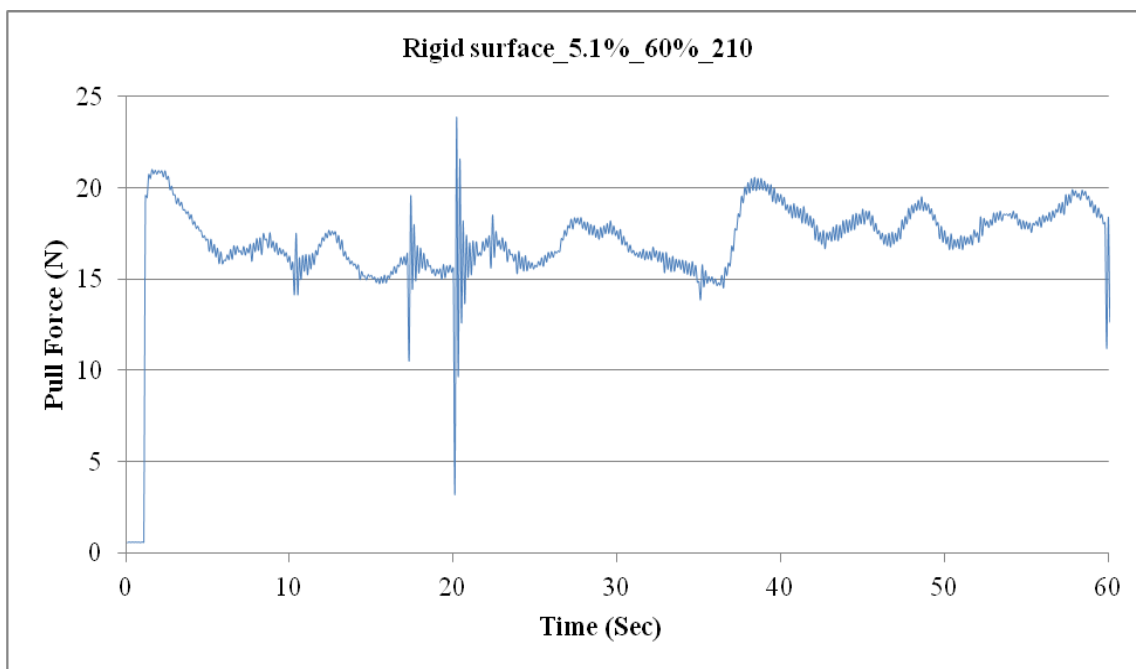
Figure 6.4: Pull forces vs. time on a rigid surface at 5.1% gradient, 60% speed with 210 lbs truck load
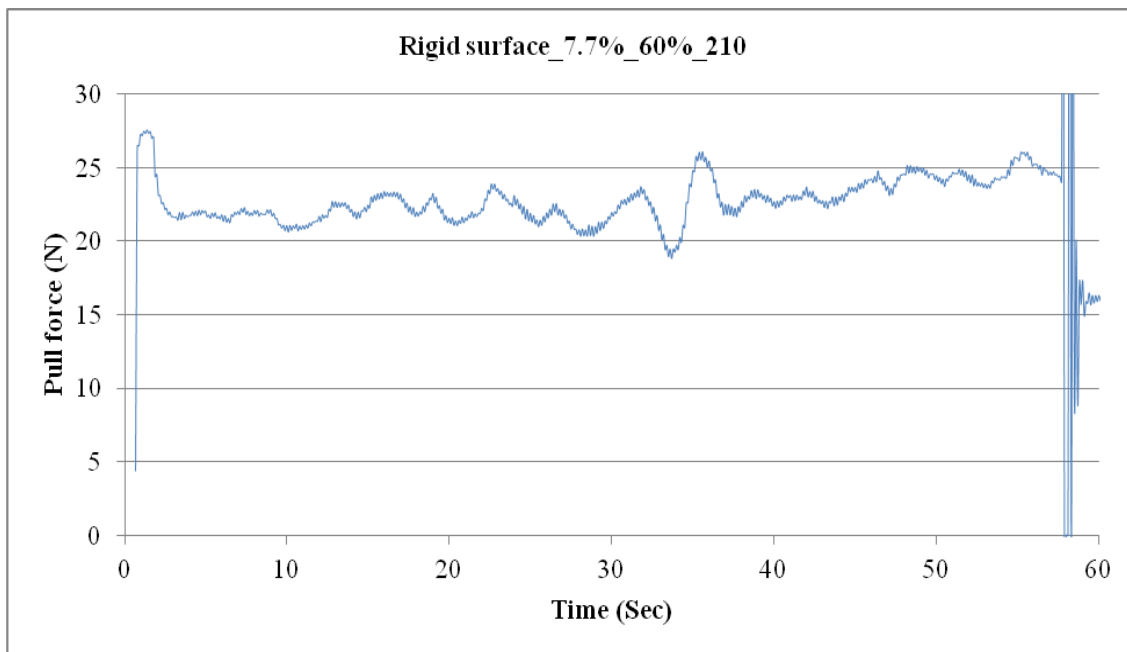
Figure 6.5: Pull forces vs. time graph on a rigid surface at 7.7% gradient, 60% speed with 210 lbs truck load
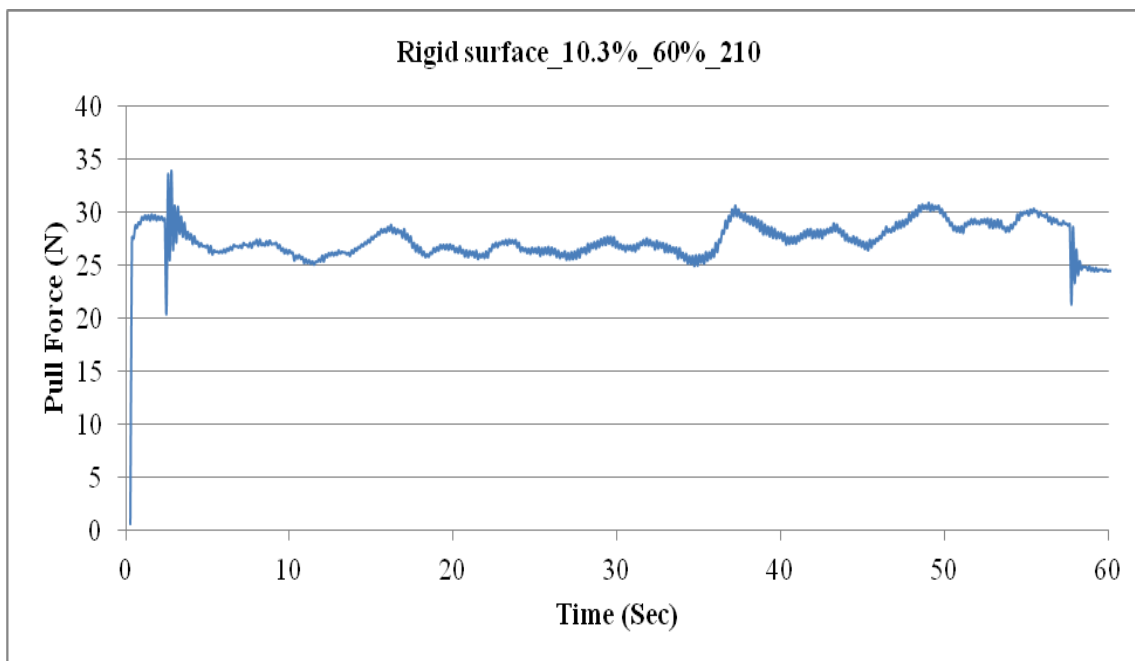
Figure 6.6: Pull forces vs. time graph on a rigid surface at 10.3% gradient, 60% speed with 210 lbs truck load
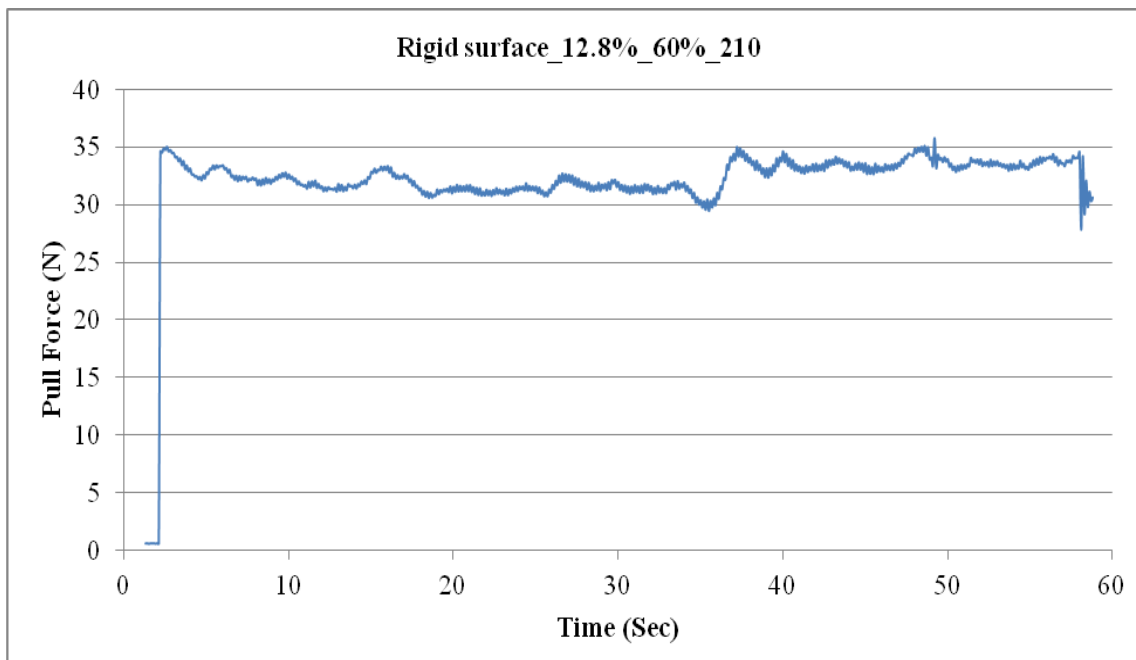
Figure 6.7: Pull forces vs. time graph on a rigid surface at 12.8% gradient, 60% speed with 210 lbs truck load

It can be observed from above figures that several peaks occurred in each plot, which is a representation of maximum force required to overcome resistance. Peak points (maximum forces) on each plot were collected in Table 6.1 through Table 6.6. The first row on each table exhibits the experiments at different speeds, while T1, T2 and T3 displayed in the second rows are the first, second and third tests performed at a particular speed. Maximum values presented in tables are in units of Newton.

	60%			70%			80%			90%			100%			AVERAGE
	T1	T2	T3	T1	T2	T3	T1	T2	T3	T1	T2	T3	T1	T2	T3	
	7.2	7.1	6.7	6.5	7.6	7.8	5.8	6.8	6.8	6.4	6.2	6.7	5.2	7.0	6.0	
	7.3	7.0	6.6	6.1	6.2	6.0	6.4	6.6	6.5	6.4	6.4	7.6	8.6	7.1	7.2	
	7.8	6.1	6.2	8.1	7.7	7.7	7.7	7.2	7.7	7.7	7.6	7.4	9.3	7.3	7.6	
	7.7	7.9	8.0	7.3	7.4	6.5	7.3	7.8	7.2	7.0	7.3	7.5	8.7	8.4	7.6	
	7.8	7.7	7.2	7.0	7.0	7.7	8.0	7.5	7.8	7.4	6.9	8.5	8.5	8.6	8.3	
	7.9	7.5	8.1	8.2	8.7	8.6	8.0	8.2	7.4	8.2	8.1	8.4		8.3		
	9.0	8.2	8.7	7.8	8.1	8.0	7.8		8.0	8.4	7.8					
	7.5	8.4	7.2	7.2	9.0	8.9	8.5		8.4		8.2					
	8.8	7.5	8.6	7.7	7.8	7.8										
	8.5	8.2	8.1	7.7												
	8.0	8.3	7.7	7.7												
				7.9												
AVG	8.0	7.7	7.6	7.4	7.7	7.7	7.4	7.4	7.5	7.3	7.3	7.7	8.1	7.8	7.3	7.6

Table 6.1: Maximum force (peak points) values at 0% gradient with 210 lbs load

	60%			70%			80%			90%			100%			AVERAGE
	T1	T2	T3	T1	T2	T3	T1	T2	T3	T1	T2	T3	T1	T2	T3	
	13.6	13.5	13.6	13.5	13.6	13.6	13.7	13.8	13.9	14.0	14.1	14.1	14.2	14.3	14.4	
	11.4	11.4	11.8	13.5	13.6	13.7	13.7	13.8	13.9	14.0	14.1	14.1	14.2	14.3	14.4	
	12.2	12.2	12.6	13.5	13.6	13.7	13.7	13.8	13.9	14.0	14.1	14.1	14.2	14.3	14.4	
	14.4	14.5	14.7	13.5	13.6	13.7	13.8	13.8	13.9	14.0	14.1	14.2	14.2	14.3	14.4	
	12.3	12.4	12.4	13.5	13.6	13.7	13.8	13.8	13.9	14.0	14.1	14.2	14.2	14.3	14.4	
	14.5	14.6	13.4	13.5	13.6	13.7	13.8	13.8	13.9	14.0	14.1	14.2	14.3	14.3	14.4	
	15.1	15.7	13.5	13.5	13.6	13.7	13.8	13.9	13.9	14.0	14.1	14.2	14.3	14.3		
	13.6	13.8	13.5	13.5	13.6	13.7	13.8	13.9	13.9	14.0	14.1	14.2	14.3	14.3		
				13.5	13.6	13.7	13.8	13.9	13.9	14.0	14.1	14.2		14.3		
				13.6	13.6	13.7	13.8	13.9	14.0	14.0	14.1	14.2		14.3		
						13.7	13.8	13.9	14.0	14.1				14.3		
AVG	13.4	13.5	13.2	13.5	13.6	13.7	13.8	13.8	13.9	14.0	14.1	14.2	14.2	14.3	14.4	13.8

Table 6.2: Maximum force (peak points) values at 2.85% gradient with 210 lbs load

	60%			70%			80%			90%			100%			AVERAGE
	T1	T2	T3	T1	T2	T3	T1	T2	T3	T1	T2	T3	T1	T2	T3	
	17.5	17.2	16.9	17.9	17.5	17.2	18.3	18.3	18.2	18.0	17.1	17.7	18.1	18.1	17.8	
	17.6	17.5	17.5	17.6	17.7	17.7	17.1	17.8	17.7	17.2	17.9	17.0	17.4	17.5	17.1	
	16.8	16.7	16.7	16.7	16.5	16.5	18.2	16.8	16.7	17.2	16.9	17.8	18.0	17.3	17.4	
	17.6	17.1	17.1	18.4	16.8	17.3	18.9	18.2	17.8	18.4	17.5	18.6	18.4	18.5	18.3	
	18.3	18.3	18.4	21.4	14.6	18.4	21.7	18.9	18.6	17.8	18.2	17.8	18.0	18.1	18.1	
	18.2	20.2	20.1	18.9	16.8	20.5	19.0	21.4	21.3	20.2	18.0	19.9	20.3	20.3	20.0	
	20.5	18.5	18.5	19.3	19.0	18.6	19.6	19.9	19.4	18.5	20.0	18.4	20.0	18.8	18.6	
	18.8	19.3	19.2	19.1	19.4	19.4	19.5	19.6	19.0	19.9	19.6	19.7	19.3	20.0	19.9	
	19.5	18.7	18.7		19.2	18.7	19.5			19.4	19.6	19.5		19.7		
	18.6															
AVG	18.3	18.2	18.1	18.6	17.5	18.3	19.0	18.9	18.6	18.5	18.3	18.5	18.7	18.7	18.4	18.4

Table 6.3: Maximum force (peak points) values at 5.1% gradient with 210 lbs load

	60%			70%			80%			90%			100%			AVERAGE
	T1	T2	T3	T1	T2	T3	T1	T2	T3	T1	T2	T3	T1	T2	T3	
	22.1	22.0	22.2	22.7	21.8	22.2	22.4	22.2	22.2	22.4	23.0	22.2	23.8	22.2	22.1	
	22.3	21.9	22.1	22.2	21.9	22.0	21.9	21.9	21.9	22.0	22.3	22.1	23.4	22.1	22.5	
	22.7	22.5	21.9	22.4	22.1	22.4	22.3	22.4	22.3	22.3	22.4	22.9	23.8	22.9	22.9	
	23.3	22.1	22.2	23.4	22.9	22.6	23.0	22.9	23.2	23.3	22.9	23.2	23.3	22.4	22.3	
	23.3	22.2	22.5	22.4	22.5	22.1	22.3	22.0	22.3	22.4	22.2	22.5	22.9	23.9	23.6	
	23.9	22.9	22.2	23.5	23.1	22.1	23.6	23.3	23.2	23.7	23.5	23.7	24.1	24.1	24.2	
	22.6	22.0	23.1	24.0	22.0	23.2	21.6	23.9	23.9	21.6	24.3	24.0	24.7	23.7	23.5	
	23.7	23.7	21.8	25.1	24.0	22.6	24.0	23.6	23.5	24.2	23.5	23.5	23.7	23.4	24.5	
	26.1	22.8	23.7	23.4	24.6	23.3	23.7	23.2	23.3	25.0	23.7	23.4	24.8		25.4	
	23.5	23.2	23.1	23.3	23.2		23.4	24.5		23.8					24.8	
	23.7	23.2	23.4	24.7	23.3					23.1						
	24.8	23.7	23.7	25.3												
	25.2		24.1	24.9												
	24.9															
AVG	23.7	22.7	22.8	23.6	22.8	22.5	22.8	23.0	22.8	23.1	23.1	23.0	23.8	23.1	23.6	23.1

Table 6.4: Maximum force (peak points) values at 7.7% gradient with 210 lbs load

	60%			70%			80%			90%			100%			AVERAGE
	T1	T2	T3	T1	T2	T3	T1	T2	T3	T1	T2	T3	T1	T2	T3	
	27.5	27.5	27.4	27.6	27.5	27.8	27.7	27.4	27.9	28.3	28.3	27.9	28.0	27.7	28.8	
	26.3	26.3	28.7	26.6	26.5	28.9	29.1	29.0	29.2	29.4	29.7	29.1	29.7	29.4	29.3	
	28.9	28.4	27.0	28.9	29.1	26.9	27.1	27.1	26.9	27.9	27.4	27.1	27.6	27.2	27.1	
	27.0	27.1	27.5	27.1	27.4	27.6	27.8	27.7	27.8	27.5	28.7	27.9	28.5	27.6	27.6	
	27.5	27.6	27.7	27.8	27.7	27.5	27.6	27.6	27.7	27.4	27.9	27.7	27.7	28.0	27.5	
	27.7	27.7	27.2	27.7	27.5	27.2	27.3	27.6	27.5	29.3	27.5	27.3	27.6	32.1	27.4	
	27.6	27.4	30.6	27.4	27.1	30.7	29.2	28.6	28.9		32.8	31.8	32.8	28.8	31.4	
	30.7	30.7	28.9	26.9	30.8	29.0	31.0	29.0	31.0		29.6	28.9	28.9	31.3	28.8	
	28.9	29.0	30.8	30.9	28.4	30.9	29.3	31.5	29.7		31.3	31.1	31.3	29.6	31.4	
	30.8	30.7	29.5	28.8	28.9	29.7		29.5			29.6	29.5	29.4		29.4	
	29.4	29.5		29.5	29.6											
AVG	28.4	28.4	28.5	28.1	28.2	28.6	28.4	28.5	28.5	28.3	29.3	28.8	29.2	29.1	28.9	28.6

Table 6.5: Maximum force (peak points) values at 10.3% gradient with 210 lbs load

	60%			70%			80%			90%			100%			AVERAGE
	T1	T2	T3	T1	T2	T3	T1	T2	T3	T1	T2	T3	T1	T2	T3	
	33.5	33.3	33.6	33.7	33.7	33.7	34.7	33.6	33.7	33.7	32.7	32.7	33.0	32.9	33.8	
	32.8	32.9	32.9	33.1	33.0	33.2	33.4	33.0	32.8	32.6	33.4	33.3	33.7	32.0	31.9	
	33.4	33.5	32.3	33.5	33.5	33.5	32.6	33.6	33.2	33.1	31.7	31.8	31.5	32.5	32.8	
	31.7	31.7	33.4	31.9	31.9	31.9	34.1	31.9	31.9	31.6	32.3	31.9	32.8	32.8	32.5	
	31.6	31.9	32.1	31.8	32.9	31.9	32.4	32.2	32.0	32.1	32.8	32.6	32.4	32.6	31.8	
	32.8	32.7	32.0	33.0	32.3	32.2	32.6	32.6	32.7	32.6	31.9	32.4	32.8	32.1	34.6	
	32.2	32.2	32.6	32.0	32.2	32.6	32.6	32.4	32.5	32.0	31.8	32.1	35.0	34.9	34.0	
	31.8	31.9	31.7	34.2	34.2	34.3	32.7	31.7	32.3	31.6	34.0	34.1	33.9	34.4	34.0	
	32.1	32.1	31.1	33.8	34.3	34.0	34.6	34.1	31.7	31.8	34.0	33.9	33.7	33.8	35.6	
	35.1	34.8	31.6	34.8	35.2	35.1	34.5	34.0	35.1	34.4	34.2	34.0	35.7	33.7		
	34.7	34.7	34.9	35.2	34.2		35.5	35.4	34.1	33.8		35.4	34.0	35.2		
	34.2	34.2	34.8				34.4	34.5	33.9	34.1		34.0		35.5		
	35.1	35.0	34.0					34.3	33.6	35.4						
	34.0	33.9	35.2						35.5							
	34.2							34.2								
AVG	33.3	33.2	33.0	33.4	33.4	33.2	33.7	33.3	33.3	33.0	32.9	33.2	33.5	33.5	33.4	33.3

Table 6.6: Maximum force (peak points) values at 12.8% gradient with 210 lbs load

All data points shown in Tables 6.1 through 6.6 were plotted against % gradient as shown below:
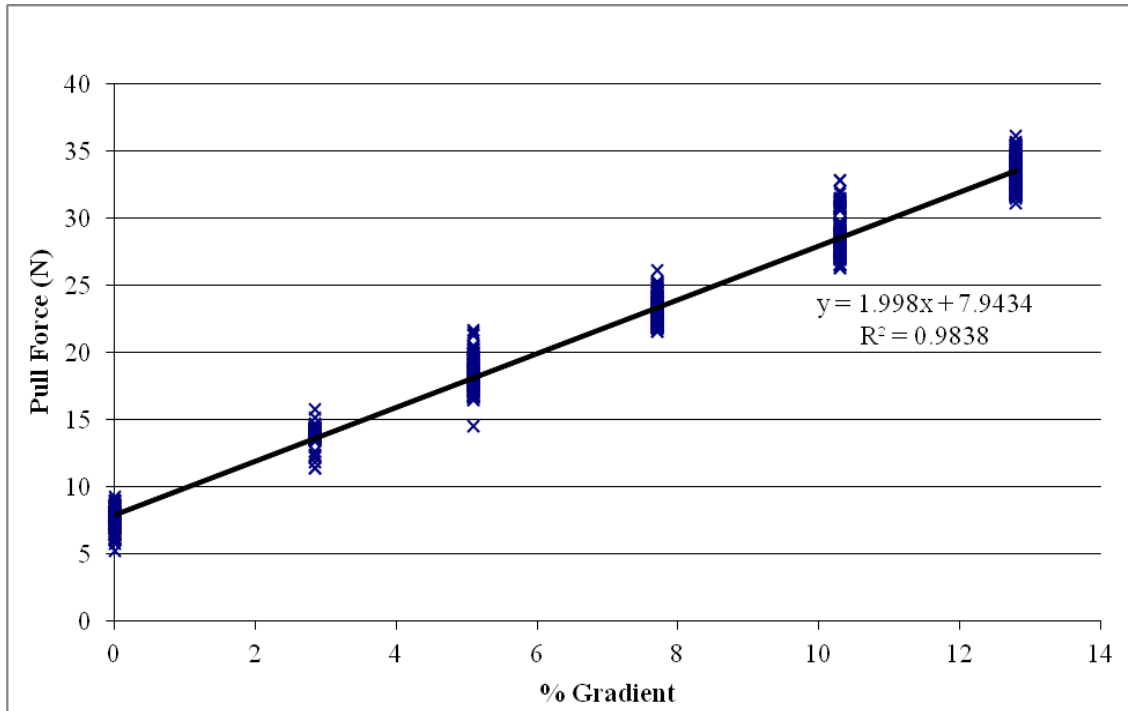
Figure 6.8: Pull force vs. % gradient on flat surface

Therefore the reference equation as taken from the above graph is:

$$Y = 2 X + 8$$

$$\text{Pull force} = 2 \ (\% \ \text{Gradient}) + 8 \qquad\qquad 6.1$$

In an ideal case, if there is no resistance to motion, the reference line should pass through origin and it can be thus concluded from the above reference that the Y-intercept is a measure of the RR which can be calculated as follows:

$$\% \ RR = (\text{Pull force} - 8) / \ 2 \qquad\qquad 6.2$$

6.2 Test results on individual materials and analysis

6.2.1 Test results on sand and analysis

Pull force obtained from the scaled truck run on a test bed filled with sand was plotted

against time. Figure 6.9 and Figure 6.12 show pull force vs. time plot at 70 % and 80 %

speed respectively. Each consecutive line represents the number of runs completed at the

respective speeds. Results were also obtained for 90 % and 100 % speeds.

It can be observed from the plot that pull force is increasing consistently along the path in

each run. It reveals the fragile nature of the sand. Initial runs required a large force to

overcome due to rut formation, which was clearly visible during the experiments. Sand

seems to have compacted after 3 to 4 runs and consecutive runs converged to a common

range of pull force. Pull force data in Figure 6.9 and Figure 6.12 were plotted against the

number of runs and presented in Figure 6.10 and Figure 6.13. As each run consisted of

more than 450 data points, a cluster of data contributes to a solid line representing a range

of pull force for each of the runs. The first run as depicted in Figure 6.9 had a pull force

range of 60 N to 84 N while the last run exhibited a pull force range of 25 N to 45 N.

Sand was tested on different gradients. Total resistance was found to be equal to the sum

of grade resistance and RR.
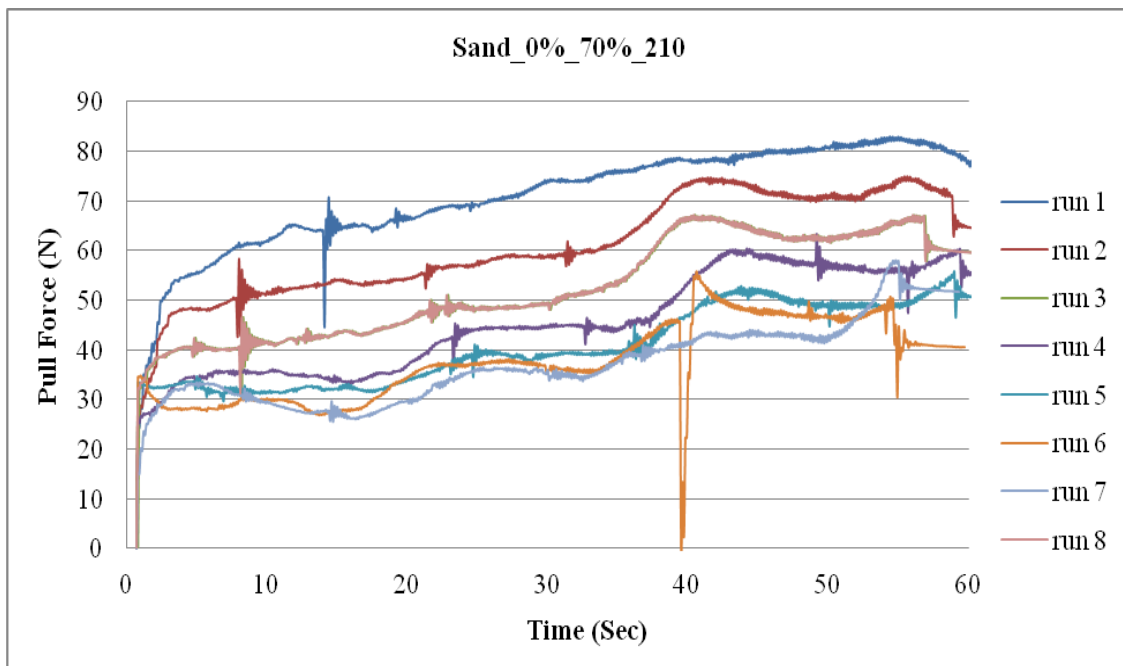
Figure 6.9: Pull force vs. time at 0% gradient, 70% speed on sand with 210 lbs load
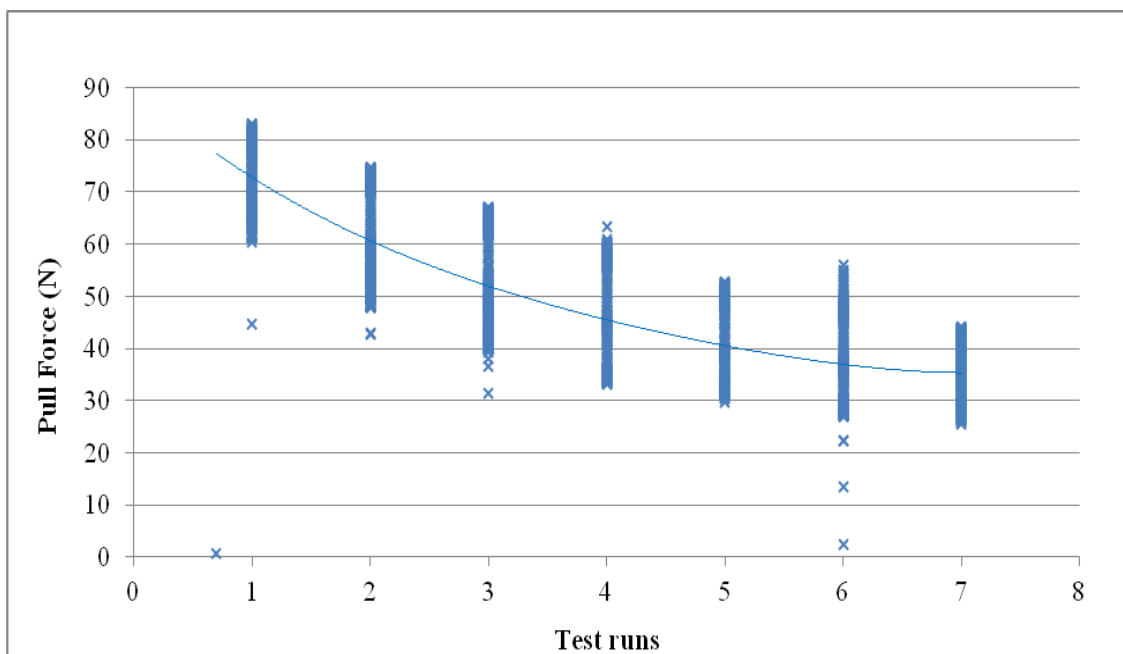
Figure 6.10: Pull force vs. test runs at 0% gradient, 70% speed on sand with 210 lbs load

Base line equation 6.2 is applied to Figure 6.10 and Figure 6.13 to obtain the range of % RR. Nature of plot for pull force vs. test runs and % RR vs. test runs were similar as the linear equation was applied to derive % RR. The first run as depicted in Figure 6.11 shows a very high RR range of 27 % to 38% while subsequent runs displayed decreasing RR due to compaction of sand. The concluding runs as displayed in Figure 6.11 have a common range of RR from 9% until the 15 % measure.
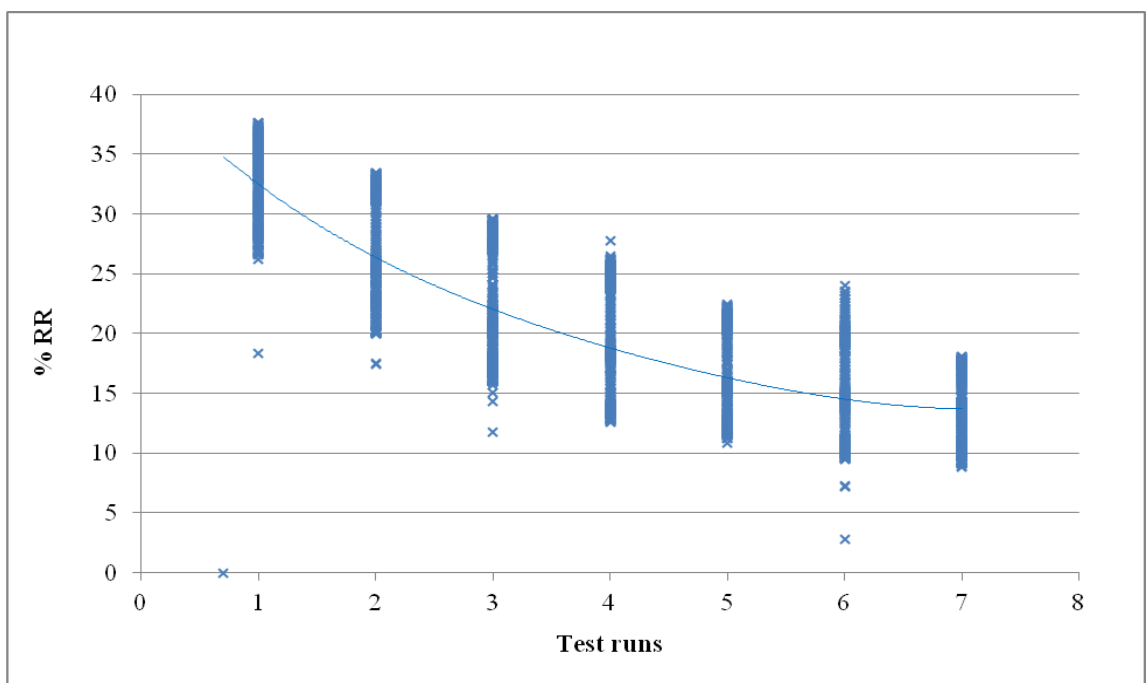
Figure 6.11: % RR vs. Test runs at 0% gradient, 70% speed on sand with 210 lbs load

Pull force vs. time and test runs plots in both Figure 6.9 and Figure 6.10 show a range of pull force from 56 N to 78 N for first run, while later runs have 23 N to 35 N. Though pull force results are comparable at both of the speeds, pull force values are slightly less at a higher speed. Further, the results portray a smaller % rolling resistace value at higher speeds as shown in Figure 6.15.
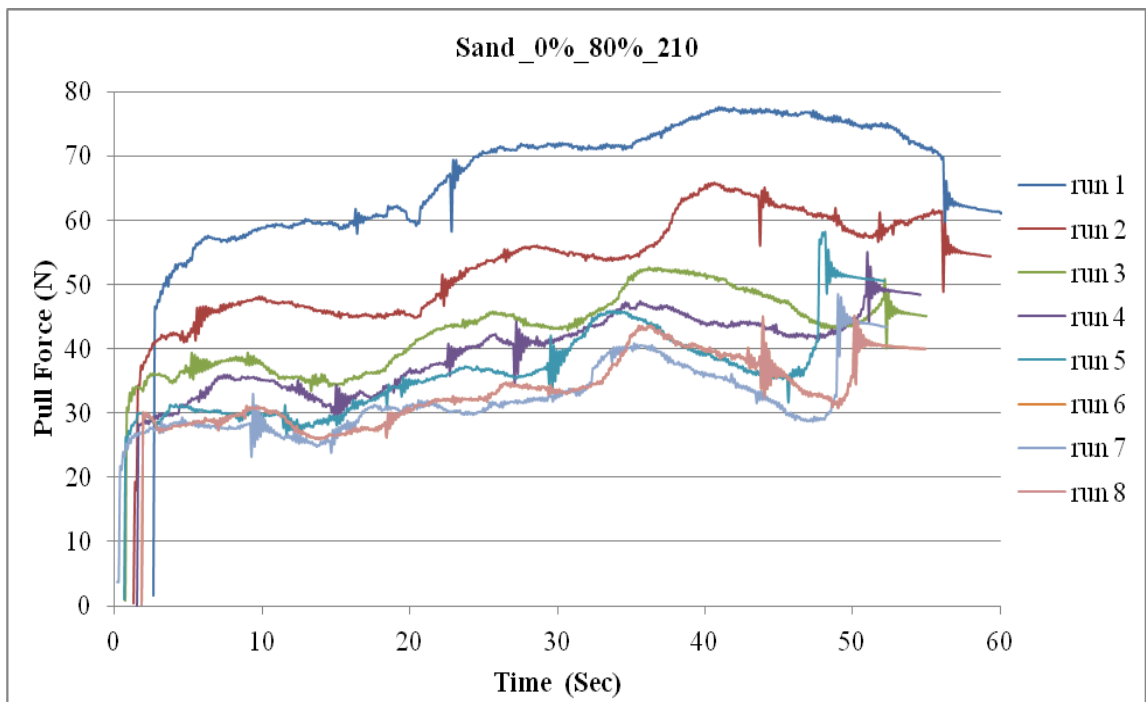
Figure 6.12: Pull force vs. time at 0% gradient, 80% speed on sand with 210 lbs load
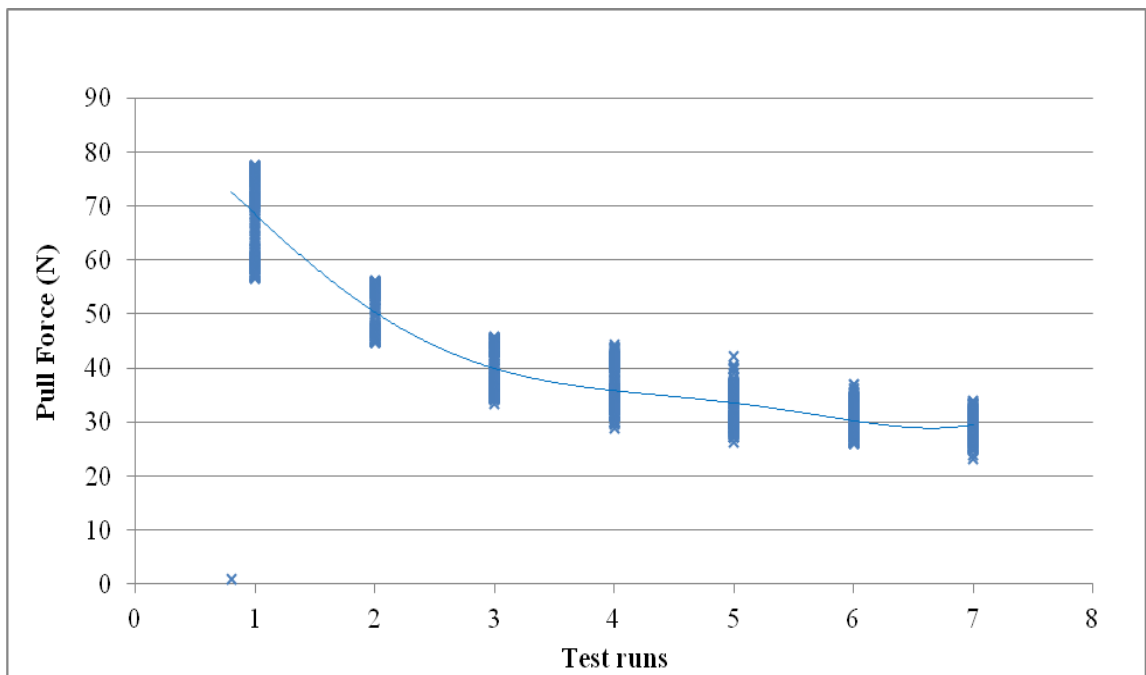
Figure 6.13: Pull force vs. test runs at 0% gradient, 80% speed on sand with 210 lbs load
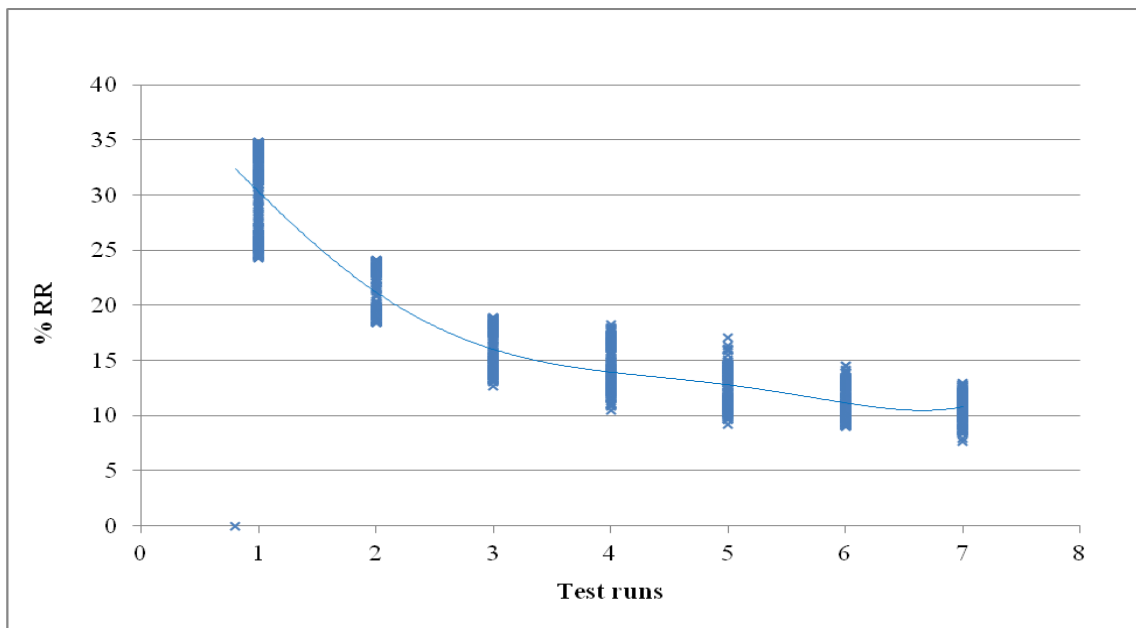
Figure 6.14: % RR vs. test runs at 0% gradient, 80% speed on sand with 210 lbs load

As evident in preceding figures, the seventh to tenth runs were completed at each speed. The average of each run was calculated for all speeds and plotted against test runs as shown in Figure 6.15 below:
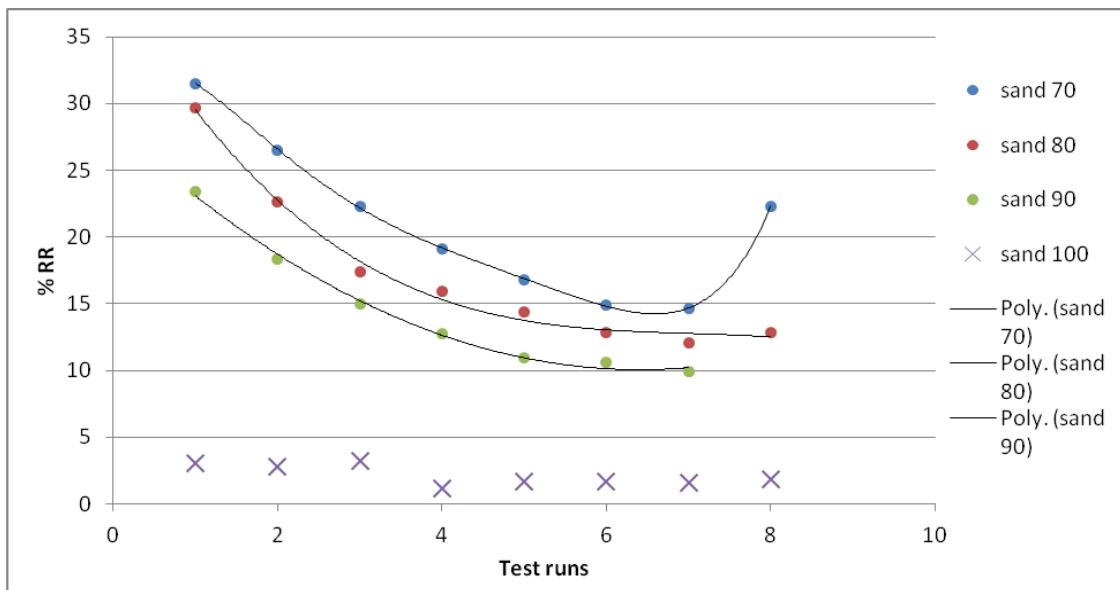
Figure 6.15: % RR vs. test runs at different speeds on sand

It can be observed from Figure 6.15 that % RR was decreasing with increasing speed. A 10% speed increment from 70 % to 80 % resulted a 2.5% improvement in RR from 15 % down to 12.5 % . Data obtained at 100% speed (Figure 6.15) are unexpectedly lower and seems to lack validity.   RR for sand when considering all speeds ranges from 10 % to 15% after a pre-compaction level is achieved.

Furthermore, data points at all speeds in Figure 6.15 was combined and a single curve was obtained to represent % RR of sand as shown in the comparison section, Figure 6.47. This was achieved by calculating the average of all data points at each run.

6.2.2 Test results on oil sand and analysis

Pull force results from the truck run on a test bed filled with oil sand are shown in Figure 6.16 and Figure 6.19. The initial two runs have higher pull forces while consecutive runs quickly converged to a common range of 12 N to 23 N as seen in Figure 6.17 and Figure 6.20. RR was calculated by applying equation 6.2 in Figure 6.17 and Figure 6.20 and plotted in Figure 6.18 and Figure 6.21. Both figures show a RR range of 2.5% to 8 %. Results at speed 70 % and 90 % were shown for comparative purposes. Results are found to be nearly equivalent at both speeds as observed in Figure 6.18 and Figure 6.21.

To have the better comparison at all speeds, average values for each run at all speeds were plotted against test runs in Figure 6.22. Average % RR for oil sand could be considered 4% to 7 % as obtained from Figure 6.22. It can be observed that variation of speed did not cause a noticeable change in % RR but a decrease in RR can be observed

with increasing speed. The related theory as discussed in section 2.8 supports the

observations in Figure 6.22. Also, number of runs required to compact oil sand was less

than sand and the difference between rolling resistances of consecutive runs are higher in

sand as compared to oil sand. The range of RR for sand is much higher than oil sand,

which proves the rut formation and fragile nature of sand.

Additionally, a single curve was obtained representing oil sand by combining data points

at all speeds and shown in comparison section, Figure 6.47.
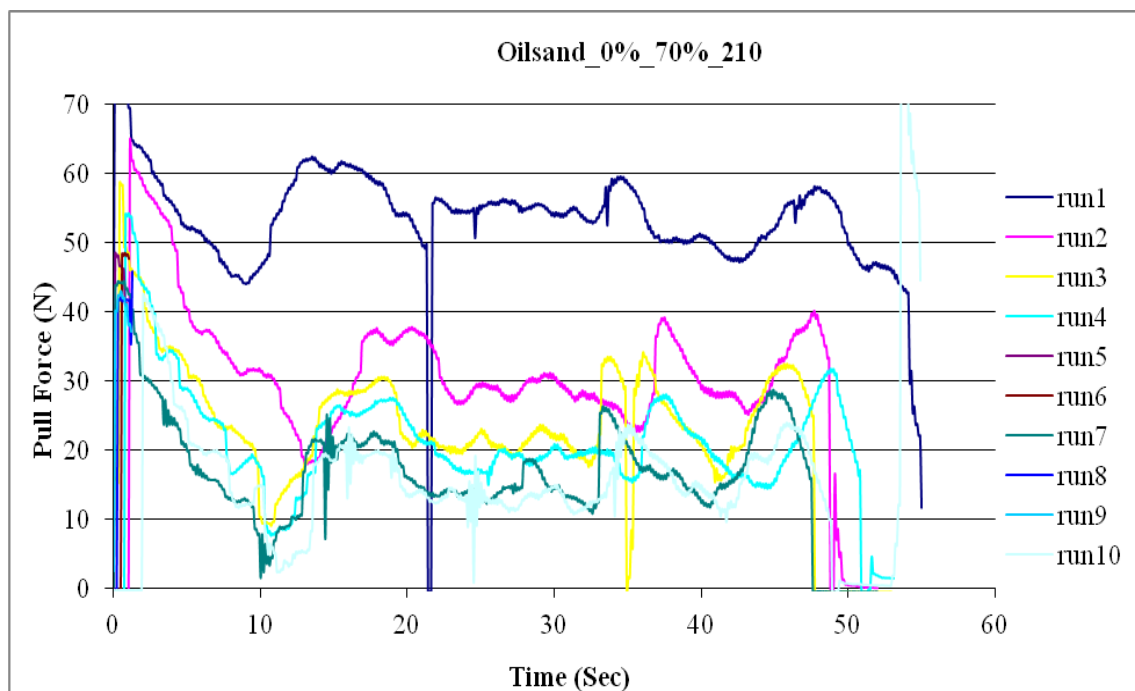
Figure 6.16: Pull force vs. time at 0% gradient, 70% speed on oil sand with 210 lbs load
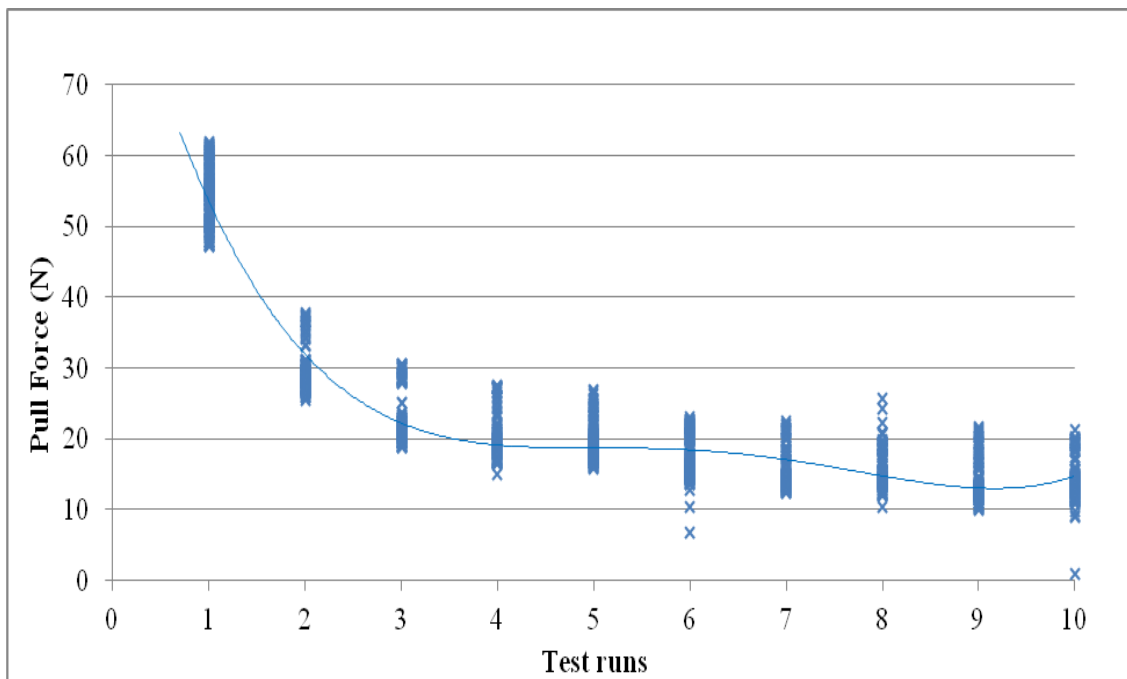
Figure 6.17: Pull force vs. test runs at 0% gradient, 70% speed on oil sand with 210 lbs load
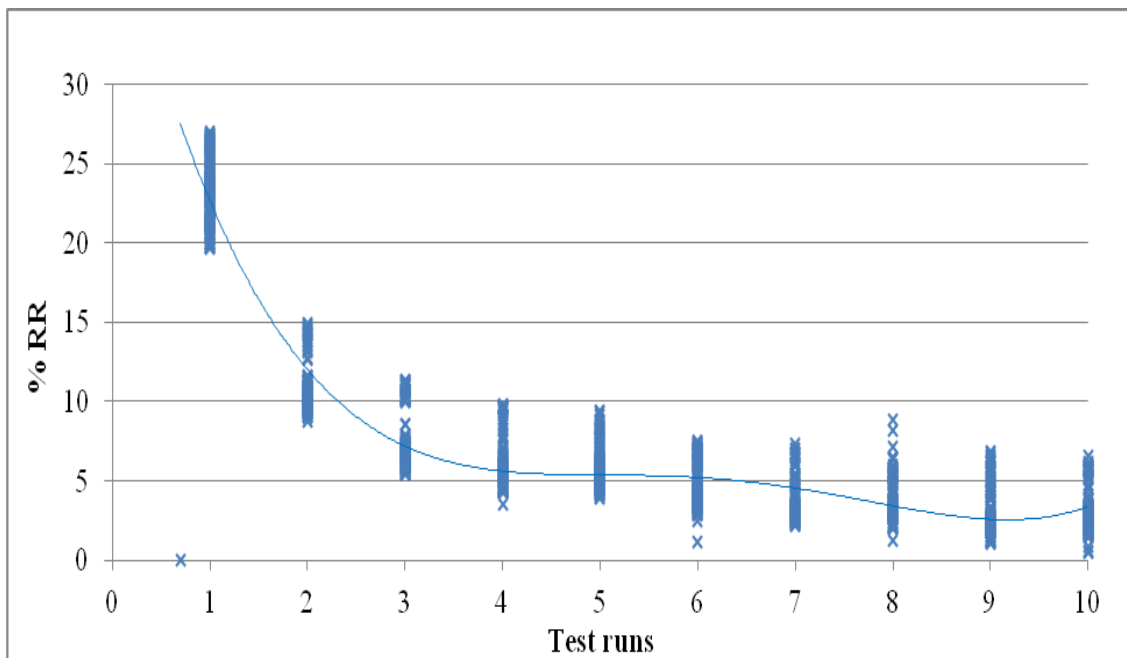
Figure 6.18: %RR vs. test runs at 0% gradient, 70% speed on oil sand with 210 lbs load
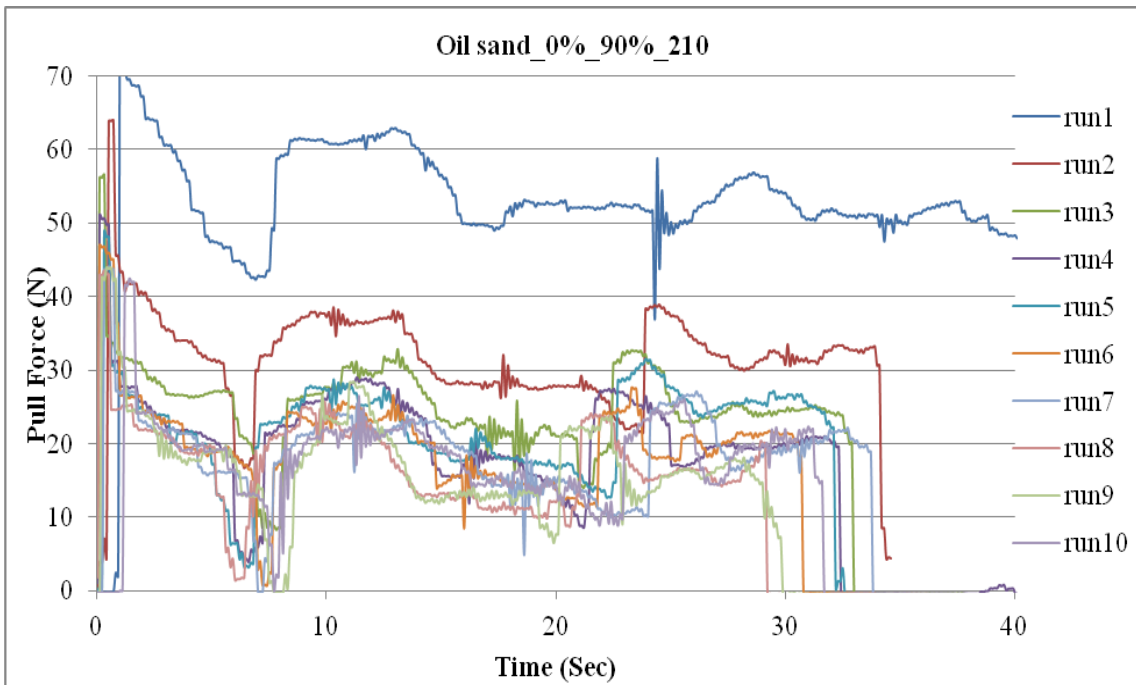
Figure 6.19: Pull force vs. time at 0% gradient, 90% speed on oil sand with 210 lbs load
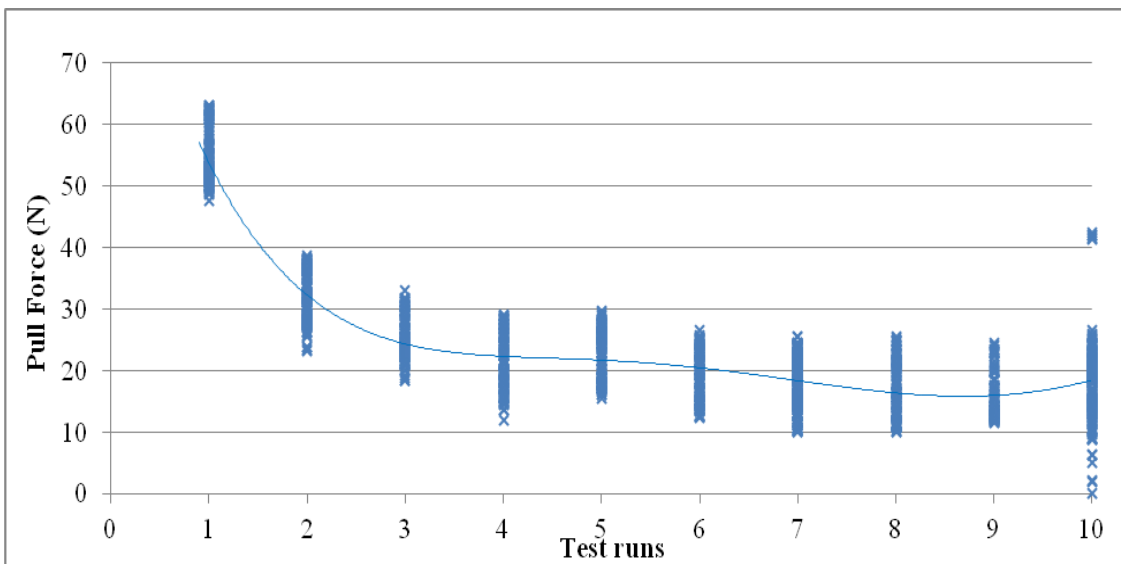
Figure 6.20: Pull force vs. test runs at 0% gradient, 90% speed on oil sand with 210 lbs load
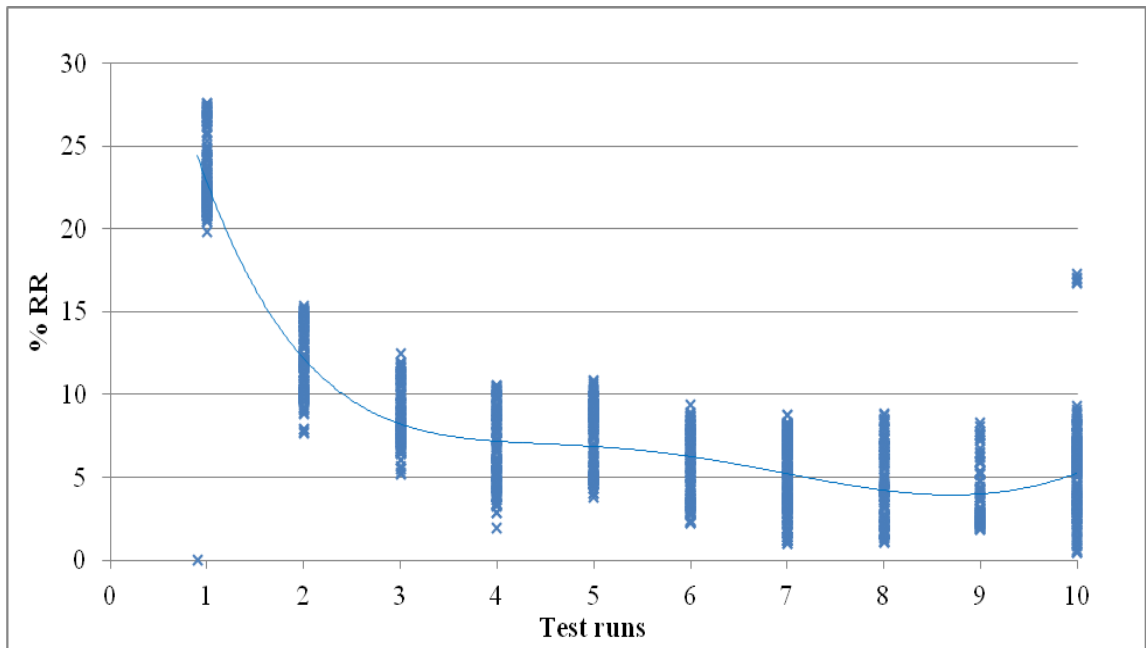
Figure 6.21: % RR vs. test runs at 0% gradient, 90% speed on oil sand with 210 lbs load
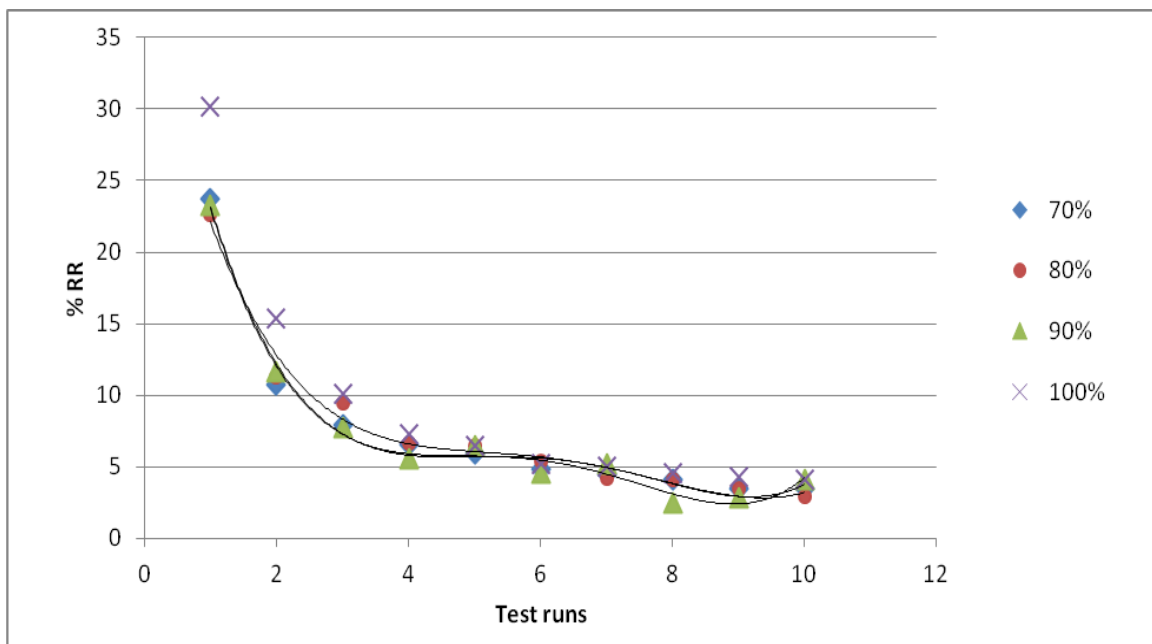
Figure 6.22: % RR vs. test runs at different speeds on oil sand

6.2.3 Test results on pit run and analysis

Pull force obtained from the scaled truck run on a test bed filled with pit run are plotted against time and test runs in Figure 6.23 and Figure 6.26 respectively. Two speeds 70 % and 80 % are considered in this section for comparison purpose. Unlike oil sand and sand, initial runs in pit run have roughly same values in later runs. There was no pre-compaction required and all test runs resulted almost same range of pull force Figure 6.24 & Figure 6.27 and consecutively same range of RR as shown in Figure 6.25 and Figure 6.28. This confirms no rut formation in the pit run material. Pull force and % RR range at 70 % speed were found 13 N to 22 N and 3 % to 7 % respectively (Figure 6.24 and Figure 6.25). These values at 80% speed were 11 N to 20 N and 2 % to 6% respectively (Figure 6.27 and Figure 6.28) which is slightly smaller than values at 70 % speed.

Average value for each run at all speeds is plotted against test runs in Figure 6.29. Range of rolling can be determined as 3% to 5% for pit run from Figure 6.28. RR comparison at different speeds show that a 10% improvement in speed results in a RR reduced from 3.6% to 3.1%, which is not significant considering the large range of rolling resistance in initial and subsequent runs. It is clear from Figure 6.29 that data points are largely scattered which brings the fact that there was a huge variation in particle sizes of pit run sample. Also, it is difficult to determine speed effects of rolling resistance due to scattered data. Further, a single curve for pit run was obtained by combining data points at all speeds and shown in the comparative section as "Pit run."
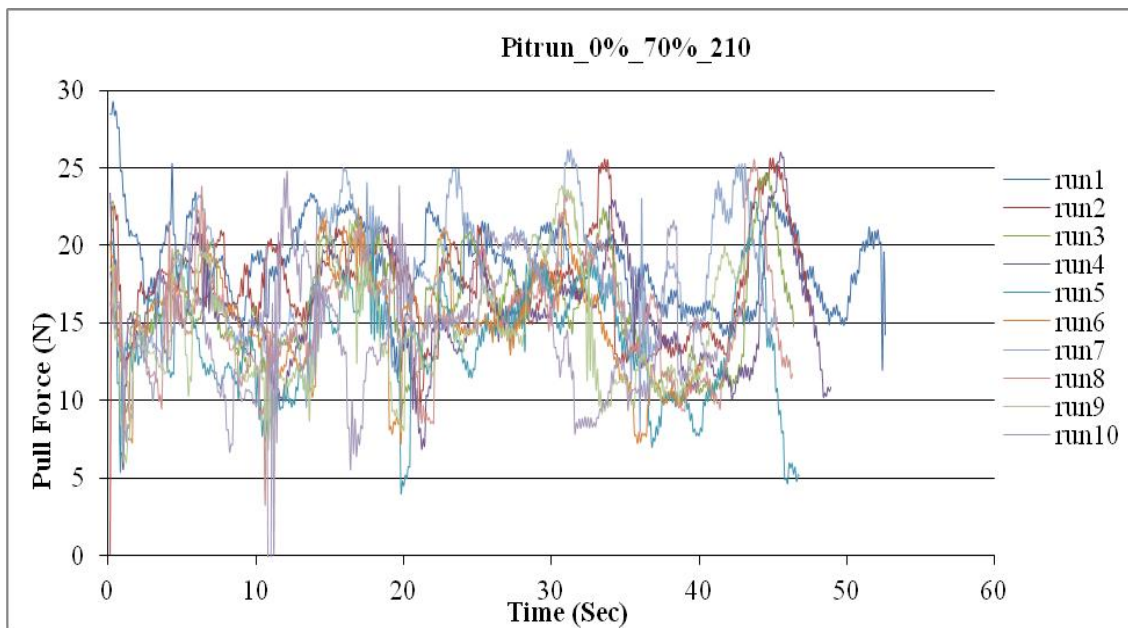
Figure 6.23: Pull force vs. time at 0% gradient, 70% speed on pit run with 210 lbs load
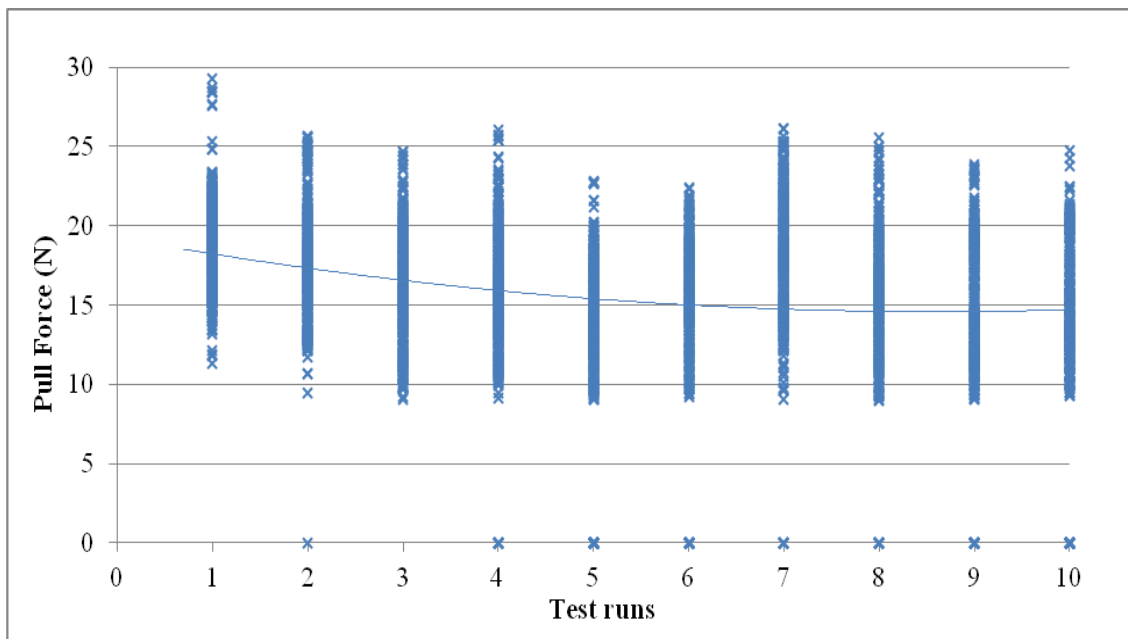
Figure 6.24: Pull force vs. test runs at 0% gradient, 70% speed on pit run with 210 lbs load
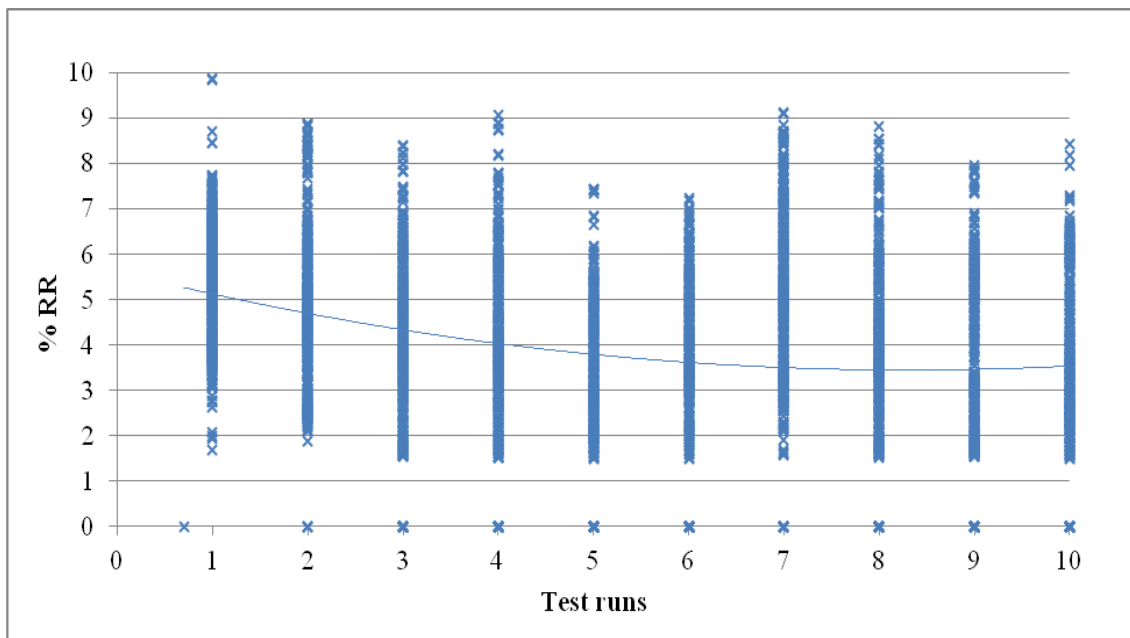
Figure 6.25: % RR vs. test runs at 0% gradient, 70% speed on pit run with 210 lbs load
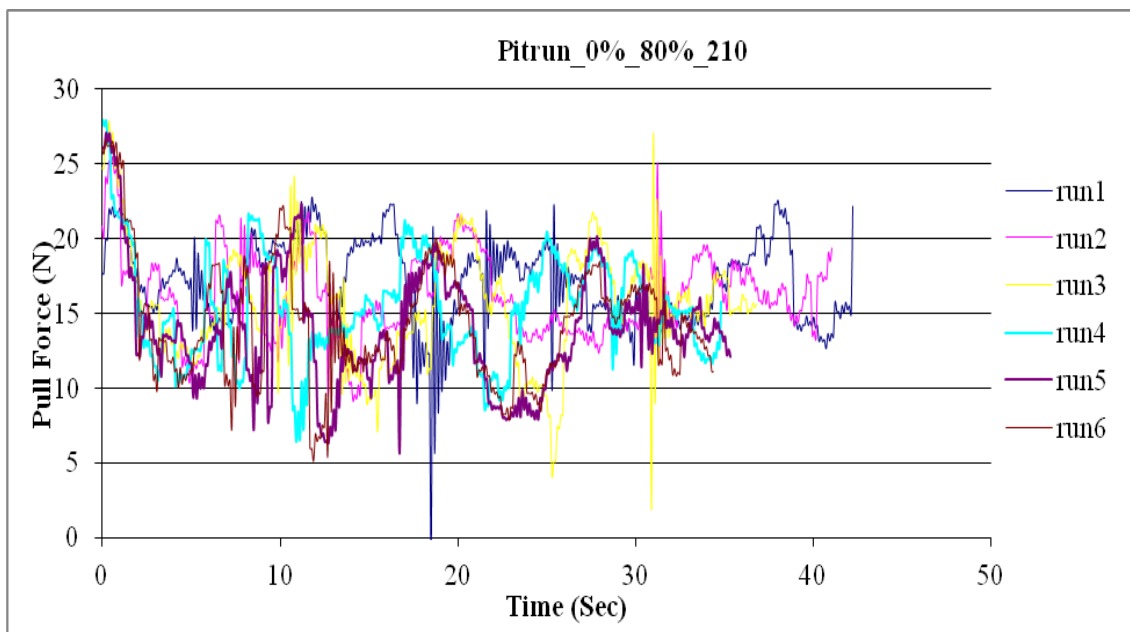
Figure 6.26: Pull force vs. time at 0% gradient, 80% speed on pit run with 210 lbs load
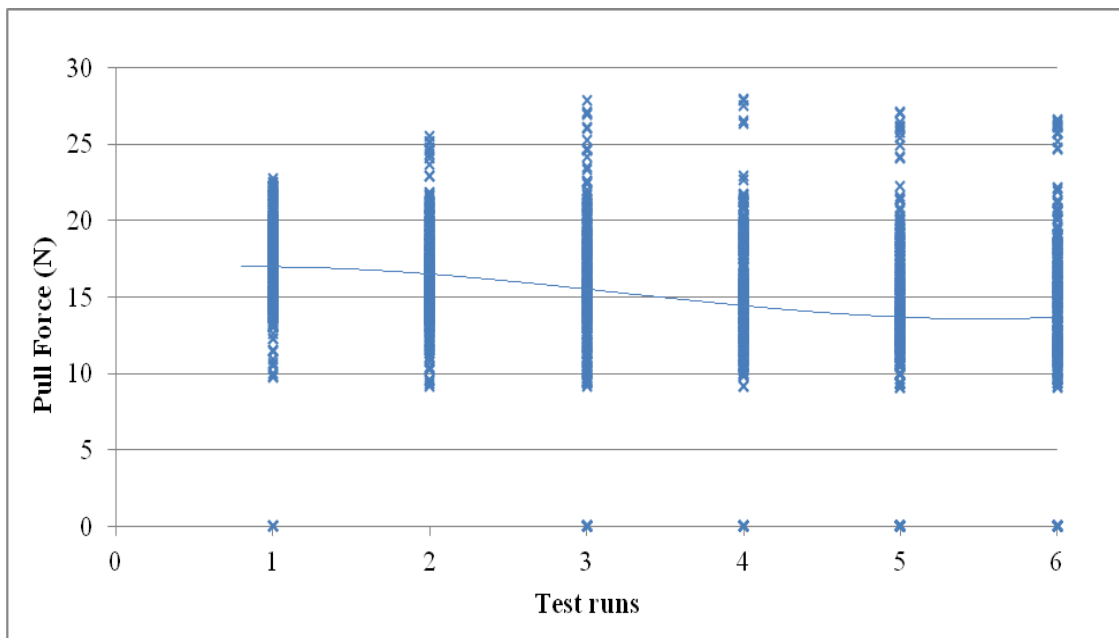
Figure 6.27: Pull force vs. test runs at 0% gradient, 80% speed on pit run with 210 lbs load
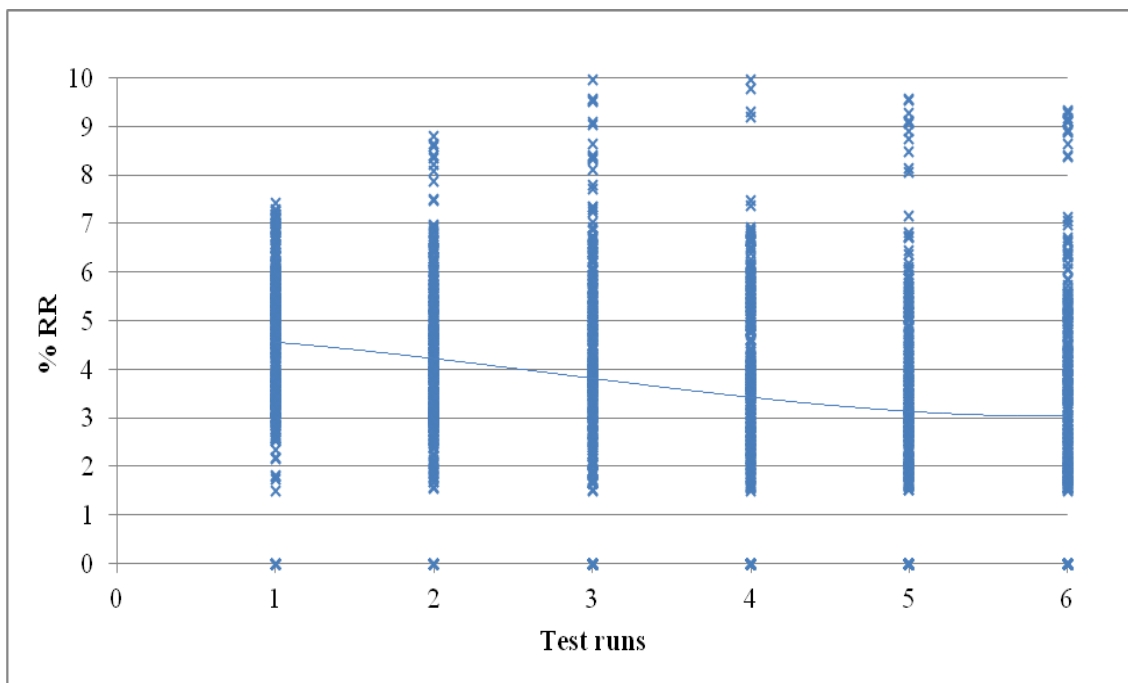
Figure 6.28: % RR vs. time at 0% gradient, 80% speed on pit run with 210 lbs load
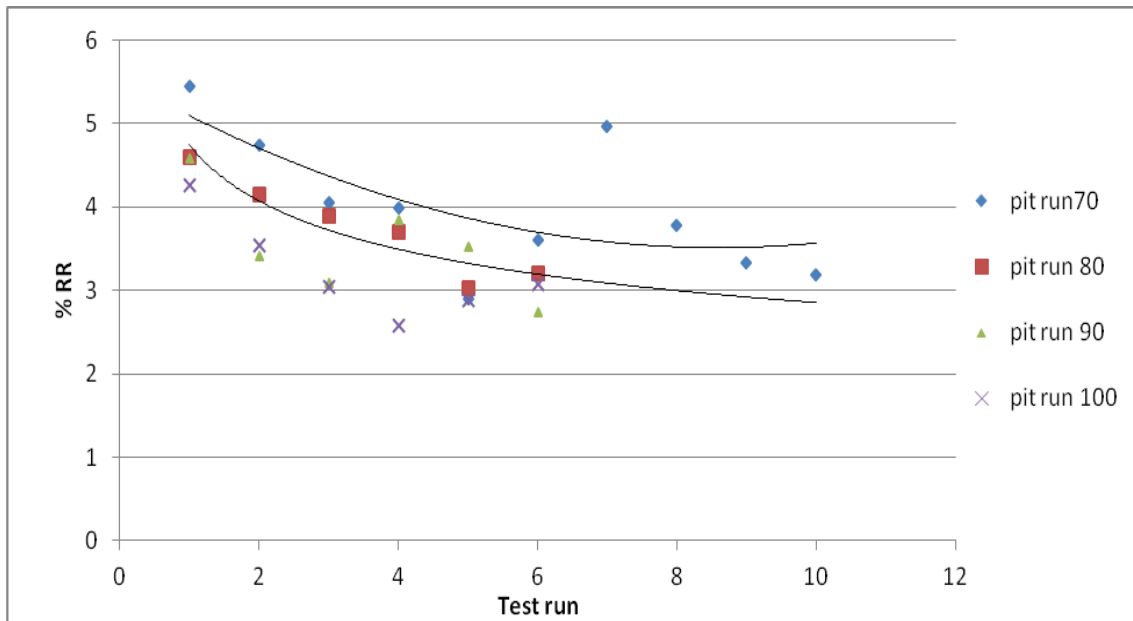
Figure 6.29: % RR vs. test runs at different speeds on pit run

6.2.4 Test results on limestone and analysis

Behavior of limestone was found to be similar to the pit run discussed in the preceding

section. Pull force data are plotted against time and test runs in Figure 6.31 and Figure

6.32. Tracking an individual run in Figure 6.31 appears difficult as all test runs yielded a

nearly equivalent range of data thus an individual test run plot is separately displayed in

Figure 6.30. It is clear from both figures that range of pull forces for limestone is 8 N to

16 N.   RR was derived from Figure 6.32 by application of base line equation 6.2 and

plotted against test runs in Figure 6.33. Range of RR was found to be between 2 % to 4

%, which ranks the lowest among all materials tested. A careful observation of Figure

6.30 and Figure 6.31 shows that peaks are frequent for limestone which could be a factor

of concern for tire life. Thus it is deemed necessary to pre compact the road and retain an

acceptable standard of smoothness to avoid high g-loading of the tire.

The average values at each run for all speeds are calculated and plotted against test runs in Figure 6.34. Average RR for limestone could be considered as 2% to 4 % which is lowest among all materials tested. Comparison of RR at different speed in Figure 6.34 shows that an improvement of 10% in speed brings RR down by 0.5 %, which is not significant considering the large range of rolling resistance in initial and subsequent runs. Further, a single curve for limestone was obtained by taking average of data points at all speeds and shown in comparison section as "Lime stone".
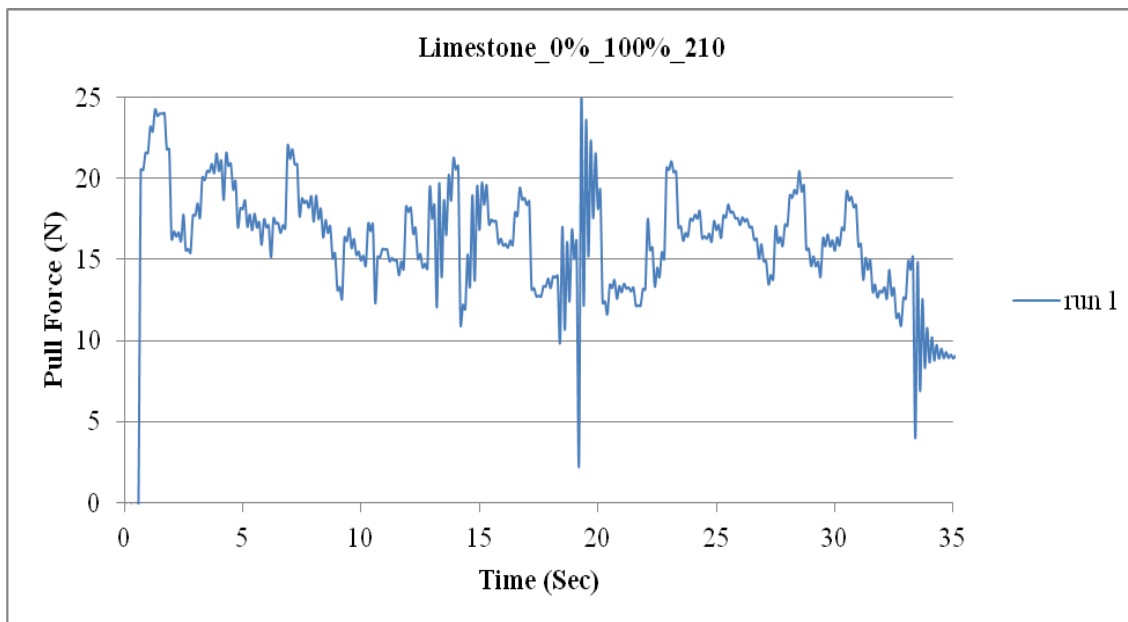
Figure 6.30: Pull force vs. time at 0% gradient, 100% speed on limestone with 210 lbs load, first run
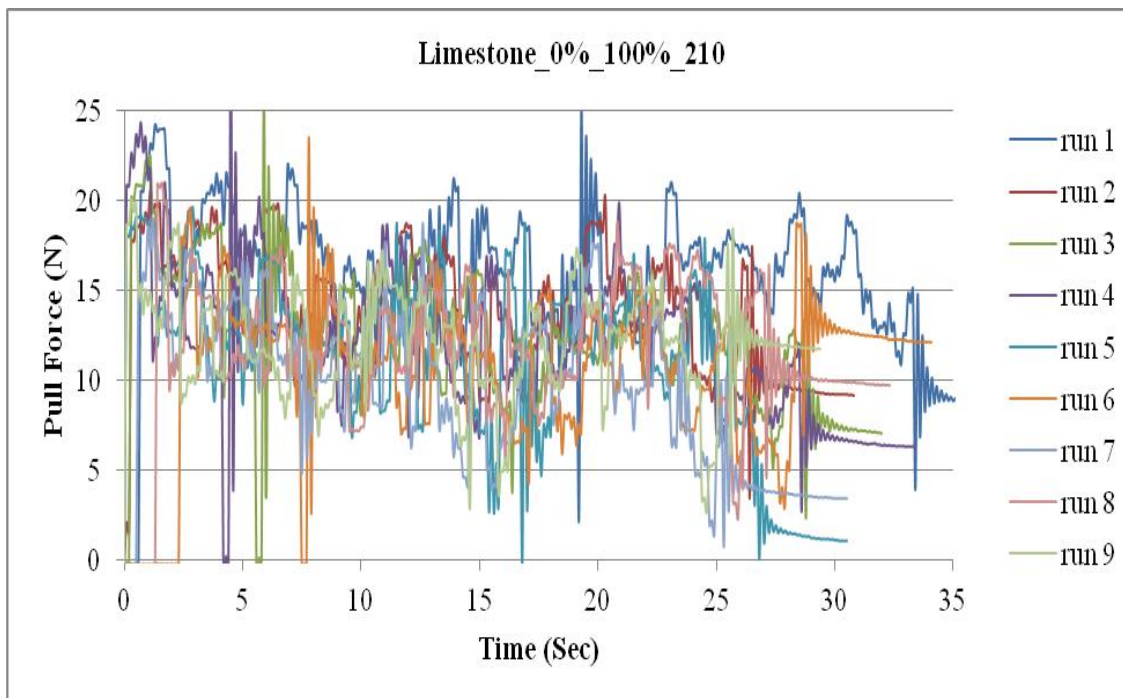
Figure 6.31: Pull force vs. time at 0% gradient, 100% speed on limestone with 210 lbs load (all test runs combined)
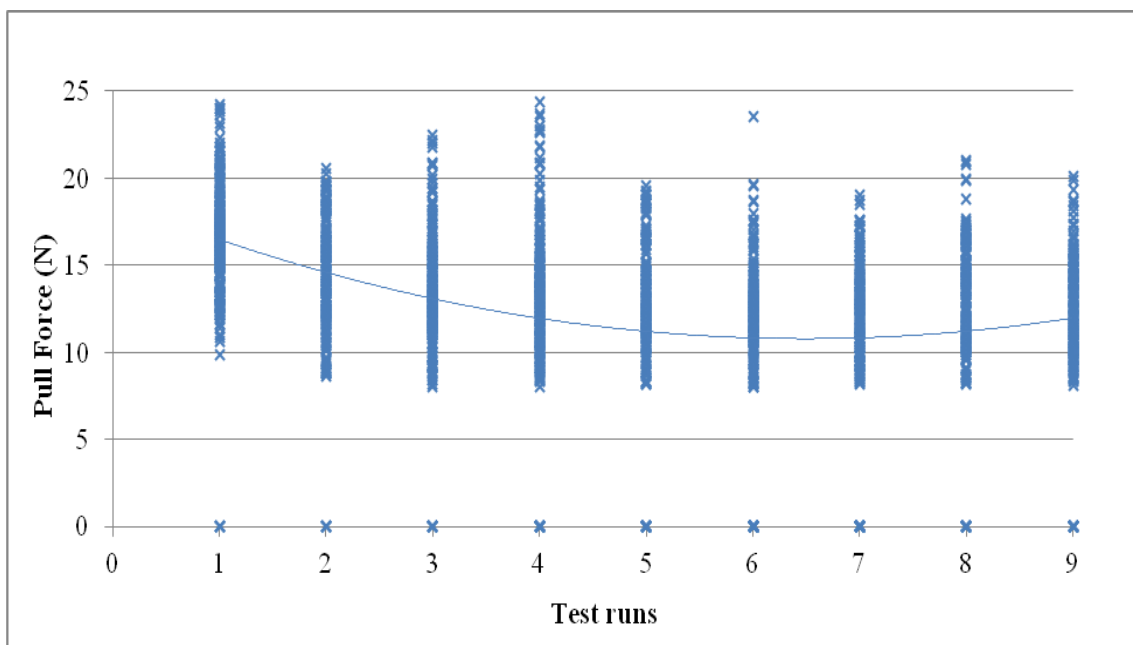
Figure 6.32: Pull force vs. test runs at 0% gradient, 100% speed on limestone with 210 lbs load
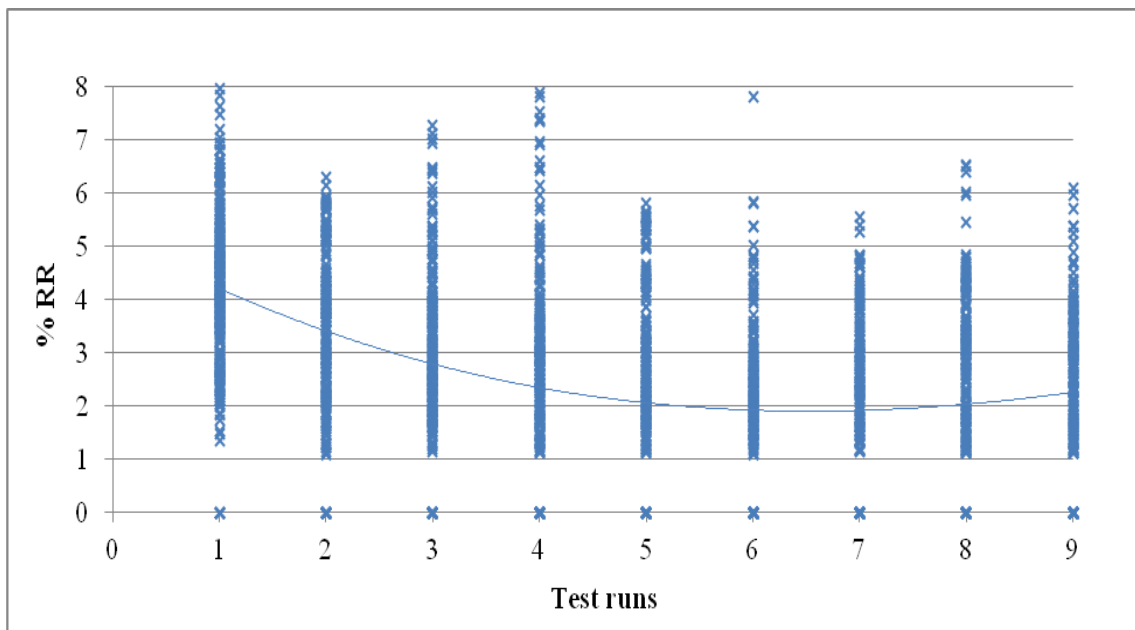
Figure 6.33: % RR vs. test runs at 0% gradient, 100% speed on limestone with 210

lbs load
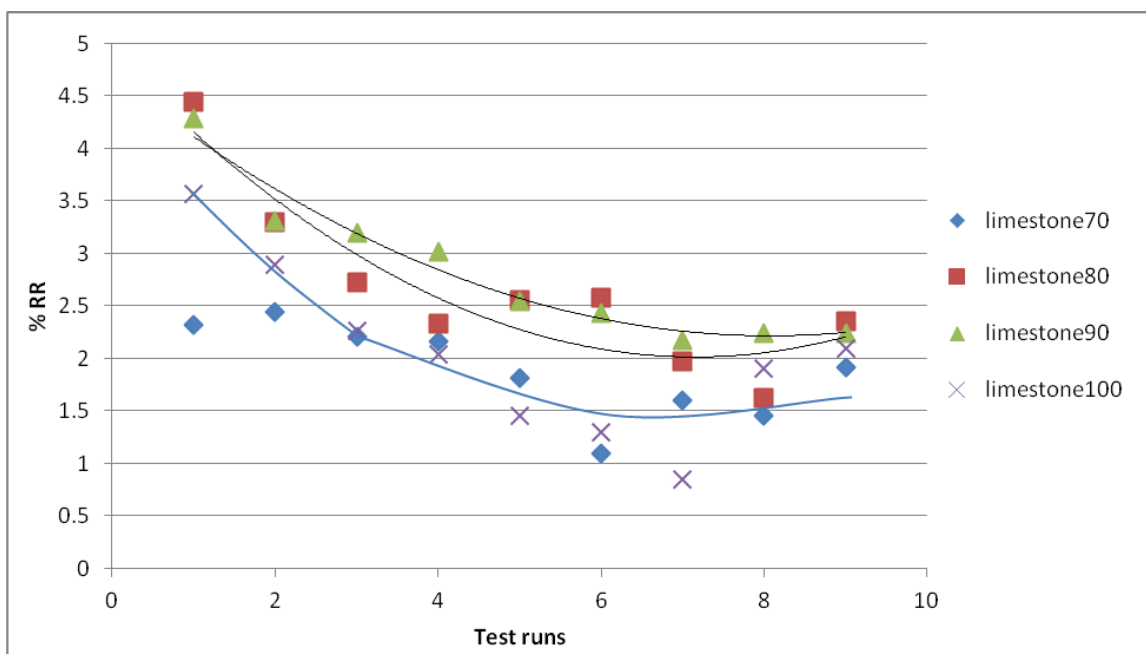
Figure 6.34: % RR vs. test runs at different speeds on limestone

6.3 Test results on composite materials and analysis

Individual materials sand, pit run and limestone were capped on oil sand and tests were performed at different speeds from 70% until 100%. Composite material was prepared by 2/3 of bed depth filled with oil sand as a base and balance 1/3 was topped with individual materials. Gradient were kept constant at 0 degrees for all composite materials.

6.3.1 Sand cap on oil sand

Figure through 6.35 to 6.37 shows the range of pull force and % RR for sand cap on oil sand at 80% speed. Behavior of sand cap on oil sand (Figure 6.35) is found similar to individual sand materials (Figure 6.9) except values are higher for cap materials. Rut formation was evident while performing the experiment similar as found in the sand phase. Higher values for sand cap might be due to deformation of both oil sand and sand. Initial runs yielded high pull force, which converged to a common range from 30 N to 45 N Figure 6.36. Plot between pull forces and test runs (Figure 6.36) shows the range of pull forces required for each run which was observed even up through the range of 72 N to 87 N in initial runs. RR for each run was obtained by application of base line equation 6.2 and shown in Figure 6.37. Range of RR was found to be 14% to 26% in later runs as shown in Figure 6.37, which is higher than individual sand material shown in Figure 6.11.
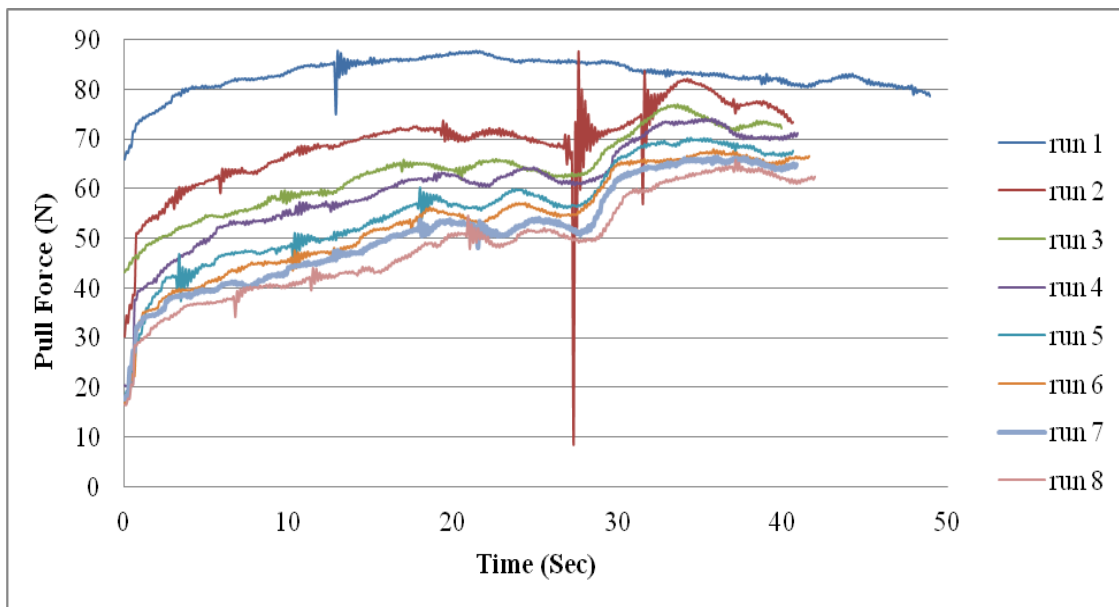
Figure 6.35: Pull force vs. time at 0% gradient, 80% speed on sand cap on oil sand with 210 lbs load
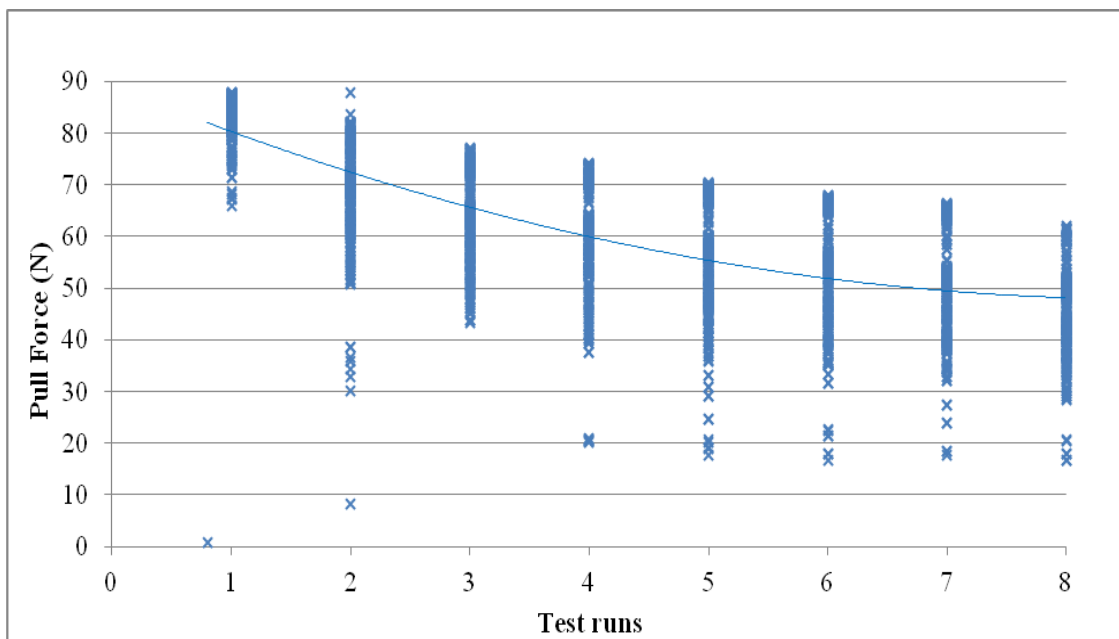
Figure 6.36: Pull force vs. test runs at 0% gradient, 80% speed on sand cap on oil sand with 210 lbs load
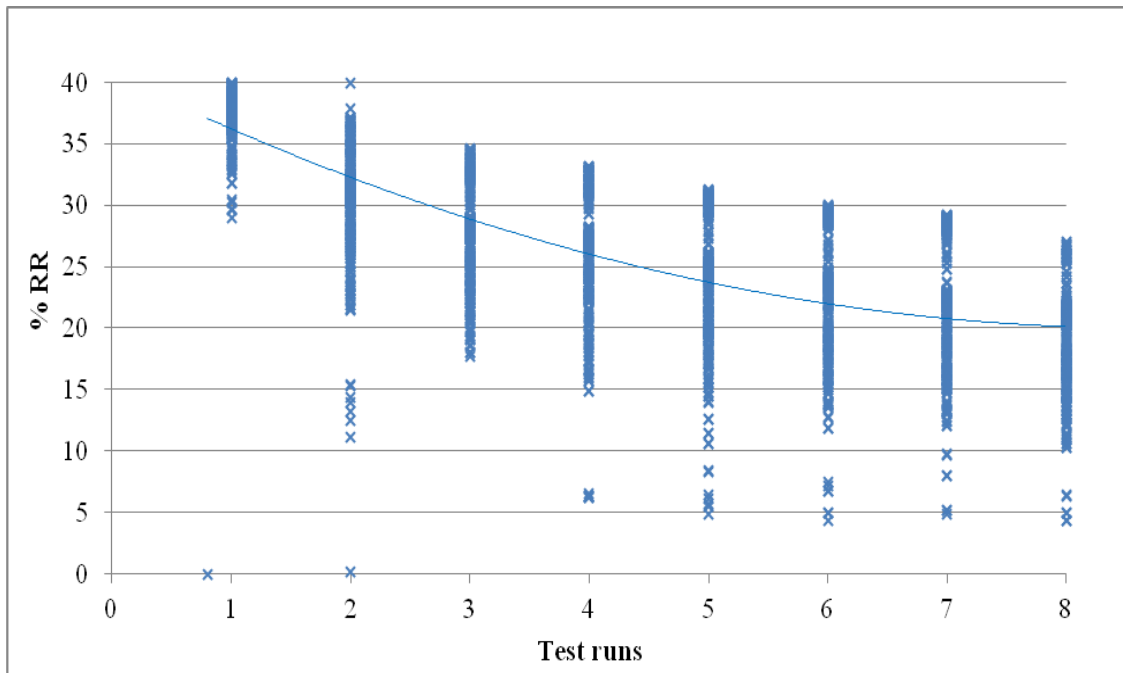
Figure 6.37: % RR vs. test runs at 0% gradient, 80% speed on sand cap on oil sand with 210 lbs load

The average values of RR at each run for all four speeds are plotted against test runs in Figure 6.38 and found to be ranging from 16% to 21%. Also, it can be observed that higher speeds yields lower RR. An increment of 10 % in speed brought RR down by 3% from 19.5% to 16.5% as observed from Figure 6.38, which is in agreement with sand materials discussed in Section 6.2.1. Also, multiple curves in Figure 6.38 were eliminated and joined into a single curve by combining data points at all speeds and shown in comparison section as "sand cap".
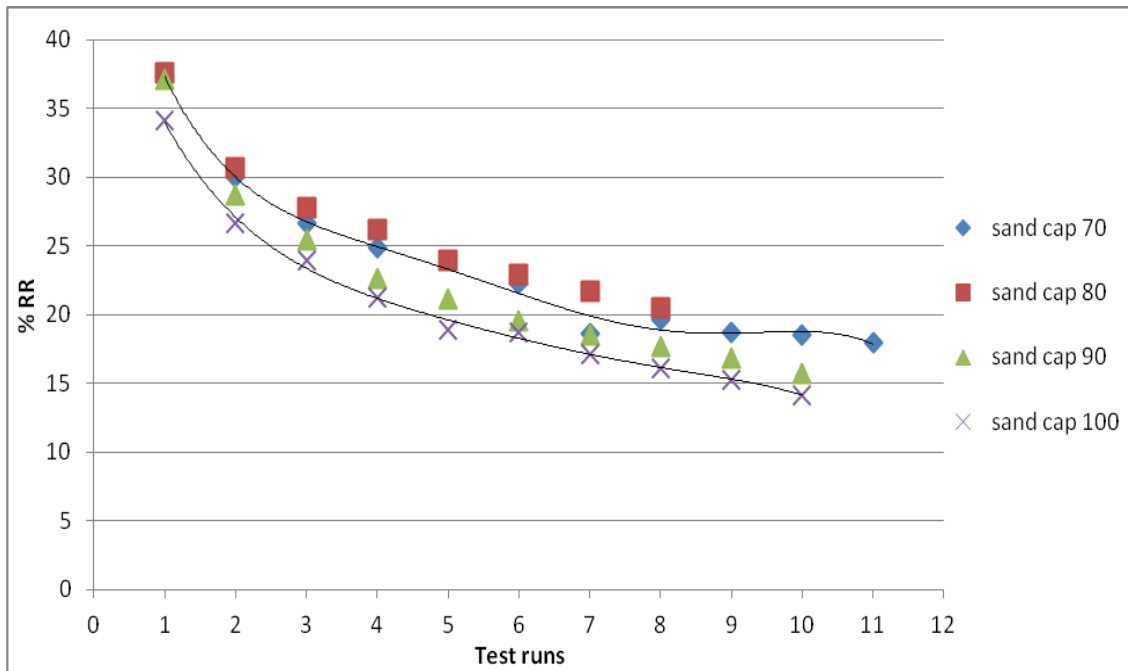
Figure 6.38: % RR vs. test runs at different speeds on sand cap composite material

6.3.2 Pit run cap on oil sand

Truck runs on oil sand capped with pit run had more of an inclination towards oil sand characteristics than individual pit run material. Pull force data obtained are plotted against time and test runs in Figure 6.39 and Figure 6.40. Initial runs required higher forces and consecutive runs converged to a common range of pull force from 16 N to 25 N which is similar to oil sand. RR was obtained by application of equation 6.2 in Figure 6.40 and plotted in Figure 6.41. Range of RR converged to 4% to 8%, which nearly equivalent to that of oil sand.
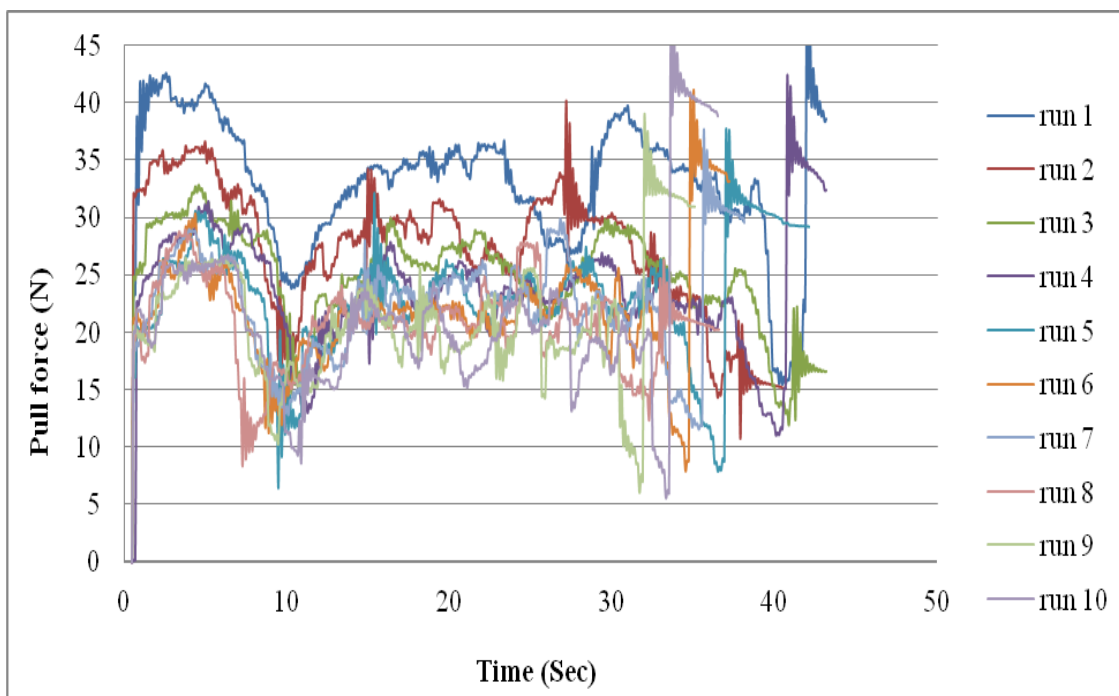
Figure 6.39: Pull force vs. time at 0% gradient, 90% speed on pit run cap on oil sand with 210 lbs load
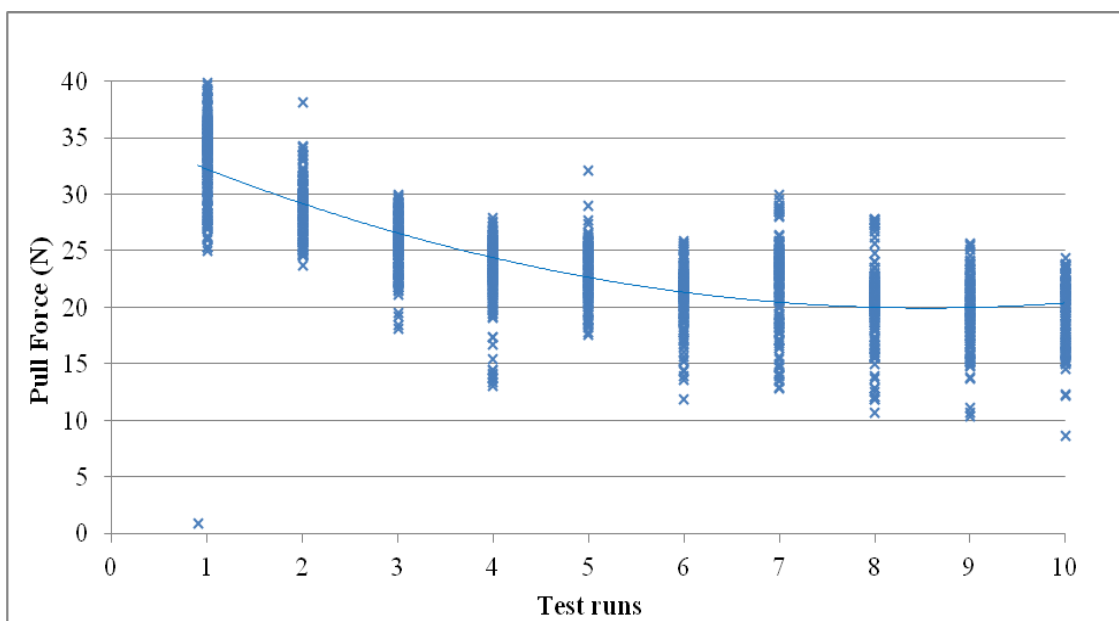
Figure 6.40: Pull force vs. test runs at 0% gradient, 90% speed on pit run cap on oil sand with 210 lbs load
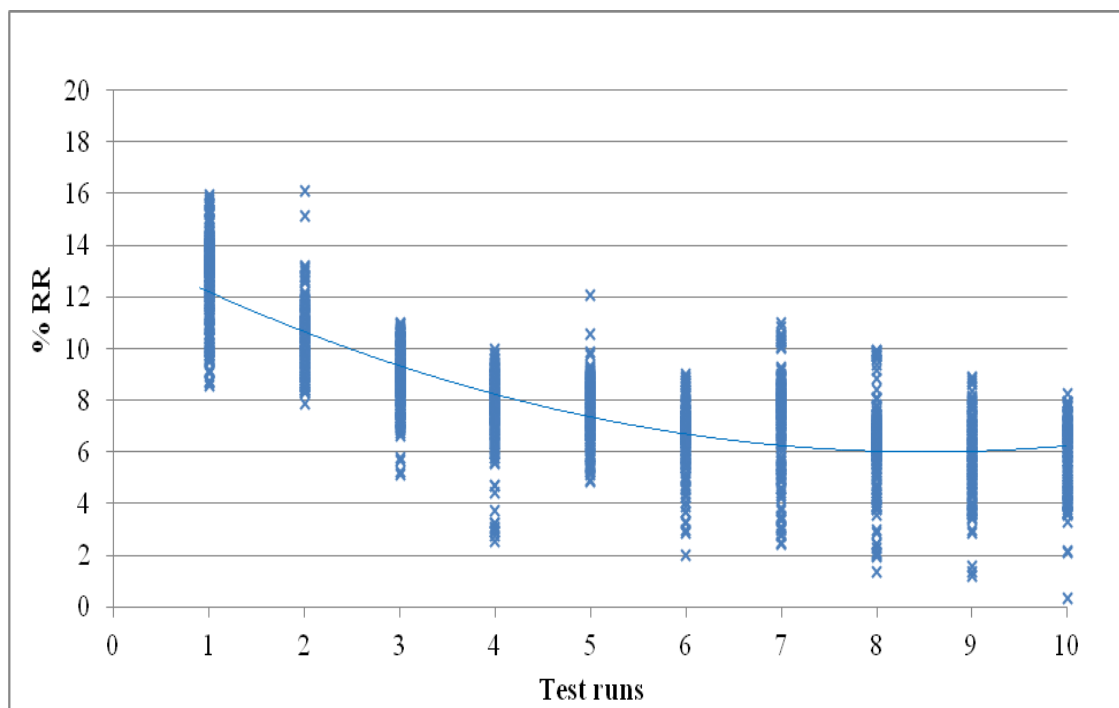
Figure 6.41: % RR vs. test runs at 0% gradient, 90% speed on pit run cap on oil sand with 210 lbs load

Average values at each run for all speeds are plotted against test runs in Figure 6.42. Data obtained at 70% and 80% speeds seems to be counterfeit while 90 % and 100 % gives a clear picture of RR on pit run. Average value of RR was found in the range of 6% to 8 %, however effect of speed on RR could not be determined from Figure 6.42. Ideal data points in figure below were combined to get single curve for pit run cap, which is shown in the comparison section as "pit run cap".
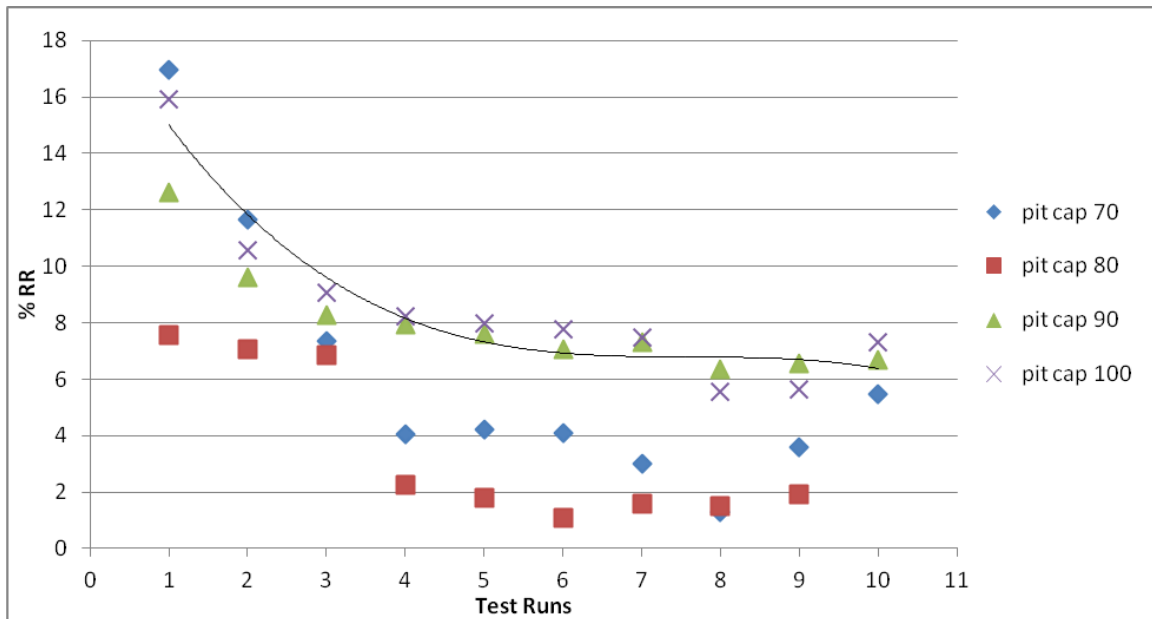
Figure 6.42: % RR vs. test runs at different speeds on pit run cap

6.3.3 Lime stone cap on oil sand

Behavior of limestone cap can be characterized somewhere between oil sand and limestone. This was the only material among all composite materials, which had lower RR than oil sand. Pull force data against time and test runs are presented in Figure 6.43 and Figure 6.44. Initial runs yielded higher forces, which converged to a common range of 10 N to 22 N consecutively a RR of 2% to 6% in Figure 6.45. It differed from individual limestone and pit run where the difference between consecutive runs was basically negligible. However, pull force converged to a common range quicker than sand and oil sand. Initial high forces have come into focus due to compaction of oil sand underneath limestone.
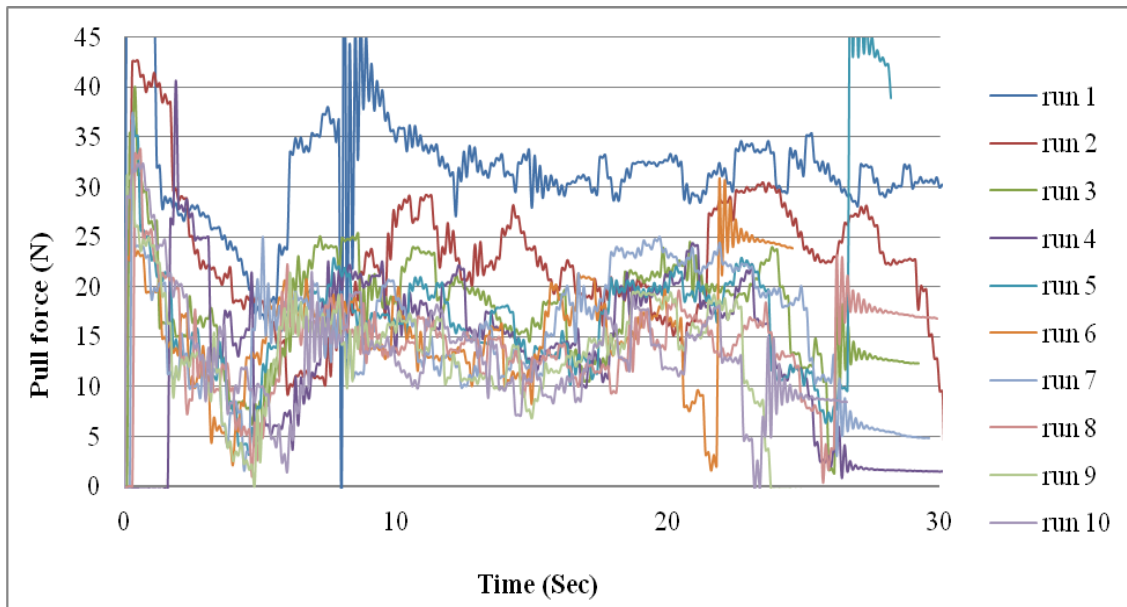
Figure 6.43: Pull force vs. time at 0% gradient, 100% speed on limestone cap on oil sand with 210 lbs load
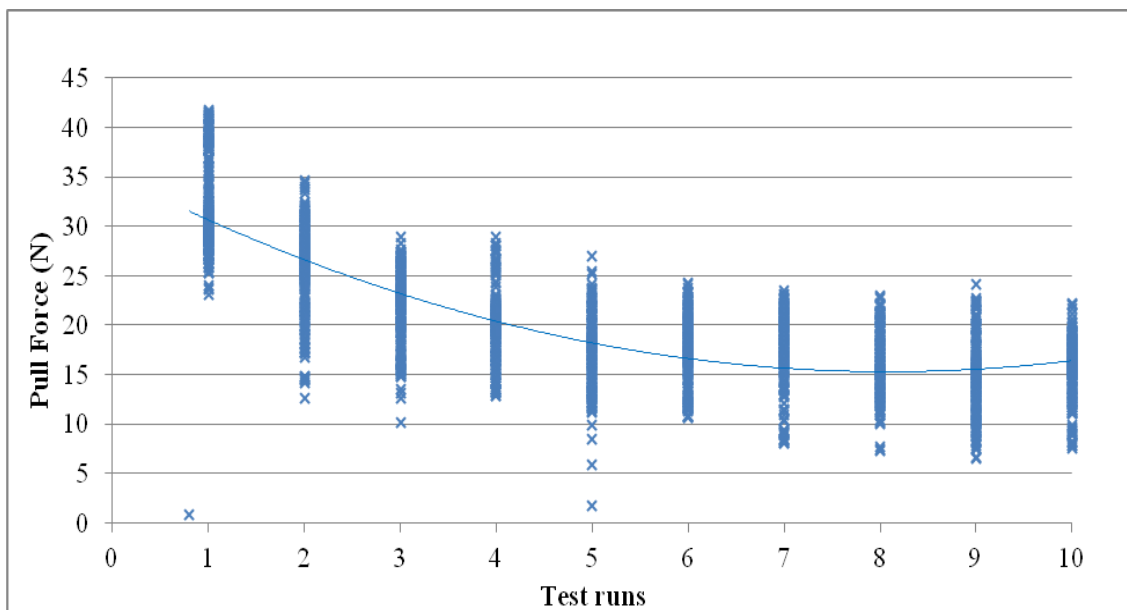
Figure 6.44: Pull force vs. test runs at 0% gradient, 100% speed on limestone cap on oil sand with 210 lbs load
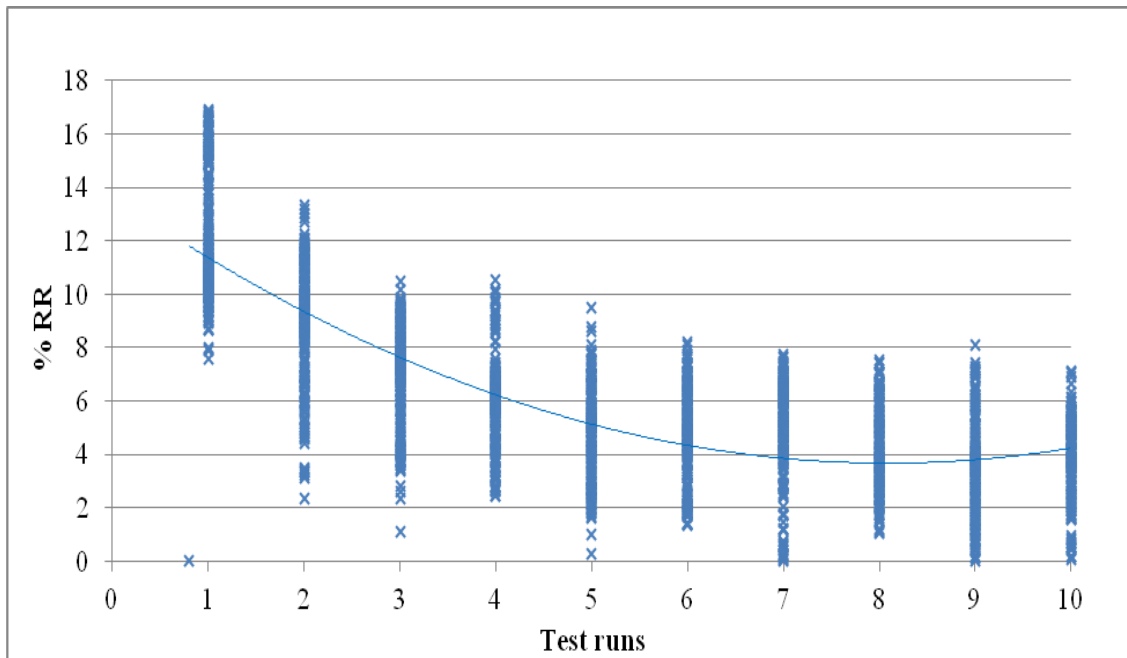
Figure 6.45: % RR vs. test runs at 0% gradient, 100% speed on limestone cap on oil sand with 210 lbs load

Average values at each run for all four speeds (70%, 80%, 90 % and 100%) were plotted in Figure 6.46. Average value of RR for limestone cap can be determined as 3% to 5%, which is smallest among all composite materials. A clear comparison of RR at different speed could not be obtained as per the data spread observed in Figure 6.46. Furthermore, a plot between % RR and test runs was created by combining data at all speeds, which represented lime stone cap as a whole, and shown in comparison section as "lime cap".
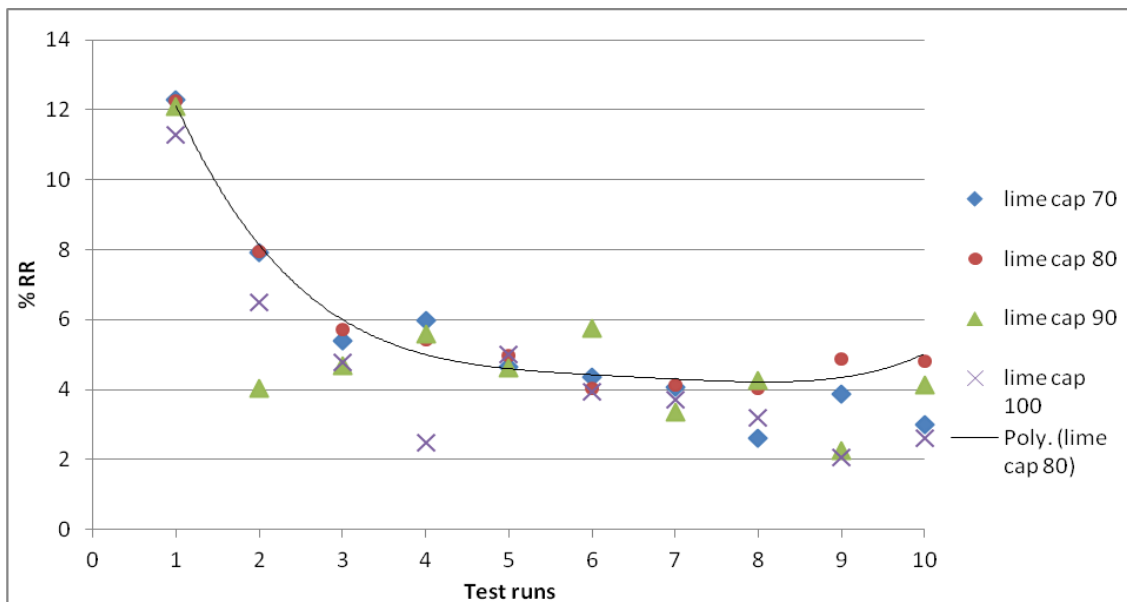
Figure 6.46: % RR vs. test runs at different speeds on lime stone cap

6.4 Comparison between individual materials, its capping with oil sand

Results for individual and composite materials have been discussed in the prior section.

A comparison of individual materials, its capping and oil sand are considered in this

section to discern the advantages of capping, along with their performance.

Results of individual and composite materials are presented in Section 6.3, where average

values at each run were plotted against test runs which resulted four points at each run

meant for 70%, 80%, 90% and 100%. If all four points are combined by taking the

accompanying average, each material will be represented by a single curve as shown in

the attached figures of current section of focus.

6.4.1 Comparison between oil sand, sand cap and sand

 RR curves for oil sand, sand cap and sand are shown in Figure 6.47. It is clear that oil

sand has the least RR among the tested materials. Sand capping on oil sand does not

improve RR; rather, it increases RR considerably. Oil sand, sand cap and sand had a RR

of 5%, 18% and 10% respectively, after the convergence.
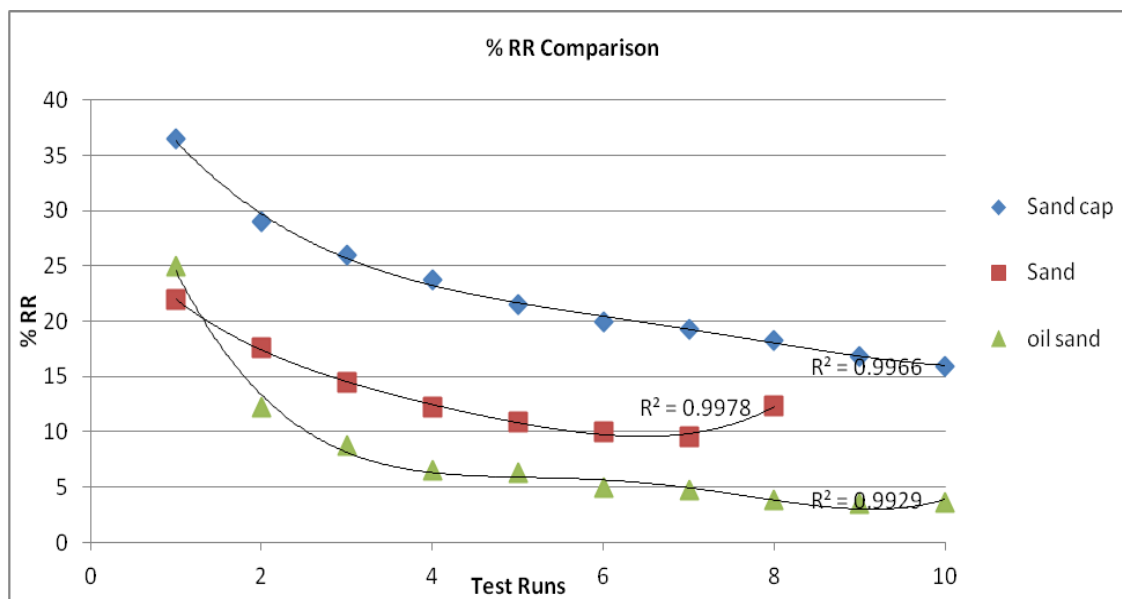
Figure 6.47: Average % RR vs. test runs for sand, sand cap and oil sand

6.4.2 Comparison between Oil sand, Pit run and Pit run cap

 RR curves for oil sand, pit run cap and pit run were collected and displayed in Figure

6.48. It can be observed that pit run has around 4% resistance which is smallest among all

three materials. Pit run cap exhibited 7% resistance with respect to 5% observed of oil

sand. The percentage resistances discussed are obtained after convergence from Figure

6.48. Therefore it can be concluded that pit run cap did not improve RR of oil sand yet

was found to be far superior to the sand cap.
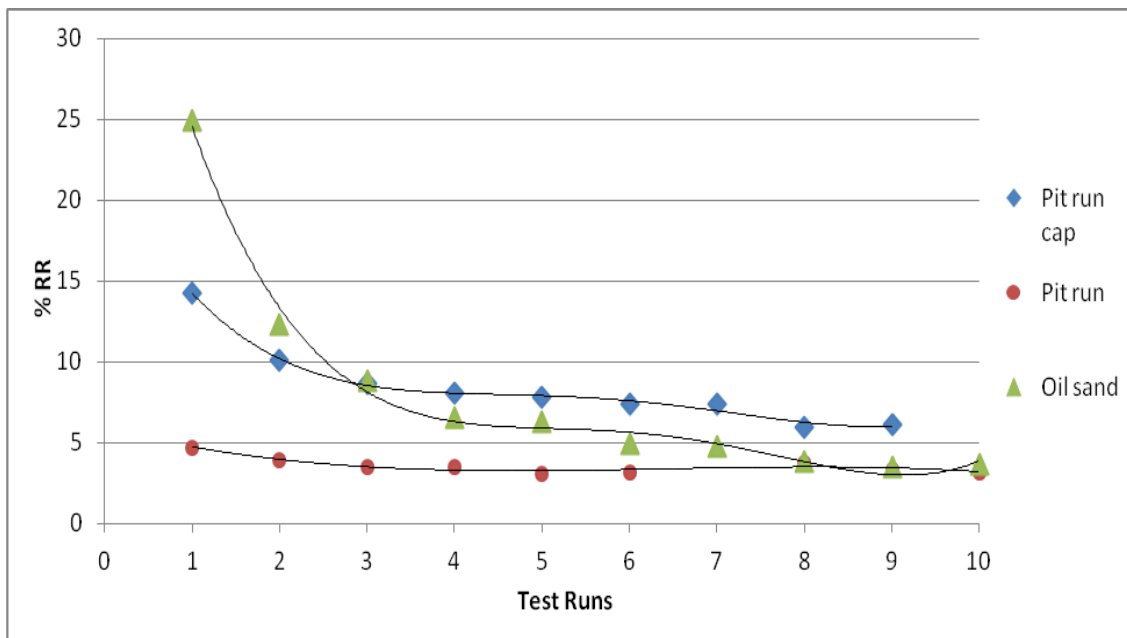
Figure 6.48: Average % RR vs. test runs for pit run, pit run cap and oil sand

6.4.3 Comparison between oil sand, lime stone and lime stone cap

Limestone cap on soil sand, limestone and oil sand are plotted collectively in Figure 6.49.

Clearly, limestone outperformed both all individual and composite materials. Limestone

as an individual material has a RR of 2.5%; while usage as a cap resistance fluctuates to

some point between that of limestone and oil sand. It can be concluded that limestone

could be the best capping solution among sand cap and pit run cap. Additionally, the

range of RR is the smallest among all composite materials tested, which signify less RR

offered by a limestone cap.
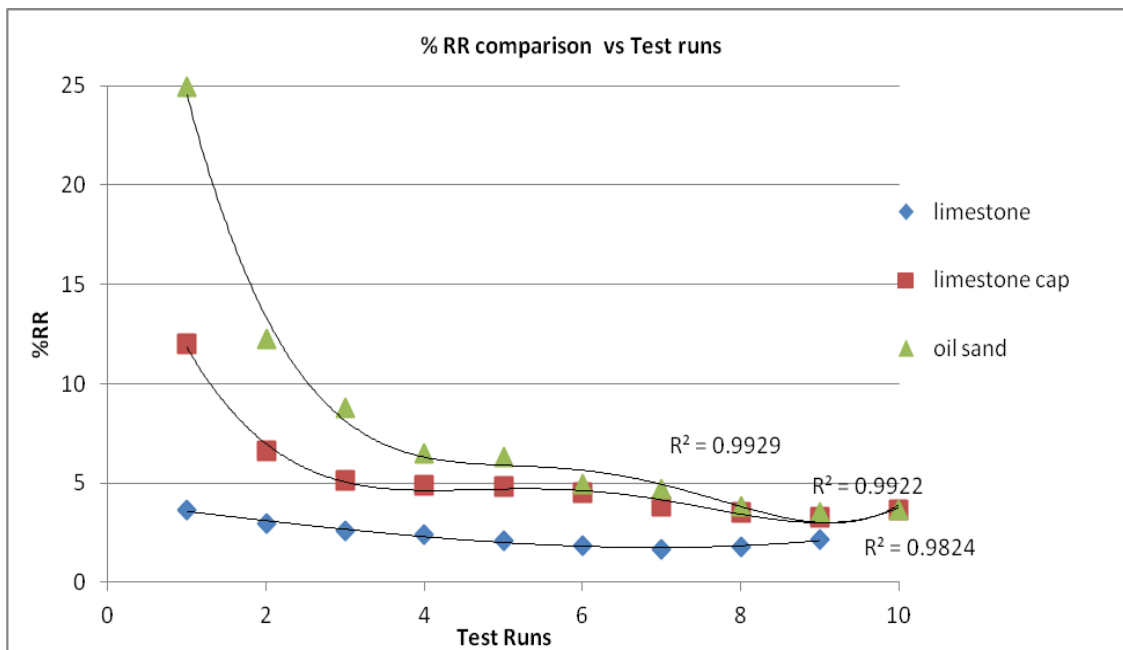
Figure 6.49: Average % RR vs. test runs for limestone, limestone cap and oil sand

6.5 Comparison between all composite materials
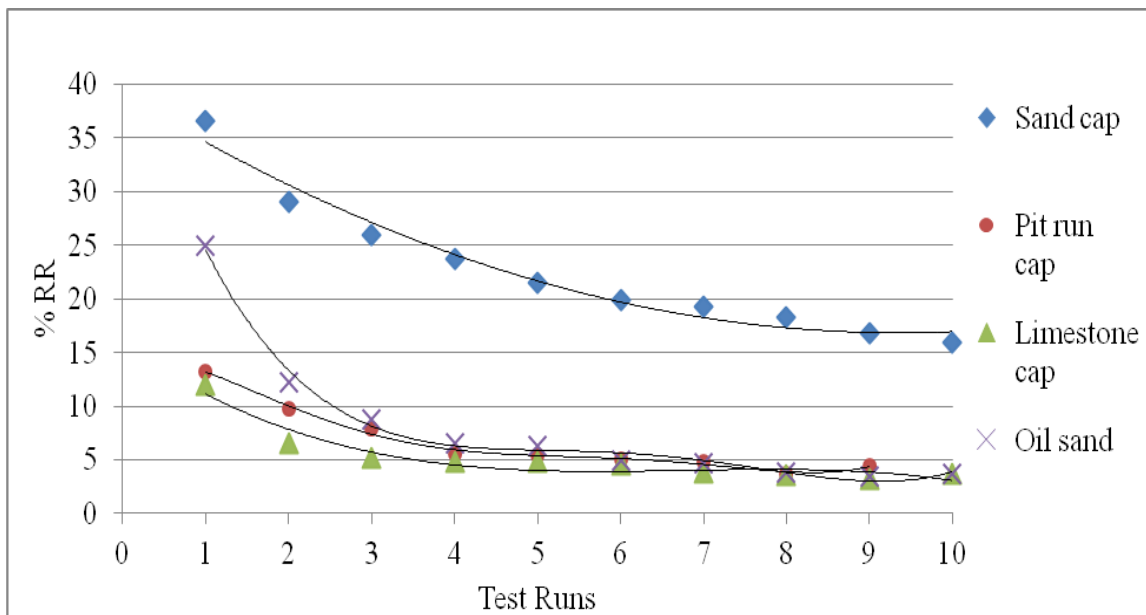
Figure 6.50: Average % RR vs. test runs on sand cap, pit run cap, limestone cap and oil sand
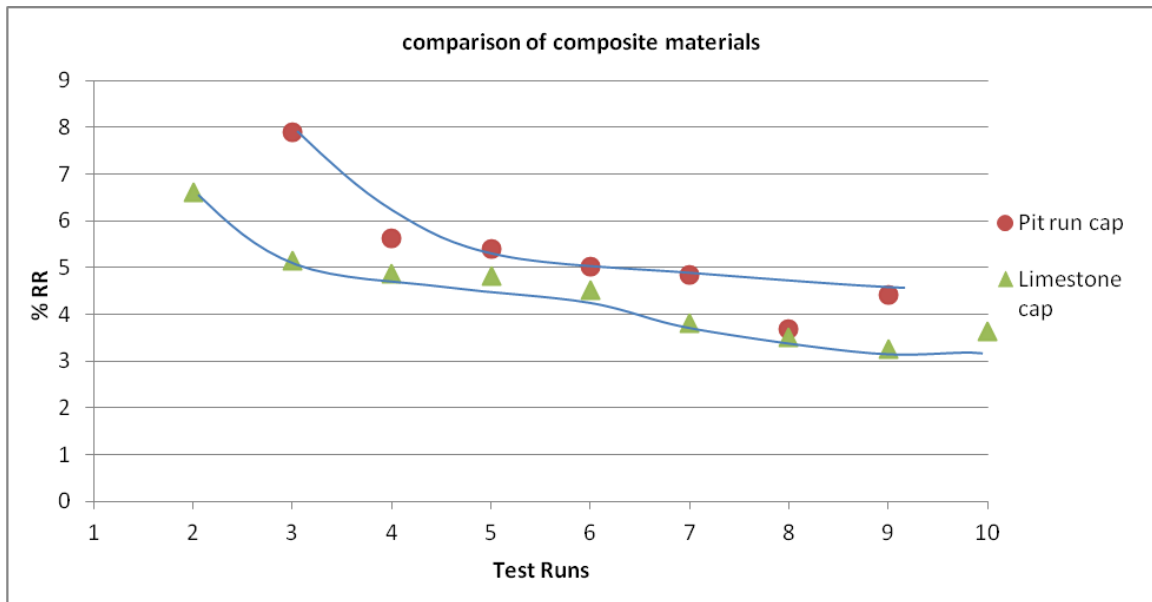
Figure 6.51: % RR vs. test runs on pit run cap and limestone cap

6.6 Different effects of rolling resistance

RR has direct effect on fuel consumption. It has been observed in an independent study by Joseph (2008) that a reduction of 5 % in rolling resistance could result 25 % to 40 % less fuel consumption in the same time period and load conditions depending upon the size of haul trucks. Consequently, emissions caused by fuel burns will decrease proportionally.

An uneven road not only creates higher rolling resistance but decreases tire life. Machine is more prone to structural damage due to rack, roll and pitch events (Joseph, 2008).

Chapter Seven: Conclusion

A series of tests were conducted on different materials commonly used in mining industry for road construction in order to predict the RR of an ultra class truck tire on a haul road. It was beyond the capacity of the University of Alberta lab to test an actual ultra class truck tire, therefore a scaled truck model was designed which was measured as fifteen times smaller than a typical heavy hauler. Accordingly, all components included while conducting the experiments were scaled and justified with scaled truck.

Tire flexure test was performed to determine tire internal pressure and load combination such that scaled truck will behave and have same impact as an ultra class haul truck on haul roads. A parameter called pressure stiffness was judged equivalent for both a scaled and an ultra class truck, which resulted a 6 psi internal tire and 210 lbs load combination in the scaled model.

Truck was run on an empty test bed to establish a reference equation, which was applied to calculate % RR of materials under consideration. A total of 275 tests at different gradients, speeds and loads were performed to establish this reference equation.

Four commonly used materials – sand, oil sand, pit run and limestone were tested in variable gradient ramp at different speeds. It was found that sand offered the highest % RR and was followed by oil sand. Pit run and limestone had considerably lower RR than

sand. Limestone was found to be best performer among all materials tested. % RR values are shown in table 7.1.

It is widely used practice to cap parent material in road construction. Materials under consideration are readily available in oil sand industry therefore its capping over oil sand was studied and % RR was calculated in each case.

A comparison between individual materials and its capping with oil sand was obtained. It was found that sand capping on oil sand yielded more % RR resistance than individual sand material. None of the composite materials performed better than its parent material but limestone was found very close to limestone capping on oil sand. Range of RR obtained for different composite materials are shown in table 7.1

Material	Converged % RR	Average RR after compaction	Initial RR
Sand	12%	10 to 15%	24 to 35%
Oil sand	5.50%	4 to 7%	20 to 27%
Pit run	4%	3 to 5%	3 to 7%
Limestone	3%	2 to 4 %	2 to 6 %
Sand cap	17%	14 to 26 %	32 to 40 %
Pit run cap	7%	6 to 8 %	9 to 16 %
Limestone cap	4.50%	3 to 5 %	9 to 16 %

Table 7.1: % Rolling resistance of different materials

A comparison of RR among all composite materials resulted that limestone offered the lowest % RR. Sand cap had considerably higher RR than sand and was observed as the

highest among all materials tested. Pit run converged to be same as oil sand, while limestone performed slightly higher than its parent material, albeit less than oil sand.

Experiments were conducted at four speeds 70%, 80%, 90% and 100% and each experiment was repeated three times to yield consistent data. Higher speed yielded lower RR on sand, pit run, limestone and sand cap. Other materials did not give a clear understanding of speed on RR. An increment of 10% on sand caused a reduction of 2% to 2.5% in RR. Similar behaviour was observed in sand cap. It was difficult to establish any relation between RR and speed for pit run, pit run cap and limestone cap due to nature of data.

This research will have application in mining industry to estimate rolling resistance of commonly used materials for haul road construction. Capital intensive mining industry has always been interested to reduce rolling resistance to a set level. Truck running on lower rolling resistance road consumes less fuel thus lower operating cost.

Chapter Eight: Future recommendations

Although, this research estimates rolling resistance of commonly used materials sand, oil sand, pit run and limestone, there are scope of further improvements. Modern development in haul road construction led to invention of many materials suitable for haul road. Claycrete is one of the examples. These materials should be tested and compared with materials under consideration. Financial implications in developing the modern road and saving due to lower rolling resistance should be judged.

Oil sand was tested on room temperature and 7 to 10 runs were completed. Situation could be significantly different during summer time when temperature is high. High temperature and cyclic loading of oil sand can cause liquefaction of material. There is future scope of research in this matter.

This research mainly focused on the material properties of rolling resistance. Materials were tested at low speed. There is a need to test these materials on higher speed and thus examine the effect of speed on rolling resistance. Also, Haul trucks very frequently accelerate and decelerate on haul road creating a dynamic rolling resistance while this research considered a constant speed. Further, Undulations on haul road bring grade resistance in focus. A further investigation in this field is required.

References

1. Baglione, M., Duty, M., Pannone, G. (2007). Vehicle system energy analysis methodology and tool for determining vehicle subsystem energy supply and demand. SAE World congress, Detroit, Michigan, April.

2. Bekker, M. G. (1956). Theory of land locomotion: The Mechanics of vehicle mobility. Ann Arbor: University of Michigan Press

3. Bekker, M. G. (1960). Off the road locomotion. Ann Arbor: University of Michigan Press.

4. Bekker, M. G., Semonin, E. V. (1975). Motion resistance of pneumatic tyres. J. Automotive Engng., 6-10

5. Bernstein, R. (1913). Probleme zur Experimentellen Motorpflugmechanik. Der Motorwagen, 9, 199-206.

6. Clark, S. K., Dodge, R. N. (1979). A handbook for the rolling resistance of pneumatic tires. Industrial development division, Institute of science and technology, The University of Michigan and Arbor, $2 - 6$.

7. Dwyer, M. J., Comely, D. R., Evernden, D. W. (1975). The development of NIAE handbook of agricultural tyre performance. Proc 5th International conference, International society of terrain vehicle systems, Detroit

8. Gee-Clough, D. (1976). The Bekker theory of rolling resistance amended to take account of skid and deep sinkage. Journal of Terramechanics, 13 (2), 87-105

9. Hetherington, J. G., Littleton, L. (1978). The rolling resistance of towed rigid wheels in sand. Journal of Terramechanics, 15 (2), 95-106

10. Heyde, H. (1913). Mechanik des Schleppers. Deutsche Agrartechnik, 7, 1-4.

11. Joseph, T. G. (2008). Scaled rolling resistance tests, Report 2: Extended analysis – Birch Mountain. 1-13

12. Knoroz, V. I. (1968). The influence of tyre rolling resistance on vehicle fuel consumption. Avtom. Prom., March (3), 11-14

13. Komandi, G. (1997). A kinematic model for the determination of peripheral force. Journal of Terramechanics, 34 (4).

14. Komandi, G. (1999). An evaluation of concept of rolling resistance. Journal of Terramechanics, 36, 159-166.

15. Morin, MA. (1841). Memoir sur le tirage des voitures. Comptes rendus de l'Academie des Sciences 1840 et 1841.

16. Onafeko, O. (1969). Analysis of rolling resistance losses of wheels operating on deformable terrain.J. Agric. Engng Res. 14 (2), 176-182

17. Onafeko, O., Reece, A. R. (1966). Soil stress and deformation beneath rigid wheels. Journal of Terramechanics, 4 (1), 59-80.

18. Perloff, W. H. (1975). Pressure distribution and settlement. Foundation engineering handbook, H. F.Winterkorn and H. Y. Fang, eds., Van Nostrand Reinhoil, New York, 148-196

19. Plackett, C. W. (1985). A review of force prediction methods for off-road wheels. J. Agric. Engng. Res., 31, 1-29.

20. Pope, R. G. (1969). The effect of sinkage rate on pressure, sinkage relationships and rolling resistance in real and artificial clays. Journal of Terramechanics 6(4), 31-38.

21. Pope, R.G. (1971). The effect of wheel speed on rolling resistance. Journal of Terramechanics, Pergamon press, 8, (1), 51-58.

22. Reece, A. R. (1965-66). Principle of soil-vehicle mechanics. Proc. Auto. Div. Instn. Mech. Engrs., 180, 2A, 2.

23. Schuring, Dieterich J. (1977). Scale models in engineering. Toronto : Pergamon press, 4

24. US Department of Energy. "Fuel Economy: Where the Energy Goes" http://www.fueleconomy.gov/feg/atv.shtml , Jan 05, 2012.

25. Terzaghi, K. (1944). Theoretical soil mechanics. New York: J. Wiley and Sons

26. Turnage, G. W. (1972). Tyre selection and performance prediction for off road wheeled vehicle operations. Proc. 4th International conference, International society terrain vehicle systems.

27. Wills, B. M. D., Barret, F. M., Shaw, G. J., (1965). An investigation into rolling resistance theories for towed rigid wheels, Journal of Terramechanics, 2 (1), 24-53

28. Wood G. S., Osborne, J. R., Forde, M. C. (1995). Soil parameters for estimating the rolling resistance of earthmoving plant on a compacted silty cohesive soil. Journal of terramechanics, 32 (1), 27 – 41.